



Design, modeling and control of inherently compliant actuators with a special consideration on agonist-anthropomorphic configuration

Ganesh Kumar Hari Shankar Lal Das

► To cite this version:

Ganesh Kumar Hari Shankar Lal Das. Design, modeling and control of inherently compliant actuators with a special consideration on agonist-anthropomorphic configuration. Automatic. INSA de Toulouse, 2016. English. NNT : 2016ISAT0030 . tel-01547435

HAL Id: tel-01547435

<https://theses.hal.science/tel-01547435>

Submitted on 26 Jun 2017

HAL is a multi-disciplinary open access archive for the deposit and dissemination of scientific research documents, whether they are published or not. The documents may come from teaching and research institutions in France or abroad, or from public or private research centers.

L'archive ouverte pluridisciplinaire **HAL**, est destinée au dépôt et à la diffusion de documents scientifiques de niveau recherche, publiés ou non, émanant des établissements d'enseignement et de recherche français ou étrangers, des laboratoires publics ou privés.

Université Fédérale



Toulouse Midi-Pyrénées

THÈSE

En vue de l'obtention du

DOCTORAT DE L'UNIVERSITÉ FÉDÉRALE TOULOUSE MIDI-PYRÉNÉES

Délivré par :

l'Institut National des Sciences Appliquées de Toulouse (INSA de Toulouse)

Présentée et soutenue le 22/12/2016 par :

GANESH KUMAR

**Design, modeling and control of inherently compliant actuators with a
special consideration on agonist-antagonist anthropomorphic
configuration**

JURY

BRAM VANDERBORGHT	Professeur at University of Brussels	Rapporteur
YANNICK AOUSTIN	Professeur at University of Nantes	Rapporteur
PHILIPPE FRAISSE	Professeur at University of Montpellier	Examineur
BERTRAND TONDU	Professeur at INSA of Toulouse	Directeur de Thèse
PHILIPPE SOUÈRES	DR CNRS at LAAS, Toulouse	Co-Directeur de Thèse
OLIVIER STASSE	DR CNRS at LAAS Toulouse	invité

École doctorale et spécialité :

EDSYS : Robotique 4200046

Unité de Recherche :

Laboratoire d'analyse et d'architecture des systèmes

Directeur(s) de Thèse :

Philippe SOUERES et Bertrand TONDU

Rapporteurs :

Bram VANDERBORGHT et Yannick AOUSTIN

Abstract

"Design, modeling and control of inherently compliant actuators with a special consideration on agonist- antagonist anthropomorphic configuration"

The research aims at the design, modeling and control of inherently compliant actuators for anthropomorphic systems. The first part of the work focuses on the study of various existing designs and look for the possibility of alternative actuators other than the conventional electric motors. Special attention is given to electroactive polymer based soft actuators which have good potential in future robotic applications. In parallel, a model of the actuator dynamics and the model-based controller (MPC and optimal control) have been synthesized for an anthropomorphic 7 Dofs arm actuated by antagonist-agonist pair of Pneumatic Artificial Muscles (PAMs) at each joint. Such model and controller is then integrated within the software environment developed by the team. Using the PAMs based anthropomorphic manipulator arm and the numerical simulator, tests are done in order to evaluate the potential of this actuator and compare with the human body capabilities.

Acknowledgement

This thesis work was achieved thanks to collaboration and support of various people who I would like to gratefully acknowledge.

First of all, I would like to thank my supervisor Phillipe Soueres and Bertrand Tondou. They kept me motivated with their great optimism and kept me pushing to do better. Without their guidance and support, it would be almost impossible to complete my thesis. Special thanks to Olivier Stasse who has always been with me whether it's technical or theoretical issues.

Thanks to Jerome Manhes who contributed in the electronic and hardware development of the project. Working with him was a great pleasure. Because of him, I was able to learn and understand all the aspects (hardware, electronics, data communication) of my experimental set-up. I would also like to acknowledge his work on NI module which is the backbone of our data capturing system on the robot.

I would thank Florent Forget for great support in the software development. Because of him it was possible to test the robot in real time with different control methods. Kevin Gerard has contributed in CAD modeling of the robot which was an necessary input the modelling of my experimental set-up. Working with Kevin and Florent was not only good for my work and my own learning but its also relaxing and fun.

I would never have been able to finish my dissertation without the support, help and love of my friends. The warm and friendly environment provided by the lab made it possible to interact with different colleagues and share jokes while having coffee. Finally, thanks to my parents and family who have been constantly providing moral support to me.

Table des matières

Introduction	1
0.1 Motivation	1
0.2 Pneumatic actuators	3
0.3 Ion-polymer actuators	3
0.4 Thesis organisation	4
0.5 Publications	5
1 State of the art	7
1.1 Compliance actuators	8
1.1.1 Compliance definition	8
1.1.2 Compliance in Human arm	9
1.2 Review of Variable Stiffness Actuators (VSA's)	10
1.2.1 Fixed compliance actuators	11
1.2.2 Variable compliance	12
1.3 Artificial muscles	23
1.3.1 Review of Artificial Muscles	23
1.3.2 Pneumatic Artificial Muscles	27
2 Identification and control of Electroactive polymer	35
2.1 Introduction	35
2.1.1 PDOT :PSS Ionic liquid actuator	36
2.1.2 Characterization of Ionic actuator	36
2.1.3 Control reviews of Electroactive polymer actuators	39
2.2 Non-linear Identification of the Artificial Muscle	41
2.2.1 Non-linear model derivation from the first order linear model	41
2.3 PI-closed loop control	43
2.3.1 Linear tuning and non-linear effects	43
2.3.2 Taking into account voltage constraints	44
2.3.3 Stability of the PI-controller	45
2.3.4 Tracking performances	47
3 Modeling of the system	53
3.1 Robotic experimental set-up	53
3.1.1 Kinematic structure of the arm	53
3.1.2 Hardware components	53
3.2 Modeling of the pneumatic system	56
3.2.1 Muscles side dynamics	57
3.2.2 Pressure side dynamics	58
3.2.3 Modeling of Agonistic-antagonistic joint actuator : Symmetric case	60

3.2.4	Modeling of agonistic-antagonistic joint actuator : Generic case	62
3.2.5	Model of the multi Dof pneumatic arm	64
3.3	Conclusion	65
4	Control of the Pneumatic system	67
4.1	Introduction	67
4.2	PID control of the pneumatic system	69
4.2.1	Model free single Integral action controller	69
4.2.2	Model based PI controller	72
4.3	iLQR control of the anthropomorphic pneumatic arm	76
4.3.1	State space representation	76
4.3.2	Iterative Linear Quadratic Regulator (iLQR)	77
4.4	Conclusion	80
5	Simulation and Experiments	81
5.1	Open loop simulation of the robot	81
5.2	Close loop control with PI controller	83
5.2.1	Trapezoidal trajectory tracking	83
5.2.2	Sine wave trajectory tracking	84
5.3	Application of iLQR in performing explosive motion	85
5.3.1	Task 1 : Position control	86
5.3.2	Task 2 : Maximizing the link speed	88
5.3.3	Task 3 : Maximizing the end effector speed	88
5.3.4	Task 4 : Ball throwing and kicking	89
5.4	Conclusion	92
	Conclusion	95
A	Characterization of PEDOT :PSS Ionic actuator actuators	99
B	Geometrical parameter of the robot	103
B.1	Kinematics of of the robot	103
B.2	Cad model of the robot	103
C	Closed-loop stability analysis of single-I controller	107
D	Electronics of the robot	111
D.1	Intensity-Pressure converter	111
D.2	NI module	112
D.2.1	From Host computer to NI module	112
D.2.2	From NI module to Host computer	114
	Bibliographie	117

Introduction

Bio-inspired robotic is one of the emerging research interests among the robotics community. In particular, the human physiology is even more fascinating which makes the human perform various manipulation tasks efficiently and robustly. From the study of the human movement, or the movement of mammals in general, we can understand that the conventional robotics development has taken a path which is quite counter intuitive to our own physiology. The conventional way of designing a robot is to make it as stiff as possible. Also the axes are aligned in such a way to facilitate computational tasks in control design. These constraints of computational power, lack of mature algorithm for modeling and controlling non-linear systems have been the motivation behind the design of robots for decades. But with the rapid evolution in computer technology and the exponential growth in computational power, it is the time now to revisit our approach to design a robot. But before that we must ask ourselves what do we expect from a robot in this modern era. Conceiving a human friendly robot is a great objective. A robot which can perform routine tasks easily and in close collaboration with human. In such environment, collision with the obstacles or with the human is inevitable. Safety and efficiency in task execution are important criteria for designing any such robots. Due to this requirements, it seems necessary to have some sort of compliance in the joint or in the structure of the robot body. The search for the most suitable actuator which can make robot efficient and compliant is ongoing. This is the main motivation behind my thesis.

0.1 Motivation

A human friendly robot should be able to imitate some human behaviour. And to make this possible, we may look back to the nature - Our own body. A simple joint model of a mammal can show the musculoskeletal structure with agonist-antagonist muscle bundles spanning the joint. In order to imitate the human behaviour, a robot should have some morphological resemblance with the human body. This motivates the agonist-antagonist actuator design. In such design, actuator can be active compliant, passive compliant or a combination of both. The shift of interest from rigid to compliance is well justified. But before comparing stiff actuators and compliant actuators, a broader definition is necessary. Stiff joint means that once the joint attain its desired position, it maintains this position (within its physical limit) even if disturbed with any external force/torque. At the opposite, a compliant joint is an actuator which allows deviations from its equilibrium position when external forces/torques are applied. Each of them has its own advantage and disadvantage. For example, rigid robots have good precision and therefore are suitable in deterministic environment. But robots are conceived to be used not only inside laboratories but in out-door environment where safety is paramount. Therefore, many desirable

properties of a rigid actuator like stability, repeatability, high payload, force and torque capability and high bandwidth control are sacrificed in a compliant actuator. But inducing the compliance in the actuators have significant advantages which are very crucial for robotics applications in an unstructured unknown environment.

- lower reflected inertia (Due to elastic component, link and drive inertia are decoupled) ;
- safer interaction with the environment (due to reduced reflected inertia) ;
- reduced impact on collision (peak forces during the collision are filtered out by the elasticity in robotic joint) ;
- stability and accuracy in force control (In many case like Serial Elastic actuators, the force control problem is translated to position control since the output force is proportional to the desired and achieved position difference multiplied by effective stiffness) ;
- energy storage capability (This could be used in application involving energy optimization or performing extreme motions).

Having understood the advantages of compliant actuators and the challenges associated with them, a closer insight of the properties characterizing the human musculoskeletal actuation system will help to design a robot which can imitate the human behaviour more closely. These properties are : antagonism, compliance, non-linearity, and muscle-tendon coupling. The different benefits that these properties can bring are described below :

- Antagonism can provide the possibility of controlling both position and stiffness. This phenomenon is widely common in mammals and therefore enables us to understand bio-inspired actuation better ;
- Compliance increases the overall safety for both the robot and its environment. It acts a passive low pass filter to absorb the impact forces. Due to energy absorbing capacity, it can be exploited to increase energy efficiency of the whole system by transferring kinetic energy to elastic energy of elastic elements, and vice versa ;
- Non-linearities pose a great challenge from control point of view. But with the capability to adjust stiffness, one can optimize a task by making a balance between accuracy and safety ;
- Tendon coupling enables faster motion as it reduces inertia, friction, backlash and static load.

Therefore, in the present thesis, antagonist inherent compliant system is considered to be our primary area of study. In addition to this, after having a wide survey of the different compliant actuators, we have also considered electro-active polymer based actuators. The motivation behind this study is coming from the previous work of our laboratory which is very inquisitive in search of potential soft actuators for the future generation of robots or microbots. In the next subsection, our primary subject of study, which is the actuators based on McKibben muscles is introduced and our contribution in the design, modeling and control is highlighted. We will then present our contribution towards the nonlinear control of an electro-active polymer based actuators.

0.2 Pneumatic actuators

Pneumatic actuators are inherently compliant and have very high power to weight ratio. These factors motivate researchers to use pneumatic actuation for exoskeleton, prosthesis, rehabilitation or even in walking robot and human robot interaction. Our goal in this thesis is to use an arm actuated by McKibben muscles to perform explosive tasks like hammering or kicking balls. Recent works [Kumar 2013] advocates other kind of actuation system which are easier to control but come with a high price tag. Our goal was to demonstrate here that with minimal modification of an existing platform [B.Tondou 2005], it is possible to perform such kind of explosive motions, and not fine manipulation as in [Kumar 2013]. The McKibben artificial muscle is known for its non-linearities and hence pose a great control challenge. These non-linearities are mainly due to hysteresis, saturation and internal friction between fabrics. So far these challenges were dealt with traditional controllers like high gain PID controller, sliding mode controller for position control [Tondou 2009]. These methods usually lead to stiff system dynamics with higher impedances. Recent developments in pneumatic actuation control [Tassa 2013, Kumar 2014] are use Model Predictive Control (MPC). For instance in [Andrikopoulos 2013], the control scheme is based on a switching Piece Wise Affine (PWA) system model approximation. The method is able to capture the high non-linearities of the Pneumatic Artificial Muscle (PAM). In [Tassa 2013] a linear formulation of the actuation system is proposed to simplify the algorithm implementation and makes it real-time.

Our contribution :

- First we propose a new model which provides a good compromise between accuracy and simplicity.
- The second contribution is to show that, on this model an iLQR control scheme can be used to generate with good precision positioning task and explosive movements.

This is achieved with the introduction of an empirical model of pressure generation from the Intensity-Pressure converter (I/P). Each of the seven Degrees of Freedom (DoFs) of the manipulator arm of LAAS-CNRS is actuated by a pair of agonist-antagonist McKibben muscles. The capabilities of the non-linear iLQR control to execute some simple tasks of reaching a point, maximizing the velocity of joint and end effector are demonstrated on this platform.

0.3 Ion-polymer actuators

Ionic polymer based actuators constitute a class of electro-active polymer. They have great potential in future nano or micro robotics applications. They have already found some applications in the medical field. It is primarily due to the fact that these polymer actuators are having a very low operational voltage range. This makes them very suitable to be used in a close environment with humans. When the

voltage is applied, it generates mechanical stress or strain. In this way, the shape and volume change of Electro-Active polymers are due to the mass transport of ions within the polymer and their uneven distribution. The challenge for such actuators is the complicated fabrication process and requirement of liquid environment for the electrode. As recent advancements have overcome this problem and such actuator could be used in open air ([Annabestani 2015, Bennett 2004]). And this makes it possible to see the potential of such actuator in the field of robotics. From the control point of view, the system being very non-linear is not so easy to model and then control.

Our contribution :

- Our first contribution is to have proposed a simpler non-linear model for the ionic polymer actuator.
- Then we have shown that using this proposed model, a simple conventional PID controller could be deployed to control accurately this system.

0.4 Thesis organisation

The thesis is organised in five chapters. The first chapter is presenting a brief survey of different existing compliant actuators. We have covered actuators which are as simple as SEA with just one linear spring up to a complex mechanical arrangement of VSA and AWAS developed by University of PISA and IIT. In order to understand these actuators, they are loosely divided in different groups based on their similar mathematical structure. In all of these groups, a mathematical model is given and it is shown with formulas and functions how these actuators vary their compliance. Later, artificial muscles and their different types and broad classification are presented. Following this, we have given an introduction to the McKibben muscles and the definition of various terminology. This is the base for later chapters in the thesis. Since our work evolved in two directions; actuators based on the McKibben muscles and Ionic-polymer actuator, a separate chapter is dedicated to our work done on Ionic polymer actuator. In this chapter, we have tried to show its potential for being a soft actuator along with the problems associated with it. More importantly, the chapter reports our effort to characterize the actuator and the control strategy for controlling this system.

The rest of the thesis presents our extensive work we have done on our experimental set-up which is a 7 Dofs anthropomorphic arm.

Chapter 3 describes in detail the static and dynamical model of joints actuated by McKibben muscles. Also the agonist-antagonist model in different configuration, namely symmetric or generic case, is discussed. After proposing the model, different control strategies are discussed in Chapter 4. We have tried to show that a generic single-I controller could be possible to avoid the modelling details. However, for practical purposes, a model based PI controller is used. The optimal control formulation and introduction to the iterative Linear Quadratic Regulator (iLQR)

algorithm is explained. This algorithm is extensively used for generating control sequences for the high performance motion. Chapter 5 reports all the simulations results and various results of the experiments performed on our robot. Many technical details regarding the parameters of the different components of the robotic arm, cad models, electronics, NI modules, data communication and software packages are given in appendix. In the appendix, we also present an analytical proof for stability of the close-loop single-I controller.

0.5 Publications

The work done on this thesis have given rise to the following publications :

- [IEEE MSC-2016] : G. K. Hari Shankar Lal Das, B. Tondu, F. Forget, J. Manhes, O. Stasse and P. Soueres, "*Performing explosive motions using a multi-joint arm actuated by pneumatic muscles with quasi-DDP optimal control*", IEEE Multi conference on System and Control, Buenos Aires, Argentina, September 2016.
- [IROS-2016] : G. K. Hari Shankar Lal Das, B. Tondu, F. Forget, J. Manhes, O. Stasse and P. Soueres, "*Controlling a multi-joint arm actuated by pneumatic muscles with quasi-DDP optimal control*", IEEE/RSJ International Conference on Intelligent Robots and Systems (IROS 2016), Daejeon, South Korea, October 2016.
- [CIMTEK-2016] : B. Tondu, A. Simaite, G. K. Hari Shankar Lal Das, P. Soueres, C. Bergaud, "*Efficient Linear Approach for the Closed-Loop Control of a Ionic Polymer Bending Actuator*", 5th International Conference Smart and Multifunctional Materials, Structures and Systems, Perugia, Italy, June 2016

State of the art

Sommaire

1.1 Compliance actuators	8
1.1.1 Compliance definition	8
1.1.2 Compliance in Human arm	9
1.2 Review of Variable Stiffness Actuators (VSA's)	10
1.2.1 Fixed compliance actuators	11
1.2.2 Variable compliance	12
1.3 Artificial muscles	23
1.3.1 Review of Artificial Muscles	23
1.3.2 Pneumatic Artificial Muscles	27

Traditionally, robots installed in the manufacturing plants and assembly lines are working in isolated confinements. The vision of robotic co-worker is still a long way to go. In fact, most today's robots are made very rigid at the joints to have good position accuracy and easier control with traditional PI controllers. But this comes at the cost of safety to human and that limits the possibility of human-robot physical interactions. As the field of robotics is evolving rapidly, the need of robots working in human friendly environment has become a necessity. It is then thought that compliance in the robots is in fact a desirable property. It cannot only minimise the damage to the human in case of collision but also saves the gears and motors of the robots. To address this question, there have been several attempts to make the robots more and more friendly to human interaction. Software controlled compliance is one of the attractive solutions used nowadays. In this way, software depends on the sensors which detects the interaction or collision and a close loop action ensures that the robot responds smoothly and softly to minimize the impact. However, the time delay due to sensing and feedback control loop could be fatal in some scenarios of sudden collision. Also the possibility of failure of circuitry or sensors makes the software controlled compliance vulnerable in many situations and limit robotic applications in high speed tasks. Therefore, it is interesting to consider inherent compliance within the structure of the robot or at the joints level. Compliance within the structure and flexibility in the links of the robot cause several complex non-linearities. Modelling these kind of robots is known to be difficult and hard to control. In this chapter we present a survey which provides a state of the art of the different actuators which can induce compliance in the robots at joint level. The ability of the stiff actuation units to interact with their surroundings

can be increased by means of active control approaches, however the existence of delays at all stages of the software system make these conventionally stiff actuated systems incapable of managing high-speed contact transients because of their limited bandwidth. This poses a requirement of inherent compliance at actuator level. A special attention has been paid to pneumatic system based actuators and two different kinds of pneumatic systems (Pleated pneumatic artificial muscles and the McKibben muscles) are explained in more details. Before that, we would like to introduce the basic definition of compliance/stiffness and some terminology that will be used throughout in the thesis.

1.1 Compliance actuators

Nowadays robots are expected to work closely with humans. Since human safety is of high priority, robots have to be compliant during interaction. Therefore, compliance in robotic is now considered as one of the desirable properties. This requirement motivates the design of a new kind of compliant actuators called Variable stiffness actuators (VSAs). In parallel, there have been several studies to learn how vertebrates control their motion perfectly while maintaining a good compliance. The design of artificial muscle is motivated by such studies. Artificial muscles are expected to have some properties found analogous to biological skeletal muscle. This section starts with a final definition of compliance in the scope of robotics and a rapid description of the functionality of skeletal muscles in humans.

1.1.1 Compliance definition

Here a brief definition of some important terms are given which will be used in the paper extensively. Stiffness is the differential of force/torque with respect to position. Compliance and stiffness are inverse to each other. Damping is the differential of force/torque with respect to velocity. Impedance and admittance are complementary terms to each other and define a mechanical interaction between two bodies using their intrinsic properties. Admittance describes the dynamical relation of force with respect to displacement [Hogan 1985]. Let us elaborate this with the help of a simple example of a single link with flexible element as illustrated in figure 1.1. [F. 2011] has defined two stiffness terms. One is called internal or passive stiffness which is due to flexible elements and another stiffness term is called external stiffness which is observed at the output link level. However, in literature slightly different definitions are also available [Grioli 2011, Ozawa 2002].

$$\sigma_{internal} = \frac{\partial \tau_e}{\partial \phi} \quad (1.1)$$

$$\sigma_{external} = \frac{\partial \tau_{ext}}{\partial q} \quad (1.2)$$

Where, θ, q are motor position and link position respectively and $\phi = q - \theta$ is the deformation. τ is the motor torque, τ_{ext} is the net torque applied on the link. τ_e is

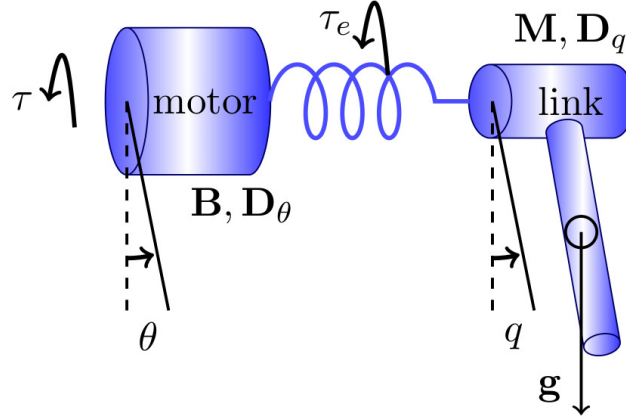


FIGURE 1.1 – A single link with flexible transmission

the flexibility torque generated due to the twisting of the flexible element.

1.1.2 Compliance in Human arm

Human joints are far more complicated due to the complex arrangement of several muscles, tendons and their insertion into the bones. However, the simplest equivalent model is the revolute joint. The force, μ , generated by any muscle is translated into torque on the joint by its moment arm [Burdet 2013]. $\tau = \rho\mu$; Where ρ is the moment arm defined as the perpendicular distance between the axis of rotation of the joint and the line of action of the muscle-tendon spanning the joint. This is explained in figure 1.2. The co-contraction of muscles changes the line of

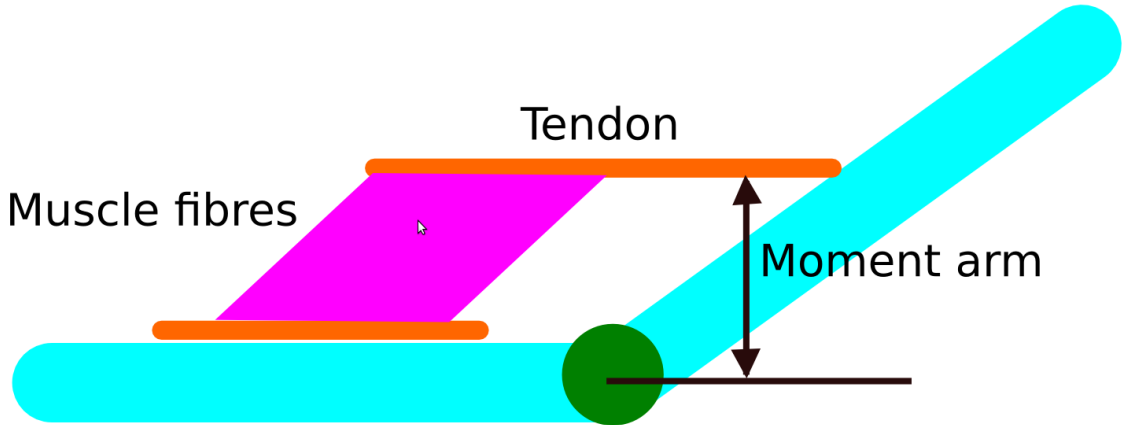


FIGURE 1.2 – Human muscle-tendon spanning a joint.

action of the muscle-tendon on the bones, thus changing the moment arm and in turn varies the torque. So the moment arm is related to muscle length (λ) and joint angle (q) in this manner $\rho = \frac{\partial \lambda}{\partial q}$. Hence, Joint stiffness and damping can be

described by the following equations.

$$K = \frac{\partial \tau}{\partial q} = \rho \frac{\partial \mu}{\partial q} = \rho^2 \frac{\partial \mu}{\partial \lambda} = \rho^2 K_\mu \quad (1.3)$$

$$D = \frac{\partial \tau}{\partial \dot{q}} = \rho \frac{\partial \mu}{\partial \dot{q}} = \rho^2 \frac{\partial \mu}{\partial \dot{\lambda}} = \rho^2 D_\mu \quad (1.4)$$

The dependency of joint stiffness and damping on moment arm and intrinsic muscle properties like muscle stiffness (K_μ) and muscle damping (D_μ) is quite evident. A pair of muscles spans the joint and acts antagonistically to move the arm. So the net torque on the joint is defined by the difference of agonist and antagonist muscle action.

$$\tau = \tau_+ - \tau_- = \rho_+ \mu_+ - \rho_- \mu_- \quad (1.5)$$

For any particular joint, τ depends on muscle force μ which in turn depends on neural activation history, muscle length and its connection to the bones. It has been established by [Milner] that a wide range of μ can satisfy the above equation due to the fact that numerous muscles are spanning a particular joint. So it is possible to find the set of μ which can just change the stiffness by modulating the moment arm by co-contraction while keeping the torque constant.

1.2 Review of Variable Stiffness Actuators (VSA's)

In order to allow safe interactions with humans, several designs have been proposed for actuators. Most of them are VSA which modulate the stiffness, some are variable damping actuators to resist to the velocity deflection and some are the combinations of both. In this section a short survey of VSAs are presented. A broad classification of these actuators has been presented in [van Ham 2009] where the four main classes have been defined on the basis of the method of stiffness control.

Equilibrium controlled : The compliance element with fixed intrinsic stiffness is placed in series with conventional motors. The stiffness is varied by moving the equilibrium position of the spring. One common example is SEA[Pratt 1995].

Antagonistic controlled : Two actuators with nonlinear force-displacement relationship are coupled antagonistically to act against each other. Using both motors simultaneously equilibrium position and stiffness can be controlled. Examples are VSA-I[Tonietti 2005], VSA-II[Schiavi 2008], VSA-HD[Catalano 2010b], PDAU[Kim 2010a], AMASC[Hurst 2004], PPAM[Verrelst 2005] and QA-Joint[Catalano 2010a].

Structure controlled : The compliance is varied by controlling the structural property of flexible element like material modulus, moment of inertia or effective length. Examples are Jack spring[Hollander 2005] and MIA[Morita 1995].

Mechanically controlled : The actuators have usually one main compliant element. The stiffness is changed by mechanically adjusting the pretension or preloading of the compliant part. Examples are MACCEPA[van Ham 2007], VS-Joint[Wolf 2008], AWAS-I[Jafari 2010], AWAS-II[Jafari 2011], CompAct-

VSA[Tsagarakis 2011], vsaUT[Groothuis 2013], SDAU[Kim 2010a] and HDAU [Kim 2010b].

1.2.1 Fixed compliance actuators

Fixed compliance actuators can be considered as one of the first attempts towards the development of compliant actuation systems. These actuators contain a passive compliant element with fixed stiffness which is usually placed between the rigid actuators and the load. These kinds of fixed compliance actuators can be implemented in antagonistic or series configuration. Here, the series configuration is discussed as it is the most common implementation. A conceptual schematic of such implementation is shown in Fig. 1.1.

The link is actuated by motor-gearbox but these two components are separated by a fixed stiffness compliant element. Such an implementation has two control variables θ and q . θ is the angle of the input pulley of the compliant element and the output angle is q which is also the angular position of the link. One of such set-up introduced in [Pratt 1995] used a DC motor coupled to a planetary gearbox and a fixed stiffness torsion spring. Some of the great advantages with SEA are their low impedance due to series compliance and low friction. These properties make SEA achieve high fidelity force control and hence make them a suitable actuators for robotic applications in unstructured environment. So far, most force/torque controlled robots rely on load cells/torque sensors [Hirzinger 2001]. These are not only expensive and sophisticated but may induce chatter in force control due to their high stiffness. On the other hand, compliant element used in SEAs (usually springs) are inexpensive, robust and stable. The following relationship describes the force delivered by a linear SEA actuator and the measurement of the compression of the compliant element :

$$F = kx, \quad (1.6)$$

where F is the force applied by the actuator, k and x are the stiffness and compression of the linear compliant element respectively. In the case of rotary implementations typically using torsional spring, the above relationship can be described as :

$$T_{rotation} = k_t S, \quad (1.7)$$

where $T_{rotation}$ is the torque delivered by the actuator while k_t and S are the stiffness and compression of the rotary compliant element, respectively. Fig. 1.3 shows the implementation of force control using SEAs. The compliant element deflection state can be used in the precise estimation of the torque or force in SEAs.

The force F_{load} is estimated from the deflection of the spring element and is compared with the reference $F_{desired}$ in order to return an error F_{error} . Thus the appropriate control signal for the electric motors are generated by F_{error} together with the measured position x_{load} and the reference. Fixed compliance actuators have been used also in rehabilitation robotics where a prosthetic ankle device has been actuated using SEA [Au 2008]. Those applications have shown significant per-

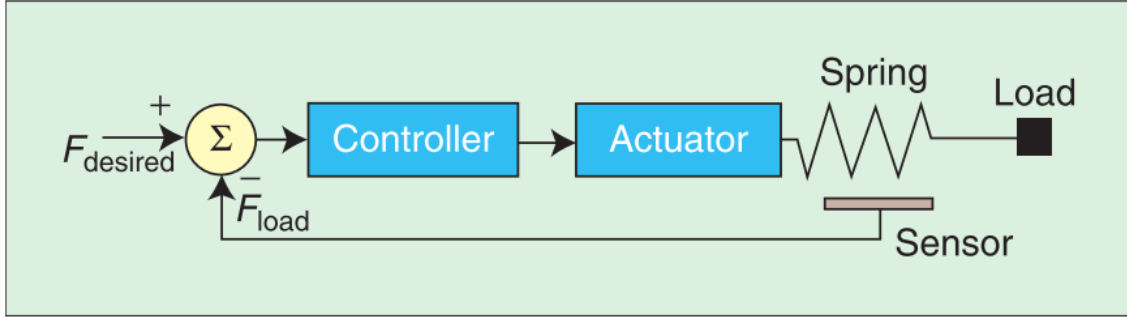


FIGURE 1.3 – Force control in SEA actuator. Figure adopted from [van Ham 2009]

formance improvements brought by SEAs. Actuators have the capability to absorb the shocks which can ultimately improved safety in human-robot interaction and protect the motor-gearbox group from shock loads generated during the foot strike. Moreover, the use of SEAs increases the torque control bandwidth which allows the prosthesis controller to imitate the torque-velocity behaviour of the human ankle in walking. SEAs were a good start for a safe human-robot interaction but the stiffness level in them is usually a fixed preset value. It is then thought to have the ability to vary the stiffness level depending on the nature of the task or the interactions with the environment. This motivates for the alternative designs of variable compliance actuators.

1.2.2 Variable compliance

Variable compliance actuators are actuators which are capable of regulating their physical compliance. Compliance and stiffness are inversely proportional and hence used interchangeably and therefore such actuators are more commonly known as Variable Stiffness Actuators or VSAs. Unlike fixed compliance actuators, they can control both stiffness and position simultaneously. Most importantly they enjoy wider range of stiffness and have energy storage capability. These actuators could make the robot more closer to the mammals with respect to the movement. It is well known that muscles and tendons in the mammals change their stiffness as a function of the motion they have to perform. For example, muscles at arm acquire a stiff configuration when the arm has to perform an accurate task, while they are compliant when they are performing the loading phase of a throw. Similarly, while jumping one can observe that leg muscles are compliant during the loading phase of the jump or during the landing phase where they absorb the shock [Cheung 2004], while during the pushing phase, they are stiff. The underline principle behind the variation in stiffness is the exploitation of the elastic energy stored within the muscles and tendons [Ishikawa 2005]. In [Hirzinger 2008], the authors had compared a rigid joint and a compliant joint. Different tasks were performed in

both cases and it was observed that there is a clear difference between the velocities of the links and the throw distances obtained in the two cases. Thus, it is concluded that joints with variable compliance actuators can achieve performance that is not possible with a conventional stiff robotic system. This motivates researchers to introduce different designs to incorporate variable compliance into the actuation systems. In the following section, various such designs are presented. The physical set-up, conceptual working principle along with their mathematical models are described. Broadly, variable compliance actuators can be categorized into two main groups : Series configuration and antagonist configuration. The division is based on the physical realization of the compliance element with respect to the motor and the load.

1.2.2.1 The series configuration

In this configuration, a variable compliance element is placed in series between the actuator and the load. Two different actuators are employed to set the equilibrium position of the joint and the stiffness independently. In both actuators one big motor changes the position and a small motor tunes the stiffness.

Adjusting the stiffness in both actuators is done through a lever mechanism (Fig. 1.5 and Fig. 1.7). A lever has three principal points; the pivot : the point around which the lever can rotate, the spring point : the point at which springs are located and the force point : the point at which the force is applying to the lever. The variation in stiffness is achieved by varying and controlling these principal points. For example, stiffness variation in AWAS ([Jafari 2010]) is carried out by moving the spring point while the pivot point is controlled to achieve stiffness variation in AWAS-II ([Jafari 2011]).

Before going into any particular design of serial VSAs, basic functioning and a simple but generic model of such actuator is presented. Fig. 1.4 shows a schematic model of a serial VSA. It consists of a principal motor and a secondary motor. While the principal motor is used to command the link motion through the flexible transmission, the secondary motor is used to modify the stiffness of the transmission.

$$M\ddot{q} + \tau_e(\theta_e, \phi) + g(q) = \tau_{ext} \quad (1.8)$$

$$B\ddot{\theta} + D_\theta\dot{\theta} - \tau_e(\theta_e) = \tau \quad (1.9)$$

$$B_e\ddot{\theta}_e + D_\theta\dot{\theta}_e + \psi_e(\theta_e, \phi) = \tau_e \quad (1.10)$$

In the above Eq. 1.8, the first line is the general robotic equation for the link side. Principle motor side dynamics is expressed in second line while the third line represents the secondary motor side dynamics. M , B and B_e are mass inertial matrix while D_θ is the viscous term. τ_{ext} , τ , τ_e and ψ_e are the external torques on the link side, torque on the primary motor side, restoration torque due to deformation and the reaction torque on the secondary motor. The device stiffness is given by the

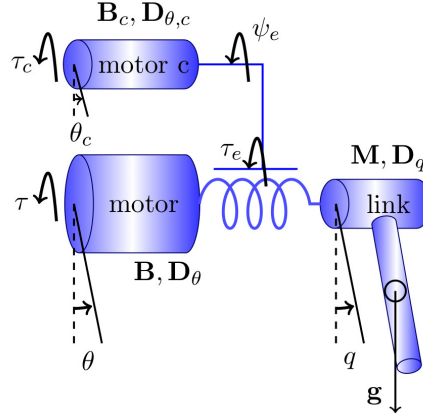


FIGURE 1.4 – Working principle of Serial VSA.

equation shown below

$$\sigma(\theta_e, \phi) = \frac{\partial \tau_e(\theta_e, \phi)}{\partial \phi} \quad (1.11)$$

Some examples of variable stiffness actuators implemented with the series approach are presented next.

Actuators with Adjustable Stiffness (AwAS) In AwAS ([Jafari 2011]), the force and pivot point are kept fixed and the spring point is changing in order to regulate the stiffness. The schematic and cad model are shown in figures : 1.5 and 1.6. The stiffness in this case can be defined as :

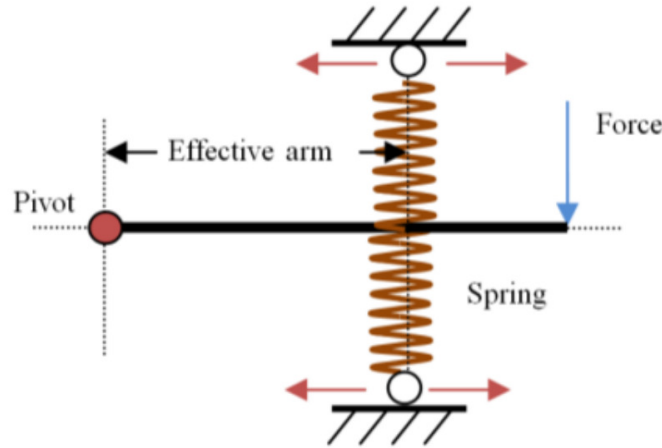


FIGURE 1.5 – Basic principle of AWAS-I actuator.

$$K = 2K_s r^2 (2 \cos^2 \phi - 1), \quad (1.12)$$

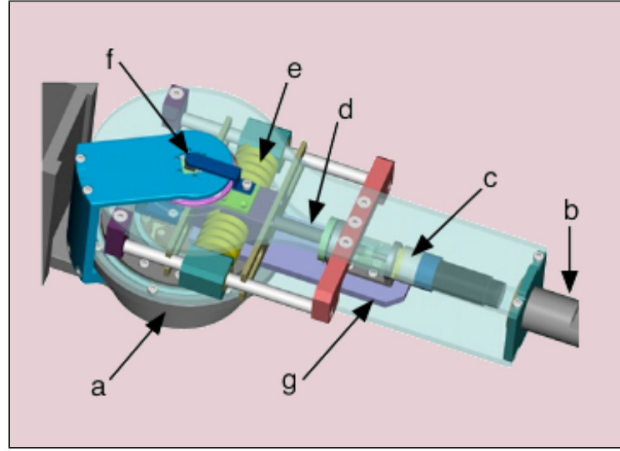


FIGURE 1.6 – CAD model of AWAS-I actuator. Figure adopted from [Flacco 2011]

where K_s , r and ϕ represent stiffness of the springs, the distance between the spring point and the pivot and the angular deflection, respectively. The range of stiffness depends on the stiffness of the springs and length of the lever. In this design, stiffness can be achieved in a good range since it depends on the square of the arm r .

Actuators with Adjustable Stiffness-II (AwAS-II) In AwAS-II ([Jafari 2011]), force and spring points are kept fixed but instead the pivot point is changing. The modification is done to make the system more energy efficient while enjoying larger stiffness range. It was made possible due to the fact that the displacement needed to change the stiffness by moving the pivot is perpendicular to the force generated by the springs. Therefore the stiffness motor does not need to directly work against spring's forces. The schematic and cad model are shown in figures below : 1.7 and 1.8. The stiffness in this case can be

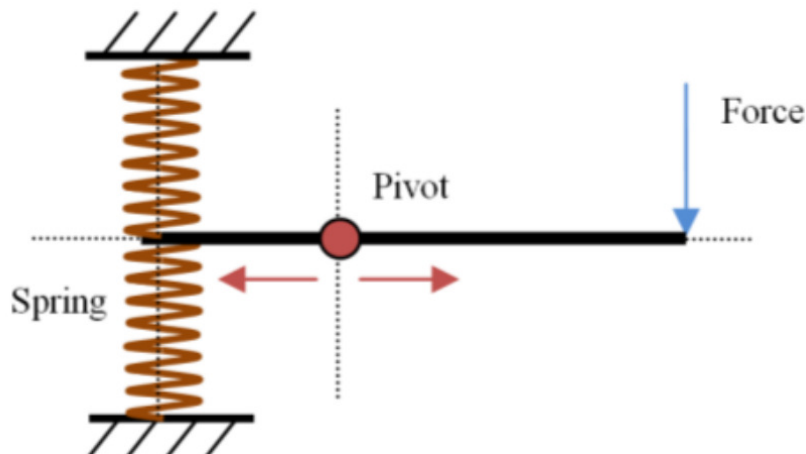


FIGURE 1.7 – Basic principle of AWAS-II actuator.

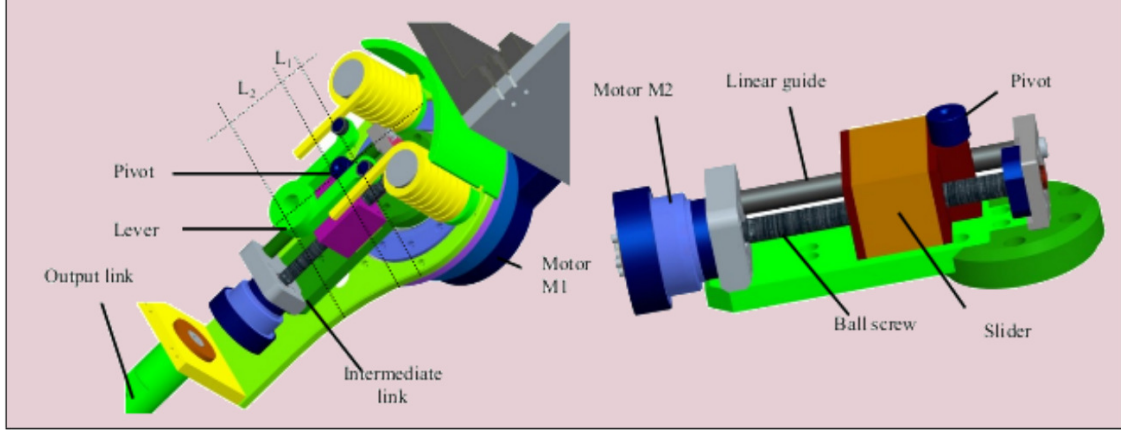


FIGURE 1.8 – CAD model of AWAS-II actuator. Figure adopted from [Flacco 2011]

defined as :

$$K = 2K_s\alpha^2(L_1 + L_2)^2\cos\phi, \quad (1.13)$$

where L_1 represents the distance between the pivot and the springs and L_2 is the distance between the pivot and the force. α is the ratio (adjustable) which is $\frac{L_1}{L_2}$. Using this mechanism the stiffness can be achieved in the largest possible range from zero to infinite since it depends on the ratio. The ratio becomes zero when the pivot reaches the spring point and it becomes infinitive when the pivot reaches the force point. This range does not depend on the stiffness of the springs and lever's length. Therefore shorter lever and softer springs can be used in this mechanism which leads to have a lighter and more compact set-up compared to the mechanism applied to AwAS.

The Jack Spring actuator A linear series-type variable stiffness actuator is the Jack Spring, [Hollander 2005]. In this solution, stiffness is varied by changing the number of active coils of the series spring. The adjustment of the stiffness is done by rotating the spring about the coil axis. This rotation is transformed into a linear motion of the spring along its axis due to the geometry of the shaft on which the spring is mounted. In fact, this shaft is machined with the same coil geometry of the spring and the inside/outside motion of the spring is achieved by screwing/unscrewing the spring on its shaft. This motion changes the effective stiffness of the actuator by varying the active spring coils. Also refer Fig. 1.9. The following formula describes a coil spring stiffness :

$$K = \frac{Gd^4}{8D^3n_a} \quad (1.14)$$

G is the material shear modulus, d is the wire diameter, D is the coil diameter, and finally n_a is the number of active coils. The Jack Spring actuator principle works on this last parameter to vary the stiffness of the overall actuator. In this concept,

one motor is used to adjust the equilibrium position of the actuator and a second motor is used to adjust the stiffness.

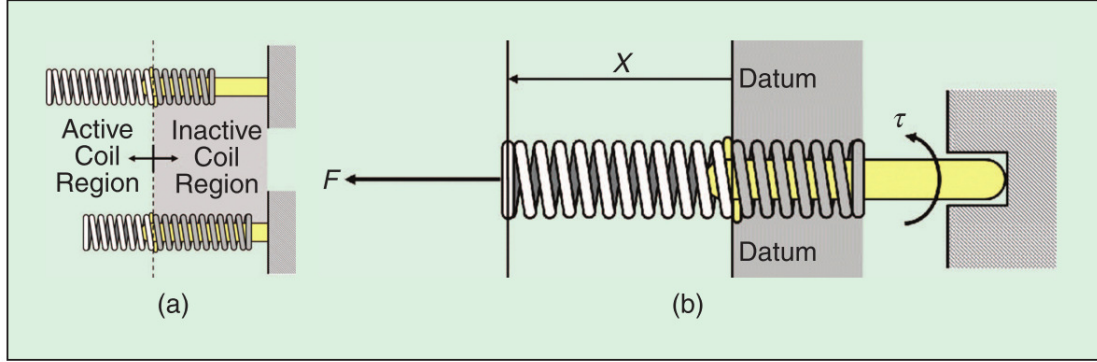


FIGURE 1.9 – Active and inactive coil region in the Jack Spring Actuator. Figure adopted from [van Ham 2009]

MACCEPA MACCEPA actuator developed by Van Ham et al ([van Ham 2007]), uses two independent actuators, M and m are used to set the equilibrium position and the apparent stiffness of the joint, respectively. Fig. 1.10 presents a kinematics scheme of the MACCEPA mechanism, showing three different bodies pivoting around a central axis a . The part of length B can rotate about the axis a and has a linear tension spring attached to one extremity. The other end of the spring is attached to a point b which is fixed on the body shown on the right by means of a cable. When the angle between the lever arm and the right body, α , is different from zero the force generated by the elongated spring generates a torque between the left and the right bodies which tends to align the body shown on the right with the lever arm of length B . When the angle α is null, the lever arm is aligned with the spring and no torque will be generated. The smaller motor m is used to pretension the tension spring at point b by pulling the cable connected to the spring. The length of the tensioned spring when the angle α is null is defined as P . The relationship between the compression angle α and the torque T can be expressed as :

$$T = kBC \sin(\alpha) \left(1 + \frac{P - L}{\sqrt{B^2 + C^2 - 2BC \cos(\alpha)}} \right) \quad (1.15)$$

where k is the spring stiffness and L is the natural length of the spring. The relationship between the compression angle and the delivered torque depends on the spring pre-load $P - L$ meaning that the overall joint stiffness can be regulated acting on the pre-load of the spring using the motor m . The angle ψ imposed by the main actuator sets the equilibrium position of the joint.

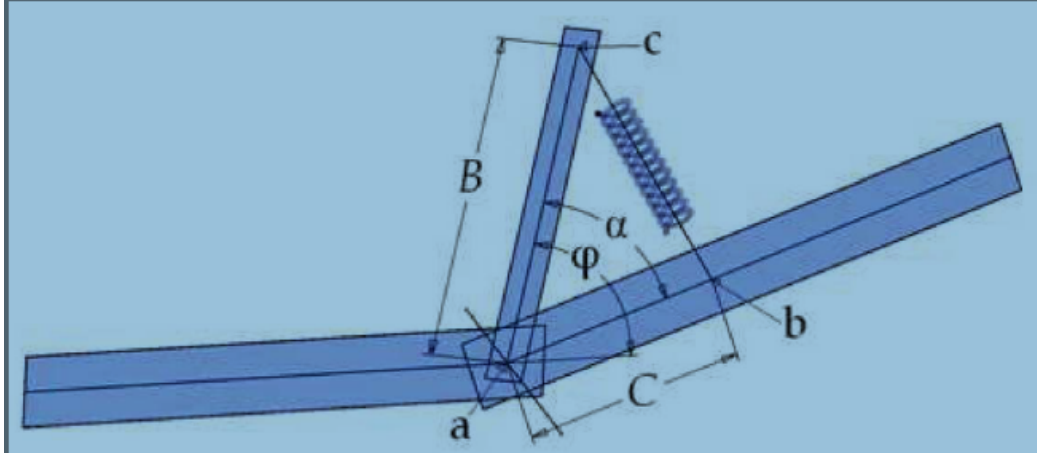


FIGURE 1.10 – Working principle of the MACCEPA. Figure adopted from [van Ham 2009]

1.2.2.2 The antagonistic configuration

Amongst all the configurations of VSAs, agonist-antagonistic actuators are closest to the mammalian anatomy. A mammalian joint is usually actuated by two muscles arranged in an agonistic-antagonistic manner. The muscles and tendon work in cooperation to have a controllable and variable compliance while driving the arm or leg. Based on the same concept, antagonist actuators have two compliant elements to power the joint. It is interesting to note that this type of antagonistic controller compliance can be achieved using both conventional electric motors and other more biologically inspired actuators such as Pneumatic Artificial Muscles (PAM). While an electrical design relies on incorporating the external compliance element (typically spring) into the system and on the other hand, compliance is an inherent characteristic of the actuator in the case of PAM. Each of these designs have their own advantages and drawbacks. PAM are mechanically easier to design and fabricate but pose a great challenge to control. Whereas electric motors driven VSAs are too bulky and cumbersome. In the following subsection, electrically driven antagonistic VSAs are considered. The conceptual basic operations and their dynamical behaviour are explained with the help of some most common VSAs like VSA-I and VSA-II.

Fig. 1.11 shows a schematic model of an antagonistic VSA where two motors working in parallel and antagonistically are connected to the link through non-linear transmissions. Non-linearity of deformation/torque characteristics of the transmissions is to be exploited for regulating the stiffness. It is achieved either by the use of nonlinear (e.g., cubic or exponential) springs or by the arrangement of linear springs in a non-linear kinematic mechanism. The two motor-transmission units are modelled with two similar equations of the form 1.16, where each motor-transmission undergoes a deformation $\phi_i = q - \theta_i$, for $i = 1; 2$. The dynamics of an antagonistic VSA is shown below

$$M\ddot{q} + D_q\dot{q} + \tau_{e,t}(\phi) + g(q) = \tau_{ext} \quad (1.16)$$

$$B_i\ddot{\theta}_i + D_{\theta_i}\dot{\theta}_i - \tau_{e,i}(\phi_i) = \tau, \quad i = 1, 2. \quad (1.17)$$

And the total flexibility torque transmitted to the driven link and the total device stiffness are given below

$$\tau_{e,t}(\phi) = \tau_{e,t}(\phi_1) + \tau_{e,t}(\phi_2) \quad (1.18)$$

$$\sigma_t(\phi) = \sigma_1(\phi_1) + \sigma_1(\phi_2) \quad (1.19)$$

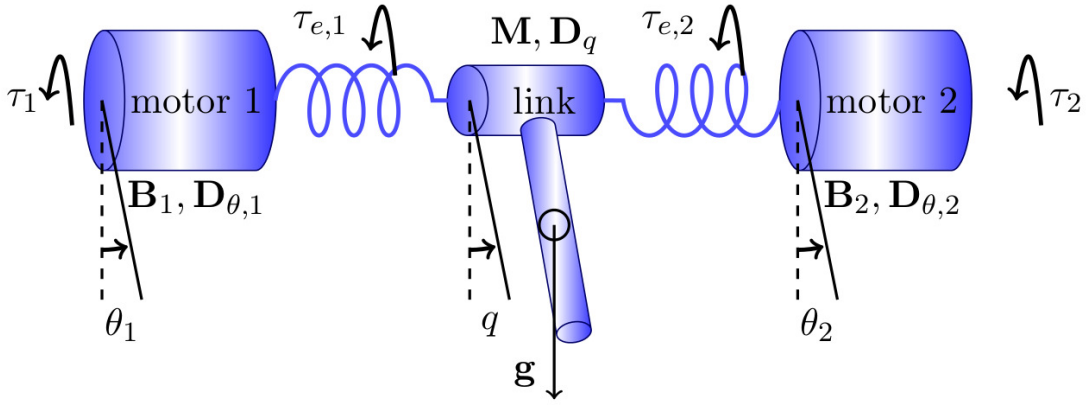


FIGURE 1.11 – Schematic model of a Variable Stiffness Actuator (VSA) in antagonistic arrangement.

There are several actuators which were designed based on the model described in 1.16. Migliore's Actuator was one of the pioneer design in this direction. In order to make the actuator more compact and energy efficient, there had been a constant ongoing effort to innovate new design which resulted into VSA-I, VSA-HD, VSA-II, vsaUT [Groothuis 2013] and compactVSA [Tsagarakis 2011]. As appeared in many literature, We present the design construction and mathematical model of few such actuators which set a new paradigm in the field of electric driven actuators.

Migliore's Actuator Migliore's Actuator proposed in [Migliore 2005] uses two conventional electrical drives connected in an antagonistic manner to the output joint through non-linear springs. A positive angle α of the agonist servo motor provides positive rotation of the angle θ of the output drive, while the antagonist actuator sets an angle β in opposition to the output joint angle, Fig. 1.12. Using linear springs in this configuration, the output joint stiffness will be :

$$S_{linear} = R_J^2(k_1 + k_2), \quad (1.20)$$

where R_J is the radius of the output pulley, k_1 and k_2 are the stiffness of the springs of the agonist and antagonist servos. The output joint stiffness depends only on the constructive parameters of the joint and on the springs stiffness which is constant. The variation of stiffness of the spring components can be set to be linearly related with the co-contraction by using elastic elements with quadratic force-elongation relationship as follows :

$$F(x) = a(x - x_0)^2 + b(x - x_0) + c, \quad (1.21)$$

where F is the force applied by the motors, x is the elongation of the spring component, x_0 is the natural length of the spring and a, b and c are constants. Using such spring components, the stiffness of the output joint, S will be :

$$S = 2\alpha R_S R_J^2 (\alpha + \beta) + 2b R_J^2, \quad (1.22)$$

where R_S is the radius of the driving pulleys. In this case stiffness can be varied by means of the co-contraction of the drives (given by the sum of α and β), with constant offset $2b R_J^2$. On the other hand, the displacement of output joint is achieved by means of the agonistic motion of the motors. Schematic shown in Fig. 1.13 elaborates the mechanical implementation of the non-linear spring component by means of a quadratic profile of the part named "Frame". The assembly shown in Fig. 1.13 replaces the conventional extension springs shown in the antagonistic set-up of Fig. 1.12 therefore permitting the regulation of the joint stiffness.

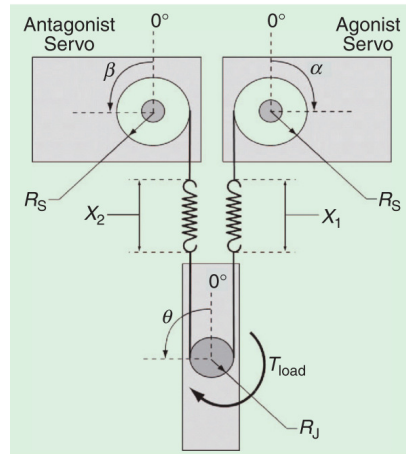


FIGURE 1.12 – Schematic model of a Milgiore's Actuator (VSA). Figure adopted from [van Ham 2009]

Variable Stiffness Actuator (VSA) The VSA is a Variable Stiffness Actuator which enjoys the cross-coupled arrangement unlike Migliore's actuator which is the simple arrangement. The modification is done to make the actuator more compact. The stiffness regulation scheme in this design can be better explained using a CAD

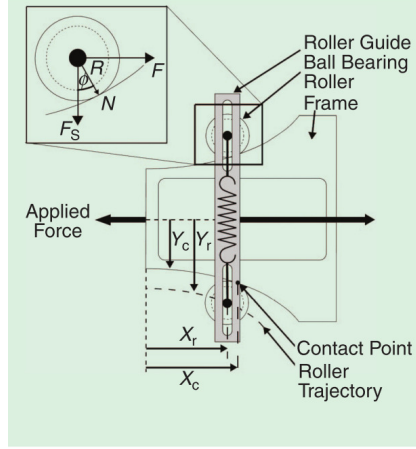


FIGURE 1.13 – Mechanism to implement the stiffness non-linearity. Figure adopted from [van Ham 2009]

model shown in Fig. 1.6. The VSA consists of three pulleys (2, 3, 4) connected by means of a timing belt (1). Pulleys 2 and 3 are actuated by means of position-controlled backdrivable DC motors, while the output pulley (4) is connected to the link. The output joint stiffness can be computed to be :

$$\sigma = 2KR\left(\frac{\bar{h}_{m,1} - h_{m,1}}{h_{m,1}} + \frac{\bar{h}_{2,m} - h_{2,m}}{h_{2,m}}\right) - 2KR\left(\frac{\bar{h}_{m,1}L_{m,1}}{4h_{m,1}^3} + \frac{\bar{h}_{2,m}L_{2,m}}{4h_{2,m}^3}\right) \quad (1.23)$$

where K is the linear spring stiffness, R is the radius of the pulleys 2, 3 and 4, $\bar{h}_{m,1}, h_{m,1}$ and $\bar{h}_{2,m}, h_{2,m}$ are the natural and active lengths of springs 5 and 7. $L_{m,1}$ and $L_{2,m}$ are the lengths of the belt between the pulley pairs 2-4 and 3-4. This means that stiffness can be changed by acting on the active length of the springs and on the belt length. In detail, by means of high/low co-contraction, high/low compression of the springs 2 and 4 (Fig. 1.15) will generate high/low apparent output joint stiffness. Fig. 1.15 further shows the geometric details of any pair of pulleys around a spring.

In practice, the antagonist motion of the drives varies changes the apparent angle between the spring axis and the belt and this creates the non-linear stiffness/compression relationship which permits the stiffness adjustment. Agonist motion of the drives only generate displacements of the output shaft.

Variable Stiffness Actuator - II (VSA-II) The VSA - II, as proposed in [Schiavi 2008], is an antagonistic actuator which uses the bi-directional actuation principle and can be represented in the schematic of Fig. 1.16. The VSA-II shows several improvements with respect to the previous VSA-I. For example, the introduction of a 4-bar mechanism which shows higher load capacity and robustness. This mechanism implements a variable transmission system used to obtain a non-linear relationship between input and output torque/displacements. Using a linear

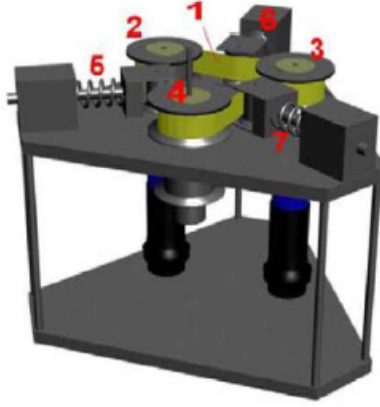


FIGURE 1.14 – CAD view and nomenclature of the VSA [19].

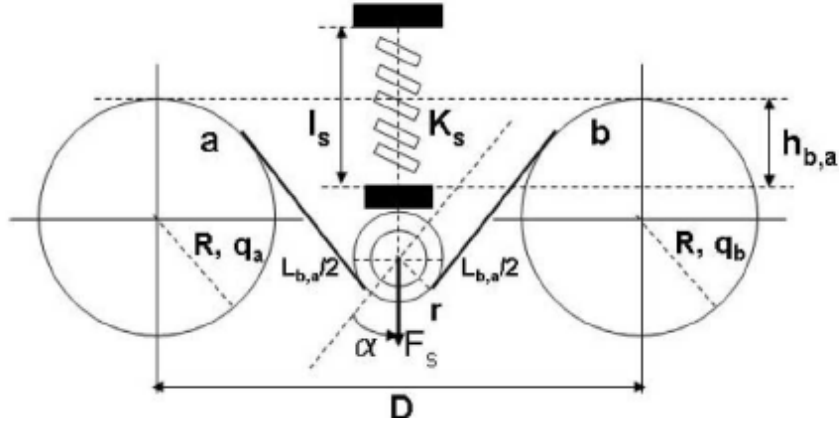


FIGURE 1.15 – CAD view and nomenclature of the VSA.

spring on the input, the relationship between deflection and torque on the output shaft can be made non-linear. Referring to the Fig. 1.17. The link OA is actuated by a motor at O. The torsion spring of stiffness k is linear, however the stiffness at O is nonlinear with angles β and θ and is described by the following relationship,

$$\sigma(\theta) = \frac{1}{4}k \left[\left(\frac{\frac{R}{L} \cos \frac{\theta}{2}}{\sqrt{1 - \left(\frac{R}{L} \sin \frac{\theta}{2}\right)^2}} - 1 \right)^2 + \frac{\frac{R}{L} \left(\frac{R^2}{L} - 1 \right) \beta \sin \frac{\theta}{2}}{\left[1 - \left(\frac{R}{L} \sin \frac{\theta}{2} \right)^2 \right]^{\frac{3}{2}}} \right] \quad (1.24)$$

$$\sigma = (a) \quad (1.25)$$

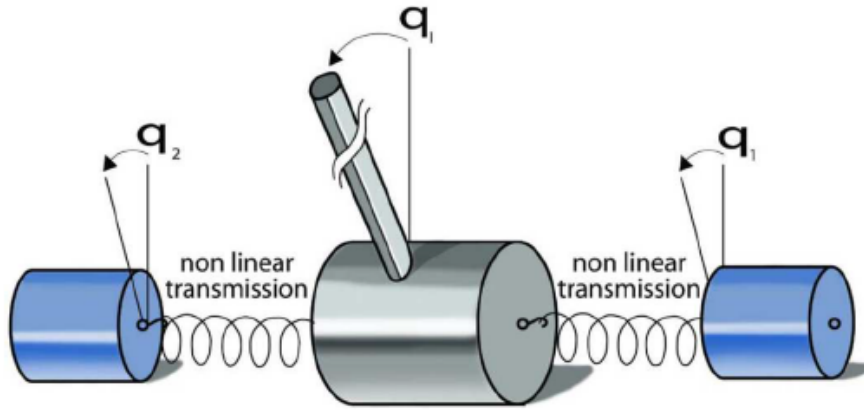


FIGURE 1.16 – Schematic of VSA-II.

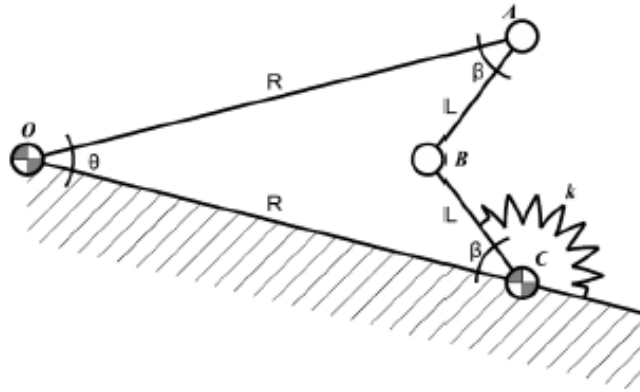


FIGURE 1.17 – The four bar transmission mechanism of the VSA-II, [21].

1.3 Artificial muscles

Traditional actuators are stiff and having high low power density, power-to-mass ratio and efficiency. VSAs are compliant however mechanical complexity, bulkiness and low power to mass ratio make them difficult to be integrated in small multi-joint robots. There is a growing interest in robots working with or in close vicinity of humans. So, it is desirable to make the next generation robots with lightweight materials having inherent compliance and adapted control strategies combined with passive compliant dynamics.

1.3.1 Review of Artificial Muscles

In this section, we are presenting briefly different types of muscle-like actuators or simply called artificial muscles. These actuators, even though they are still in development, have shown a good potential to replace prevalent ac-

tuators. It is possible to extend the applications of robotics in medical devices like invasive surgical or diagnostic instruments [Guimard 2007, Ruiz 2015, Tozzi 2011], prosthetics, rehabilitative exoskeleton, soft robotics (as grippers and manipulators) [Choi 2007] and recreation toys using such actuators due to their fabrication flexibility.

Artificial muscle can generate reversible contraction, expansion, or rotation within the body by the application of an external stimulus. These stimulus could be voltage, current, pressure, temperature etc and are the basis of division of the artificial muscles into different types [Mirvakili 2013]. They can be divided broadly into (1) pneumatic, (2) thermal, (3) electric field and (4) ionic actuators. The comparison of the currently investigated artificial muscles is shown in Fig. 1.1. Even though, the combination of the efficiency (40), strain rate (50/s) and specific power (284 W/kg) of a human skeleton muscle are hard to compete (Fig. 1.18b), artificial muscles are often compared to it.

The current state-of-the-art tendencies and challenges of prevalent artificial muscles are discussed in the following sections.

Pneumatic actuation Pneumatic actuation generates contraction force using elastomer stress. So the linear motion, thus generated, is due to inflating and deflating a rubber tube beneath the structure. This actuation system has been used widely [Daerden 2002, De Volder 2010, Ilievski 2011, Zhang 2011] because it is extremely lightweight and inherently compliant. One of the most common type of Pneumatic actuators are McKibben-type actuators which have been further developed in order to improve their lifetime and control [Meller 2014, Tondur 2012, Zhang 2011] due to their mechanical design of braided sheath structure. However, there is a constant development going on in pneumatic based actuators and new inflatable materials are being suggested such as the pneumatically-driven flexible microactuators (FMAs) [Gorissen 2011, Gorissen 2014] or the embedded pneumatic networks of channels in elastomer (PneuNets) [Ilievski 2011]. These actuators are capable of generating complex motions with the single source of pressure and hence different motions like gripping, bending or crawling can be created simply by changing their configurations and size [Martinez 2014, Morin 2014, Mosadegh 2014, Shepherd 2013]. As the experimental setup considered in this thesis will be using McKibben muscle, we will extensively discuss in the latter sections, the model, geometric and mechanical construction, advantages and challenges of using McKibben muscle based actuators.

Thermal actuation Thermal actuation normally uses a Shape-memory alloy (SMA) materials which can undergo a phase and shape change with temperature or stress. To use SMAs as actuator, they are usually heated by running current through them (reviewed by [Kheirikhah 2011]). Nitinol is one of the most well known lightweight solid-state SMA. However, the major drawback with most of the solid-state materials is that they have limited life cycle and they fail due to the micro-

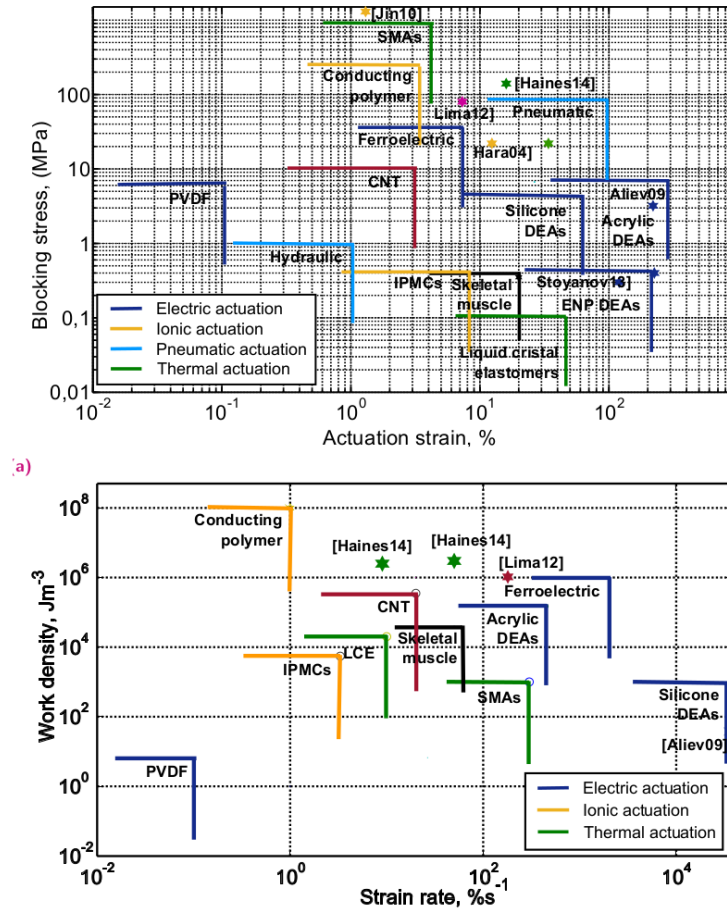


FIGURE 1.18 – (a) Stress versus strain and (b) work density versus strain rate of typical artificial muscles (defined by lines) and some state-of-the-art actuators (stars). Types of actuations : blue - electric, orange - ionic, green - thermal, red - CNTs, gray - others, black - mammal skeletal muscle. Adopted from [249, 269] and other sources mentioned in the text.

structural crack propagation and fracture. Furthermore, cooling of the actuator is significantly slower than heating and causes a response asymmetry. In order to deal with this problem, Shape memory polymers (SMPs) are proposed. They are low cost and are able to produce larger strains of up to 700% [Koerner 2004] (typical strain of SMAs is 0.1%). Furthermore, due to easier processing and synthesis flexibility, SMPs could be tailored to required applications (reviewed by [Behl 2013, Sun 2014]).

Thermal expansion phenomenon has been recently used for actuation purpose by the twisted yarns of metals [Mirvakili 2013], carbon nanotubes (CNTs) [Lima 2012], nylon or polyester [Haines 2014]. When the length of the yarn is kept constant during heating, the yarn untwists and its diameter increases. Alternatively, when the change in the twist is restrained, during the actuation yarn contracts in length and its diameter increases. multiwall carbon nanotubes (MWCNTs) are one of the first actuators of this kind [Zhang 2004]. MWCNTs have very high strength (up to

300 MPa), tensile stroke (upto to about 10%) and the work capacity. However, the complicated and expensive fabrication methods lead to the development of the artificial muscles, based on the twisted metal nanowires [Mirvakili 2013]. Moreover, it was shown that much cheaper materials, such as nylon or polyester can be twisted, coiled and used as torsional muscles [Haines 2014]. These actuators are able to contract by 49% and can be used for millions of cycles. One of the drawback of this nanowire is its electro-thermal energy conversion efficiency that is currently only about 1 to 2%.

Electric field actuation Electric field actuation can be used as actuators when certain materials produce mechanical stress under the influence of the electric field. Piezoelectric ceramics, ferroelectric polymers, i.e. polyvinylidene fluoride (PVDF) are one of such materials. They can generate large strains (5%) due to the field-driven alignment of their polar groups. The main advantages of such polymers are low heat dissipation and fast response (ms). Therefore, actuators based on them can be used for applications such as varifocal microlenses [Choi 2011]. Nevertheless, their actuation requires high voltages (150 MV/m), they are sensitive to defects and difficult to mass produce [Madden 2004a, Mirfakhrai 2007]. Dielectric elastomers (DEAs) based electroactive polymer actuators are the most widely known. They are typically made of a passive elastomer film that is sandwiched in between two compliant electrodes. When a voltage is applied, the electrostatic pressure between the electrodes (Maxwell Stress), arising due to the Coulomb forces, compresses the thickness and expands the area of the elastomer in between. DEAs usually produce large strain 3 (Fig.1.18a). The fabrication of DEAs requires low-cost, lightweight and conformable materials [Brochu 2010], [Kornbluh 2013]. One of the challenges of DEAs based actuator is the need of flexible and stretchable electrodes. Also DEAs require high electric fields (150 MV/m) and, consequently, voltages up to 5 kV, therefore their applications in the fields that require contact with humans is very limited [Madden 2004a, Mirfakhrai 2007].

Ion-based actuation Ion-based actuation relies on the production of mechanical stress or strain of several percent by application of voltage within a very small range (1 – 3V). In this method, the shape and volume change of Electro-Active polymers are due to the mass transport of ions within the polymer and their uneven distribution. It is essential to have a low voltage devices when working in the vicinity of human. For this reason, these Ion-based actuators have already found various applications [Doring 2013] in biotechnology and medicine [Bawa 2009, Cabane 2012]. Several types of ionic EAPs are being investigated for applications as artificial muscles : ionic gels [Maeda 2010], ionic polymer-metal composites (IPMCs) [Jo 2013, Tiwari 2011], conducting polymer actuators (CPAs) [Baughman 1996] and, more recently, carbon nanomaterial based composites [Baughman 1999, Kong 2014]. Ionic gels could potentially match the force and the energy density of a skeletal muscle at low voltages But its weak mechanical pro-

perties need to be improved [Bassil 2014, Imran 2010]. Ionic polymer-metal composites (IPMCs) have potential applications in the underwater robotics (e.g. grippers [Ford 2015], swimming devices [Chen 2011, Kim 2005, Palmre 2013]) and medicine (e.g. microgrippers [Feng 2014], steerable catheters [Ruiz 2015]) due to the low actuation voltage and relatively large bending. But one of their drawbacks is that the actuation is followed by a slow relaxation due to the water diffusion. Moreover, IPMCs are sensitive to dehydration, hydrolysis above 1.23 V and tend to drift in the position or get permanently deformed. Carbon nanotubes, since from the time of its discovery, have found their applications in several fields. These have been recently used as an ionic actuators. When carbon nanotubes (CNTs) and their composites suspended in the electrolytes [Baughman 1999] or ionic liquids (ILs) [Barisci 2004] and the voltage is applied (1–4V), the CNTs surface is charged and electrolytes form an electric double layer around them. The electrostatic repulsion of the charges on the nanotubes causes the elongation of the carbon-carbon bonds, that consequently elongates the nanotube. Due to their stiffness, networks of entangled nanotubes or yarns are needed to cause macroscopic deformations and even then, a very small strain ($< 1\%$) are achievable [Baughman 1999]. Also these CNTs actuators can have good strain rate, high elastic modulus and huge work densities. After the discovery of the Bucky gel, which is a single walled carbon nanotube and ionic liquid gel-like composite, it is considered for ionic actuators. It is due to the possibility of facile fabrication and the fast response time of the actuators. However, so far, the mass production of CNTs and Bucky gel are quite expensive and difficult and so their applications in the design of actuators are limited. [Li 2008, Tunckol 2012]. There is an ongoing effort to look for cheaper alternatives. Carbon black and carbon fibre mixtures with ILs are being investigated [Terasawa 2014]. Also, there is a growing interest in composite material electrodes that would combine advantages and reduce disadvantages of each type, e.g. carbon - conducting polymer composites [Torop 2014, Surana 2015].

Ionic based polymer actuator has shown the great potential to be a good soft actuator for several robotic applications. Hence, we have considered Ion-based actuation for our study. In the laboratory, an Ionic polymer based bending actuator has been developed and various experiments are conducted to characterize the actuator. We will present our work and contribution in this field in latter chapter (Chapter 2).

1.3.2 Pneumatic Artificial Muscles

Pneumatic Artificial Muscles (PAMs) are contractile and linear motion engines operated by gas pressure. Their core element is a flexible reinforced closed membrane attached at both ends to fittings along which mechanical power is transferred to a load. The membrane is inflated or squeezed when gas is filled in or sucked out of it. It creates a radial expansion or contraction of the membrane which in turn contracts axially and thereby exerts a pulling force on its load. The force and motion thus generated by this type of actuator are linear and unidirectional.

The most common driving force for a PAM's is gas, usually air which is either forced into it or extracted out of it. This way the actuator is powered by the pressure difference of the inside gas with regard to the surroundings. Although, under-pressure operating muscle have been proposed in [Marcincin 1993, Morin 1953], PAMs usually operate at an overpressure. It is easier to generate and supply compressed gas and a lot more energy can be conveyed by over-pressure than by under-pressure.

Various fluid-driven muscle-like actuators have been there now for almost a century. A classification review of PAMs to cover most of the commonly used PAMs in the research have been presented in [Daerden 2002] where these are broadly classified according to their design and operation : (1) pneumatic or hydraulic operation, (2) overpressure or under-pressure operation, (3) braided/netted or embedded membrane and (4) stretching membrane or rearranging membrane. The distinction between PAM designs were done on the basis of structure of the tension carrying element of the muscle and the way membrane inflates. The tension carrying structure can embrace the membrane or can be embedded into the membrane. Also the inflation of membrane can happen in radial direction either by stretching the membrane material or by rearranging the membrane's surface. Hydraulic operation has been used in humanoid set-up and robotics applications. However, due to the flexibility needed for inflation and deformation, material strength poses a limit and consequently the pressure difference across the inflating element needs to be limited. Hydraulic operations have usually bad power to weight ratio, typical in the range of about 500 kPa to 800 kPa. This makes hydraulic based actuators less viable as actuators for soft robotics. Below presented the most frequently used PAMs which is the Braided Muscles. Also a short description of Pleated Pneumatic Artificial Muscle (PPAM) is presented, which is one of the recent improvement to counter the drawbacks of the braided design. In fact, we present two kinds of pneumatic system in more depth in order to understand their characteristics. These are PPAM and Mckibben muscles. The former study is based on the work of Daerden ([Daerden 1999, Daerden 2001, Daerden 2002]) and the latter work is directly inspired from Tondu ([Tondu 1995]) These studies will further help us to propose model for our own Mckibben muscles which are used as an actuator for our experimental set-up.

Pleated Pneumatic Artificial Muscle (PPAM) This actuator was developed by Daerden [Daerden 1999, Daerden 2001] in which inflation of muscles occurs by the rearrangement of the membrane. This means no material strain is involved when it is inflated. The way this is done is shown in Fig. 1.19.

The muscle membrane has a number of pleats in the axial direction. The contractile motion due to expanding of the muscle membrane is carried out by unfolding these pleats. There is almost no friction involved in this process. Furthermore, membrane stresses in the direction perpendicular to the axis are kept negligibly small and decrease with an increasing number of folds. This results into a very low energy

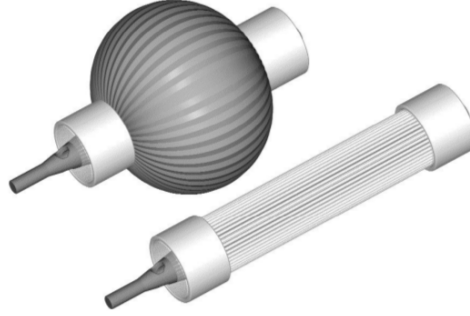


FIGURE 1.19 – Pleated Muscle, fully stretched and inflated [Daerden 2002].

demanding expansion of the membrane. One of the great advantage of this kind of PAM that there is almost no hysteresis because of the absence of the friction. Since the membrane's expansion needs a very small amount of energy, threshold pressure could be restricted to a low value, e.g. less than 10 kPa for the muscle used in the experiment [Daerden 1998].

The characteristics of this type of muscle depend on the ratio of full length to minimum diameter, on the strain behavior of the membrane's material, on the contraction rate and, finally, on the applied pressure. Contraction force can be derived mathematically [Daerden 1999] and expressed as

$$F_t = -pL^2 f_t(\varepsilon, \frac{L}{R}, a), \quad (1.26)$$

in which L represents the muscle's full length, R its minimum radius and a is a dimensionless factor that accounts for the membrane's elasticity. Please refer 1.19. From Eq. (1.26), it can be seen that f_t is a dimensionless function which depends on contraction rate, geometry and material behavior. Fig. 1.20 shows f_t for different values of muscle thickness $\frac{R}{L}$.

It has been shown by the author that the thick muscles contract less than thin ones, but generate higher forces at low contraction rates. Although, infinitely thin muscle has a maximum contraction of about 54%, practically the maximum contraction of the this type of muscle can reach upto 45%. It is because a minimum thickness of the muscles has to be ensured in order to able to assemble the muscle.

A typical Force-contraction characteristic of PPAM type muscles has been identified experimentally in [Daerden 2001]. In the experiment, the muscle used was made of a para-aramid fiber unidirectional fabric made air-tight by a polypropylene liner. The end fittings are made of aluminium. Its total weight is about 60g. The maximum contraction of this muscle was experimentally found to be 41.5%. The pressure was limited to 300kPa and threshold pressure was below 10kPa. In

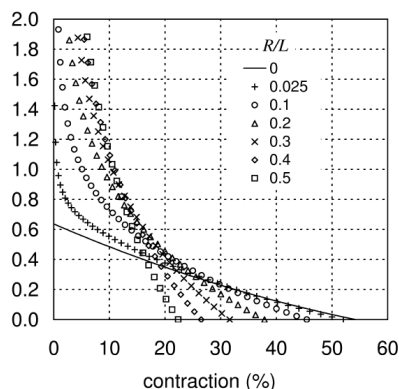


FIGURE 1.20 – Pleated Muscle dimensionless force function [Daerden 2002].

order to keep the muscle safe, the maximum force was limited to 3500N. Fig. 1.21 shows the measured force diagrams for a range of operating pressures of a muscle of $L = 10\text{cm}$ and $R = 1.25\text{cm}$ or ($R/L = 0.125$).

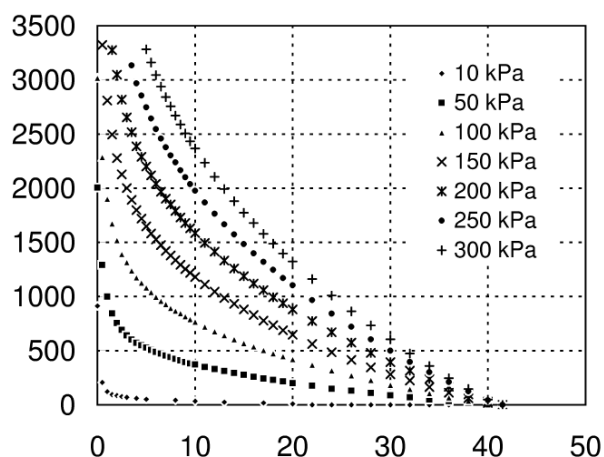


FIGURE 1.21 – Pleated Muscle dimensionless force function [Daerden 2002].

Since the muscles in unidirectional force generator, two muscles are used in antagonistic setup to move a joint [Daerdan 1999, Daerdan 1998]. In comparison to the similar set-up using Mckibben muscles, it is concluded that PPAM based actuator has better position accuracy of about 0.1° for a motion range of 60° . Also it has lower rise time. Besides positioning, compliance control was performed [Daerdan 1998]. Both position and compliance control was achieved just by using classic linear PI-control techniques. This was possible mainly because of the absence of hysteresis. In the case of positioning experiments with the Mckibben muscle [Caldwell 1993, Inoue 1987, D. G. Caldwell 1995, Hesselroth 1994a, Tondu 1995], in spite of using more or less complex control algorithms, e.g. pole placement, feed-

forward, adaptive control, fuzzy control or neural networks, the step response times are in the order of magnitude of 1s and higher and positioning accuracy worse than 1° for similar motion ranges as above. This shows the tremendous impact hysteresis due to friction has on controlling these actuators.

McKibben Muscle McKibben muscles show great similarity with biological muscles. They have very good power to weight ratio. Moreover, they can be used in rigorous environment whether it is dusty, humid or even wet. In contrary to conventional electrical or mechanical actuators which require very clean and dry place. Despite of having hysteresis phenomenon and requirement of threshold pressure, McKibben muscle is the most studied and used as pneumatic artificial muscles. One of the reason is that this kind of muscle is very easy to fabricate, maintain and mass produced. For these reasons, we have considered McKibben muscles for our actuators in our work. The following section is dedicated to present a review of different modelling attempts of the McKibben muscle along with its resemblance to the biological muscle. McKibben muscle is composed of an inner tube surrounded by a double helix braid, characterized by its initial braid angle (α_0) as illustrated in Fig. 1.23.



FIGURE 1.22 – McKibben Muscle

The McKibben muscle behavior depends largely on the dynamics of the inner tube, surrounding braided sleeve and the pressure supply. In literature, several models of McKibben muscles can be found. The most prominent are [Chou 1996, Tondu 2000, Colbrunn 2001]. In [Chou 1996, van Ham 1996a], the pneumatics are taken into account in the modelling while the muscle is subjected to a dynamic load. In [Colbrunn 2001], a complex relation of the valve is included in the model of the muscle. In most cases however, the pressure is considered as an input to the system. As indicated in [Schroder 2003], it is interesting to note that these three models, even though they do not use exactly the same parameters, can be transformed into each other. In this section we will present the most referred model which is the

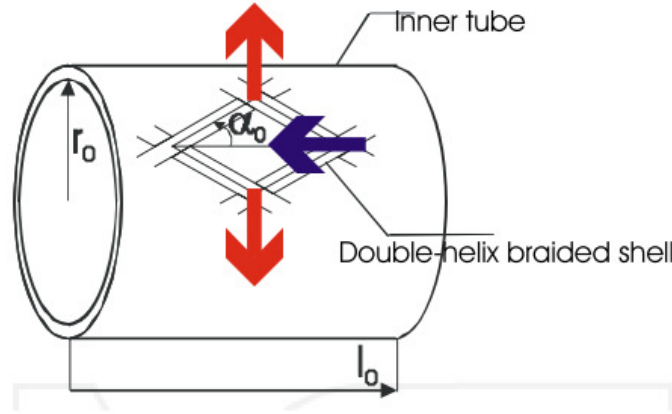


FIGURE 1.23 – operation principle of the McKibben muscle

Chou-Hannaford model [Chou 1996] :

$$F_m = \frac{\pi d_o^2 p_m}{4} \left(\frac{3}{\tan^2 \alpha_o} (1 - \varepsilon^2) - \frac{1}{\sin^2 \alpha_o} \right) \quad (1.27)$$

with the muscle force F_m , the resting diameter d_o , the muscle pressure p_m , the rest braid angle α_o and the elongation ε . The pressure in a McKibben muscle is modelled by Boyle Gay Lussac's law, while the generated force is defined using a force balance. The parameters α_o used in Eq. (1.27) is not a well defined parameter, since it is not constant over the length of the muscle and it is hard to measure. The results of this model are good in the high-pressure range typically above 2 bar and it is suitable to model Rubbertuator like Festo's MAS. However, in this thesis, the model proposed in [Tondou 2000] is taken as the base. This model includes the cylindrical volume error correction and has the close resemblance to biological muscle. It could also be applied in the application of smaller pressure range (1-5 bar). This model is deal in detail in the Chapter 3.

McKibben muscles resemblance with biological muscles has been studied in [Klute 1999] where the experimental based comparison was made between pneumatic and biological muscles. The McKibben muscles are compared to the Hill model, a model describing the behavior of biological muscles in [Tondou 2006]. The Hill model describes the relationship between muscle shortening velocity V and its corresponding tension, F_{Hill} which can be mathematically defined as follows

$$(F_{Hill} + a)V = (F_0 - F_{Hill})b, \quad (1.28)$$

where F_0 is the isometric contraction force at zero contraction ratio in given stimulation conditions. a is a constant having the dimensions of a force and b is a constant having the dimensions of a velocity.

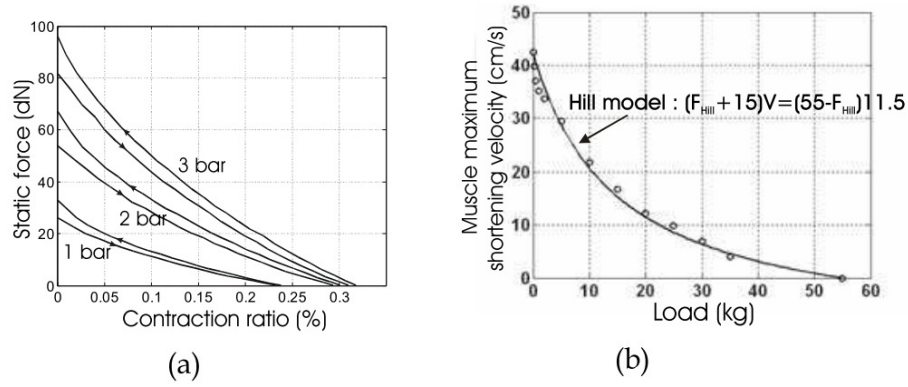


FIGURE 1.24 – Characteristics of a typical pneumatic McKibben muscle (of initial length $l_0 = 335mm$, initial radius $r_0 = 10mm$ and initial braid angle $\alpha_o = 23^\circ$, (a) Tension-Displacement curves at constant pressure 1, 2 and 3 bar, (b) Tension-Velocity curve at constant 2 bar pressure.

Identification and control of Electroactive polymer

Sommaire

2.1 Introduction	35
2.1.1 PDOT :PSS Ionic liquid actuator	36
2.1.2 Characterization of Ionic actuator	36
2.1.3 Control reviews of Electroactive polymer actuators	39
2.2 Non-linear Identification of the Artificial Muscle	41
2.2.1 Non-linear model derivation from the first order linear model	41
2.3 PI-closed loop control	43
2.3.1 Linear tuning and non-linear effects	43
2.3.2 Taking into account voltage constraints	44
2.3.3 Stability of the PI-controller	45
2.3.4 Tracking performances	47

2.1 Introduction

As discussed in the Chapter 1 in "The state of the art" where various types of artificial muscles are presented, conducting polymer actuators (CPAs) are found to have several advantages when compared to other kinds of artificial muscles. They show faster response and require less voltage up to $2V$. Furthermore, they are lightweight and compliant. These advantages make CPAs as one of the best potential choice in biomedical applications. It was shown in Chapter 1 Fig. 1.1a, they can produce large strain and stress and work in electrolytes or biological fluids [Daneshvar 2014, Harlotte 2002]. CPAs can be configured as free-standing or bi-layer and trilayer actuators. In the free-standing CPAs, a single film is submerged in liquid electrolyte polymer and the volumetric expansion can be measured directly [Melling 2002]. Such actuator is characterized by out-of-plane strain. However, bending actuators are usually employed for most of the practical applications as they can take advantage of much higher in-plane strains. The bending motion is achieved by laminating an electromechanically active conducting polymer with an inactive substrate creating bi-layer or tri-layer structures. During volumetric expansion of the polymer, stress gradient is generated at the interface subsequently leading

to bending. Most commonly studied configuration is bilayer structures, but their operation requires a counter electrode which motivates the use of trilayer devices for application purposes. In our laboratory at LAASCNRS, PEDOT :PSS trilayer CPAs are extensively studied and reported in [Simaite 2015a]. Various advantages of PEDOT :PSS trilayers CPAs and the challenges are compared to the most commonly used conducting polymer based actuators. In [Simaite 2015a], the author has reported, in detail, about the structure, fabrication, basic functioning and the characterization of the actuators based on PEDOT :PSS trilayer CPAs. Since scope of my thesis is to study the dynamical model of such actuators and propose a control strategy for such actuators. For the sake of better understanding and completeness, a very brief introduction of the PEDOT :PSS trilayer CPAs are presented.

2.1.1 PDOT :PSS Ionic liquid actuator

poly(3,4-ethylenedioxythiophene) polystyrene sulfonate (PEDOT :PSS) based actuators are trilayer conducting polymer actuators (CPAs). Fig. 5.1 shows the structure of the trilayer actuator. So far, Polypyrrole (PPy) is one of the most used conducting polymer for applications in CPAs. It can produce volumetric swelling of typically 2 – 3% during oxidation. In comparison to others, polypyrrole based actuators produce largest displacements and forces [Gaihre 2013, Temmer 2013] and maximum electrochemical strains of up to 29% [Hara 2004, Hara 2005]. Despite having all these features, electrical conductivity of polypyrrole decreases by 2 - 3 orders of magnitude in the reduced state. This reduces the over all active part of the film which ultimately results into electrochemical creep during actuation [Hara 2011]. Furthermore, PPy films are usually very rigid leading to low ion diffusion speed and slow actuation rates [Otero 2003, Temmer 2013]. Therefore, use of polythiophene derivatives as electrodes is now preferred which motivates the consideration of actuators based on poly(3,4-ethylenedioxythiophene) (PEDOT) and one of its possible counterions - polystyrene sulfonate (PSS). The performance of the actuators based on PEDOT in comparison to PPy are still not so significant. Similar strains and strain rates are expected [Temmer 2013]. However, PEDOT is a well known polymer for its chemical, electrochemical (in doped state) and thermal stability. PEDOT also has high electrical conductivity that could reach up to 2000Scm^{-1} [Mengistie 2014]. Furthermore, it shows faster actuation. It is because of doping with the immobile anions (DBS, PSS, etc.) makes it more soft and porous which lead to a better ion diffusion [Otero 2003, Temmer 2013, Zainudeen 2008]. Therefore, PEDOT could eventually emerge as an advantageous alternative to conventional CPAs electrodes.

2.1.2 Characterization of Ionic actuator

The mechanical work produced by the Ionic actuator is mainly due to the processes involved in the volume changes in conducting polymers during their redox reactions. While polypyrrole (PPy) secondarily doped with immobile anion (DBS)

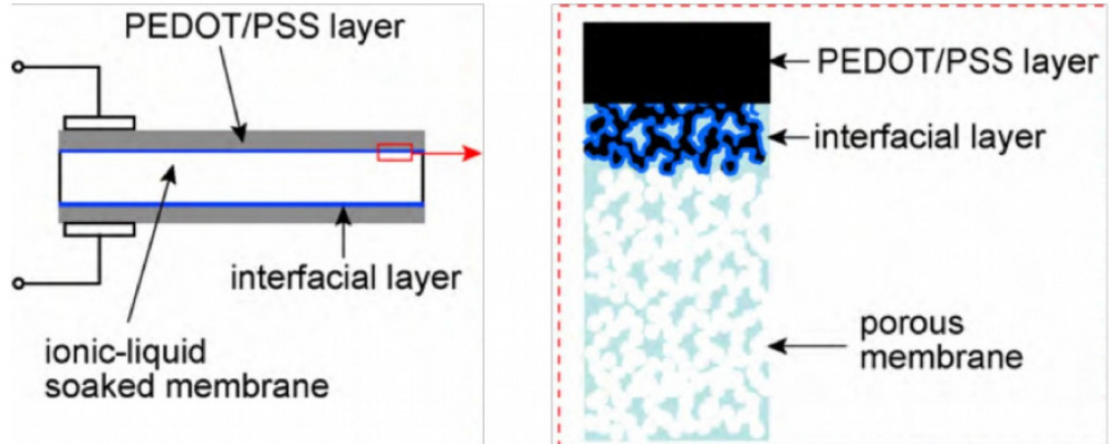


FIGURE 2.1 – Structure of the tri-layer actuator considered in this study

during its synthesis, is widely studied, the ion transport and volume expansion of the PEDOT :PSS is barely studied. So, in order to explain the behaviour of PEDOT :PSS in ionic liquid, the current understanding of the actuation mechanisms of PPy(DBS) based actuators is used. Characterization measurements were mostly done with trilayer actuator (PEDOT :PSS/mPVDF/PEDOT :PSS) clamped at one end (Please refer to the Fig. 5.2). at one end and supplied with a voltage in $[-2V + 2V]$ range.

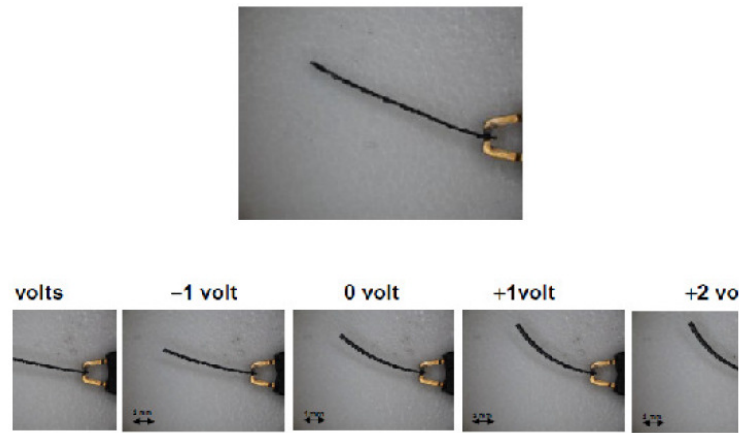


FIGURE 2.2 – Trilayer actuator (PEDOT :PSS/mPVDF/PEDOT :PSS) clamped at one end and supplied with a voltage in $[-2V + 2V]$ range

The actuators were cycling by applying a potential waveform between two electrodes and the response was recorded by recording the video of the bending or by laser displacement sensor. Detail set-up and explanation could be found in Appendix A. The change in the displacement was then extracted from the video and is shown in Fig. 5.3a. The transferred current was simultaneously measured and was

used for calculations of the dissipated power (Fig. 5.3b).

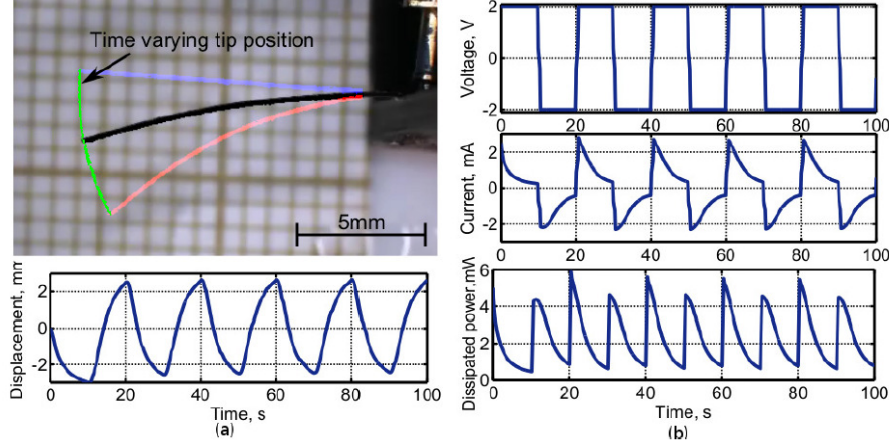


FIGURE 2.3 – Merged images of the actuator at its extremities during actuation applying square wave with frequency of 50mHz and 2.0V amplitude. Blue and red actuators show its maximum and minimum displacement position, green dots show the tip position calculated from recorded videos. Actuator displacement profile in time is shown in the figure below. Actuator is bending towards the negative electrode. (b) Applied voltage, current and power dissipation measured during the actuation. Figure adopted from [Simaite 2015a]

Strain The actuator bending is often expressed as strain. The use of displacement and curvature to characterize the performance of the actuator is quite trivial as they do not take into account the dimensions of the actuators. Strain can be defined simply, in the context of artificial muscles, as a displacement normalized by the original material length in the direction of actuation [Madden 2004b]. Measurement of strain can be done by direct means in the case of free-standing polymer films or indirectly using bending beam theory. Sugino et al. in [Sugino 2009] proposed an equation to estimate the difference in strain (ε) during bending of the actuator

$$\varepsilon = \frac{2DW}{L^2 + D^2}, \quad (2.1)$$

where L, W are the length and the thickness of the actuator and D is the measured displacement. The Eq. 5.1 is valid for a simplified geometrical model assuming low displacements, it is still viable for the measurements in the case of PEDOT :PSS based actuators. Due to the mechanisms other than ion transport involved in volume expansion, irreversible expansion (creeping) is often observed as shown in Fig. 5.4a. The term "active strain" is defined as the difference between the maximum peak strain and the following minimum strain of each voltage cycle (shown in Fig. 5.4a as δe_{max}).

Strain rate Strain rate is the measure of the speed of the actuator and thus it is an another important characteristic of the actuator. Formally speaking, it is the average change in strain per unit time during an actuator stroke [Madden 2004b] (Please refer Fig. 5.4a. It has been observed that the strain rate expressed in this manner is highly dependent on the actuation frequency. In fact, speed of the actuation is not constant and its bending significantly slows down once 70%(approx) of the maximum strain is reached. Therefore, sometimes for comparison purposes, the maximum speed of expansion is used. It is calculated at each time interval ($\delta\epsilon/\delta t$ as shown in Fig. 5.4b). PPy based actuators typically have strain rates of approximately 1%/sec. The strain rate is mostly limited by how quickly ions can move through the polymer film. Therefore, size of the ion, the microstructure of the polymer and history of the cycling have large influence on the speed of actuation [Melling 2002, Pytel 2007]. Another implication of the diffusion model is that it takes more time to diffuse deeper into the film and the full depth might not be reachable.

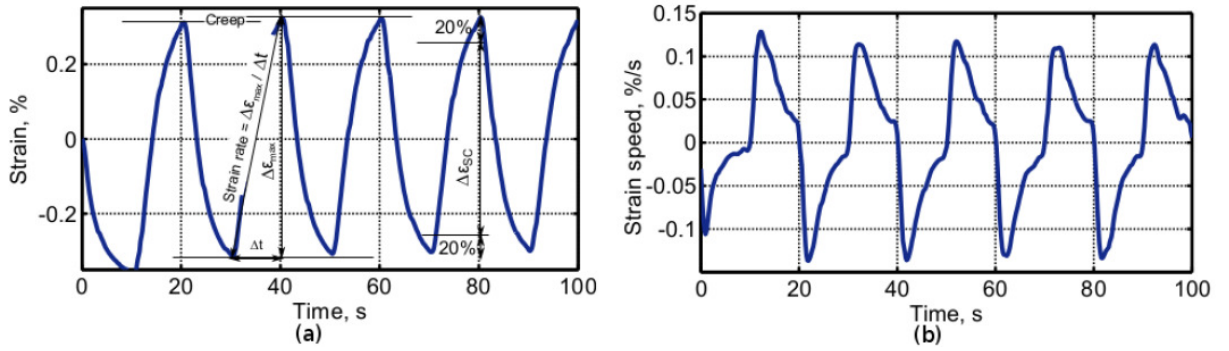


FIGURE 2.4 – (a) Actuator bending profile shown as calculated strain versus time. Strain is calculated using Equation 5.1 for every point detected during video processing. Min to max strain ($\Delta\epsilon_{max}$) is defined as strain difference between extremities during one actuation period (T), strain rate is a ratio of ($\Delta\epsilon_{max}$ and $T/2$). (b) The speed of the actuator is calculated at every point as $\delta\epsilon/\delta t$. Figure adopted from [Simaite 2015a]

2.1.3 Control reviews of Electroactive polymer actuators

Closed-loop control of artificial muscle is a difficult challenge due to the general non-linear character of the artificial muscle dynamic contraction but also due to its associated feeding requirement. Among possible energy choices, electric tension is particularly relevant as a clean, simple supply mode easy to put into work, especially when a quick contraction can be got from low voltage and low electric energy. Ionic polymer bending artificial muscles belong to this class of low energy electroactive polymeric actuators. While, in their earlier development, such bending strips needed a liquid environment for contracting, the recent use of non-evaporable ionic liquid

made possible their use in open air [Lu 2002, Bennett 2004] and so expanded their application field. Although the positioning of this kind of actuator can be controlled in open-loop with an input voltage, the typical "drift"-phenomenon of the actuator under a constant input voltage - i.e. the fact that the actuator continues to slowly bends without giving the impression to converge towards a steady-state position - makes necessary the need of a closed-loop control. Several attempts have been made for developing closed-loop control for the accurate positioning of this bending artificial muscle including linear PID-control [Yao 2008], feed-forward control [John 2010], sliding mode control [Wang 2013] or fuzzy and neuro-fuzzy control [Druitt 2014]. The highly non-linear character of the bending phenomenon would actually leads to give priority to sophisticated control approaches as done by Druitt and Alici in their paper [Druitt 2014]. Alternatively, in this preliminary work on soft actuators, we would like to analyze the relevance to come back to simpler control approaches. The motivation for such approach comes from our work made on the control of robots actuated with the pneumatic McKibben muscle. Due to its highly non-linear nature, several sophisticated control approaches have been tested such as sliding mode control, fuzzy control or biomimetic control. Although interesting results were obtained for various trajectories, all these approaches actually suffer a degree of complexity due to the relatively high number of parameters or rules to tune without to be sure to keep the same level of performances in a large field of experimental conditions. More recently, we attempted to control a single artificial muscle and a joint made of two antagonist pneumatic McKibben muscles by considering a simple I-controller taking advantage of the own stiffness and damping of any artificial muscle [Tondou 2016]. The electroactive polymers considered in our work contracts by bending while the McKibben fluidic muscle contracts along its long axis. A linear closed-loop control approach with a limited number of parameters are proposed to apply to a tri-layer PEDOT :PSS/PVDF/ionic liquid sample [Simaite 2015b]. Carbon nano-tubes [Simaite 2016] have been added in order to increase its resistance to delamination in the full working range $[-2V, +2V]$, as illustrated in Fig. 2.2. In a broad sense, the originality of our approach is based on the intuitive idea that the classic PID can be especially adapt to the peculiar nature of any artificial muscle. Such an approach finds its place, according to us, in current thinking about redefinition of PID gains tuning rules as done, for example, by Fruehauf et al. [Fruehauf 1994] — mentioned in [Druitt 2014]. The choice of a PI control, as proposed in this thesis, is motivated by the identified model developed in section 5.2. Before we attempt to apply it for steps and sine-wave trajectories in the next section, by means of the classical experimental set-up shown in Fig. 2.5. The sample tip positioning is measured using a laser with respect to a zero horizontal position, and the feedback control combines a NI-card with the LabView software.

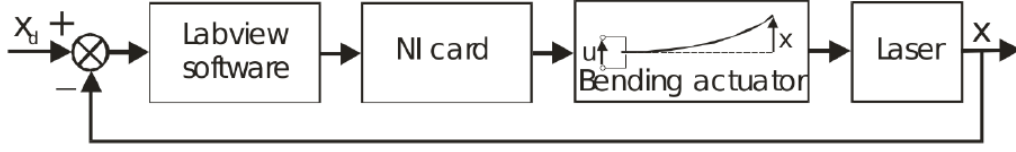


FIGURE 2.5 – Structure of the tri-layer actuator considered in this study (a) under the form of a sample of 15mm long, 2mm wide with a thickness of about $140\mu\text{m}$ (b) and classical set-up for a closed-loop control of the actuator tip position x towards a desired position or time-trajectory x_d (c)

2.2 Non-linear Identification of the Artificial Muscle

In a recent article [Tondou 2015], we attempted to propose a general definition of any artificial muscle as an open-loop stable system when input is the muscle activation variable and output is one positioning dimension. In the case of a tri-layer bending polymeric sample, the input is an electrical voltage while the output is generally specified as a vertical distance measured at the tip of the sample. The open-loop stable character of the artificial muscle points the way towards open-loop identification, especially from step recording of its positioning dimension in response to various step amplitude. Such an identification problem can be tackled by using various methods as the ANFIS-NARX paradigm, recently applied to IPMC (Ionic Polymer Metal Composite) [Annabestani 2015] for getting an advanced non-linear model of the full bending actuator or, in a more conventional way, classical techniques of linear system identification applied to the time variation of the sample : in [John 2010], the authors are proposing a sixth-order transfer function with a constant gain for identifying their polypyrrole tri-layer actuator.

2.2.1 Non-linear model derivation from the first order linear model

Our approach is a bit different in the sense it is based on a preliminary observation of two characteristics of any open-loop step-response of the type of bending actuator we try to control : whatever the u -control voltage, no overshoot occurs and the slope at the origin is never close to zero. In the framework of linear systems, these two points are characterizing a first-order system. If, for low voltage open-loop steps, a linear first-order system can give a satisfying model, as illustrated in Fig. 2.6a for $+0.25\text{V}$ and 0.5V -steps, this is not the case for upper voltage open-loop steps due, in particular, to the "drift"-phenomenon which makes the convergence to the steady-state slower than expected for a linear system. This is the reason why we propose the following non-linear model directly derived from the expression of a first-linear model, as follows :

$$x(t) = k(1 - e^{-\frac{t}{T}})u \quad (2.2)$$

where u is the step amplitude, x is the artificial muscle tip position, k is a

TABLE 2.1 – Identified parameters of the proposed non-linear model

$u(V)$	0.25	0.5	0.75	1	1.25	1.5	1.75	2
$k(mm/V)$	2.5	2.5	2.45	2.5	2	1.9	1.8	1.75
$T(s)$	6	5.5	4	3	2.5	2.15	2.15	2.1
r	1	1	0.8	0.7	0.6	0.475	0.45	0.4

gain, T a time constant-like parameter and r a positive coefficient lower than 1, without dimension. If $r = 1$, the system behaves like a first order linear system. For each considered open-loop u -step, k was identified as the ratio between steady-state position over u , and the T and r parameters were identified by successive trials, T being chosen for matching rising slope while r was chosen for matching the final convergence speed. Fig. 2.6a gives the result of this identification in the case of positive u -steps whose corresponding estimated values for k, T and r are given in Table 1. A linear interpolation between identified parameter values for getting continuous change for k, T and r is proposed in Fig. 2.6b. It can be noted that we voluntarily limited the interpolation to the range $[+0.25V, +2V]$: if it is clear from identified step responses at low voltage, that the assumption of a linear behaviour of the bending artificial muscle at very low voltage is relevant, data are however missing about k and T parameters in this voltage-range. We see little problem with this situation due to the fact that control voltage close to zero is rarely used in practice.

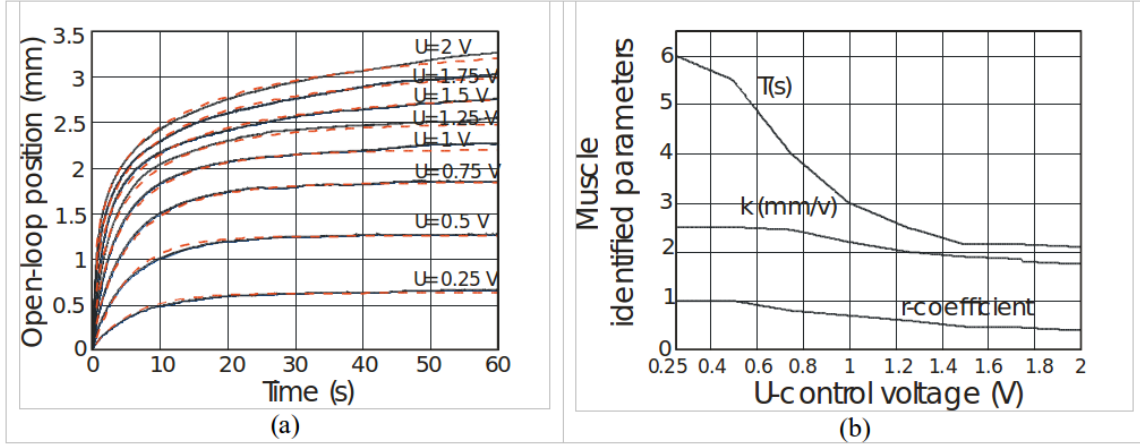


FIGURE 2.6 – Nonlinear open-loop identification of the actuator : (a) Comparison between x -position in response to u -voltage steps (full line) — only positive u -steps are considered — and the proposed non-linear model (dashed line), (b) Variation of the parameters (T, k, r) of the proposed non-linear first-order for a u -control voltage varying in the range $[+0.25V, +2V]$

2.3 PI-closed loop control

2.3.1 Linear tuning and non-linear effects

It is well known that a first linear system can be controlled in closed-loop by a PI-controller whose proportional and integral gains can be determined from a direct comparison between the resulting characteristic polynomial and this of a standard second order system. Let us write the PI-control as follows : (equation)

$$u = k_P(x_d - x) + k_I \int_0^t (x_d - x)(\tau) d\tau \quad (2.3)$$

where u is now the closed-loop control voltage, x_d the desired output, x the real output and k_p, k_I are constant gains. For a linear first order, open-loop system, in the form of the transfer function $\frac{k}{1+Ts}$, the characteristic equation resulting from the PI-controller is given by :

$$1 + \left[\frac{1 + k k_P}{k k_I} \right] s + \left[\frac{T}{k k_I} \right] s^2 = 0 \quad (2.4)$$

whose terms can be identified with those of the classical form : $1 + 2z\omega_n s + (1/\omega_n^2)s^2 = 0$, where z is the damping factor and ω_n the undamped pulsation of the corresponding linear second order. Because it is also well known that response time of a linear second-order system without zero is, for a given z , inversely proportional to ω_n , it is then possible to choose z and a given response time T_r — for example, the time beyond which the response keeps inside the 0.95/1.05 desired position-range — for deriving the gains k_p and k_I as follows :

$$k_P = \frac{1}{k} \left[\frac{2z(\omega_n T_r)T}{T_r} - 1 \right] \quad (2.5)$$

$$k_I = \left[\frac{(\omega_n T_r)^2 T}{k T_r^2} \right] \quad (2.6)$$

In the limit-case $z = 1$ — corresponding to the quickest step-response before overshooting — the $(\omega_n T_r)$ -term is equal to about 5 and we can so compute k_P and k_I for any given T_r . This approach has, however, a severe limitation : the presence of a zero in the closed-loop transfer function equal to $(-k_I/k_P)$ whose effect can be an overshoot impacting also the response time. If we apply this approach to the linear version of the identified model of our sample developed in section 5.2 by considering $r = 1$, constant k and T parameters respectively equal to the mean value of identified k and T parameters of Table. 2.1, we get, for $z = 1$ and $T_r = 2s$, the result shown in Fig. 2.7a in the case of a $1mm$ desired step position — we get k_p equal to about $8.1V/mm$ and k_I to about $10.65V/mm.s^1$, while k is about equal to $2.2mm/V$ and T is equal 2 to about $3.7s$. The response time is a bit greater than the expected 2 seconds with, however, a slight overshoot exceeding a bit 5%. If we now apply the same values for k_p and k_I to the non-linear model proposed, it is interesting to remark that the overshoot is now negligible with, as

a consequence, a reduced response time divided by more than 2. Such a way for tuning the controller gains is however not able to take a strong constraint peculiar to the considered artificial muscle : control voltage control must be lower than $+2V$, in absolute value, which is clearly not satisfied as shown in Fig. 2.6b.

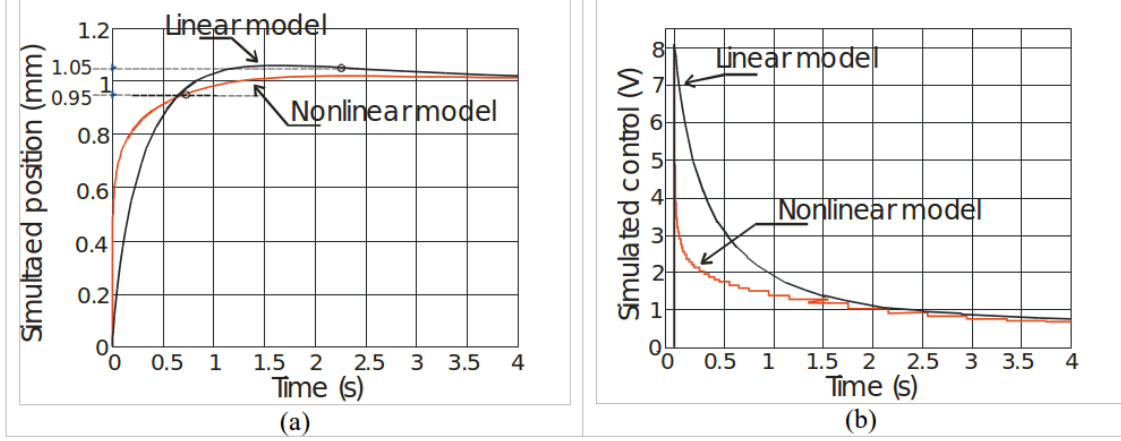


FIGURE 2.7 – Simulation of a closed-loop PI-linear control applied to a mean linear model of the artificial muscle and to the proposed non-linear model : (a) Simulation of step responses — circles correspond to the time beyond which response belongs to the 0.95/1.05 desired position-range, (b) Corresponding control voltage.

2.3.2 Taking into account voltage constraints

Theoretically, closed-loop control should avoid to reach the bounds of the permitted control range but, in the case of our tri-layer sample, the consequence would be the need to adapt the controller gains — or rules if a logics-based controller is considered — to the desired position. The consequence can be a great complexity as already mentioned in the case of the recent study by Druitt and Alici [Druitt 2014]. Our alternative approach proposes to consider the $[-2V, +2V]$ voltage range as a practical range whose $-2V/+2V$ bounds can be reached without damage for the artificial muscle at the condition that the steady-state position does not require to indefinitely stay at one of these bounds. From open-loop identification developed in section 5.2, this condition is satisfied by limiting the desired position in the range $[-3mm, +3mm]$. If we admit that closed-loop control can be performed with saturation periods, it is clear that classical rules for tuning a PID-type controller cannot be applied anymore. Our approach for tuning the PI-gains is based on the fact that, on the one hand, only two gains are considered and, on the other hand, on the knowledge of the identified non-linear model. In the case of steps, the following two-stage strategy is proposed, where u_{lim} designates the maximum value for a safe control :

1. A reference x_{ref} -position is chosen, typically at the middle of the positive, or negative, admissible range. The gain k_P is then tuned according to the following

relationship :

$$k_P = \frac{u_{lim}}{x_{ref}} \quad (2.7)$$

Such a k_P -gain leads to a control value equal to u_{lim} at $t = 0^+$ just before the integral action starts to play its role ;

2. For the same reference position, the gain k_I is then tuned by simulation of the PI closed-loop controller applied to the proposed non-linear model with, as an aim, a limited overshoot combined to the lowest possible response time. The obtained (k_P, k_I) couple can then be applied to lower and upper desired positions.

Let us consider, in our case, a reference equal to $1mm$ and $u_{lim} = +2V$. We deduce : $k_P = 2V/mm$. As shown in Fig. 2.8a, a choice of $k_I = 1V/mm.s$ leads to a response time of about $2s$ with no overshoot. As expected, the control voltage is saturated at $t = 0^+$ and then tends to a non-saturated value. On the same plot, we considered the simulated step-response for $x_d = 0.5mm$: no overshoot occurs and response time is still close to $2s$. On the same plot, the corresponding real step responses are also given. There is some discrepancy between simulated and real responses. This is, especially due, according to us, to the way the non-linear differential equation has been solved : we used Matlab software and its ode113-solver which, in the case of our problem, generated solution with a mean sampling time of about $300ms$ when the Labview control program was sampled at $10ms$. It is, however, interesting to check that the real step response both for $1mm$ and $0.5mm$ exhibit no overshoot, as expected. We give in Table. 2.2 the performances in step response time and overshoot for steps between $-3mm$ and $+3mm$ whose corresponding position and control versus time are respectively shown in Figs. 2.9a and 2.9b. In every case, the same (k_P, k_I) -couple equal to $(1V/mm, 2V/mm.s)$ was used. For any desired position greater, in absolute value, than $1mm$, the control is initially saturated to $+2$ or -2 volts before almost instantaneously leaving this value limit. In the case of bounds $-3/+3mm$, the control value is initially maintained to the voltage limit during several seconds. This limitation of our actual electroactive artificial muscle makes impossible to get short time responses for desired positions in the lower and upper-range between -3 and $-2mm$ and $+2$ and $+3mm$. It is worthy to note that for steps less than $1mm$, in absolute value, another tuning of the gains would make possible to get a faster contraction but our first aim in the reported experiments was to analyze the possibility of keeping the same gains whatever the step-value and, especially, to check the very limited overshoot resulting of such an approach, as verified in Table. 2.22. We also give in Fig. 2.9c the steady-state error for positive steps $0.5, 1, 2$ and $3mm$: in every case, the steady-state error belongs to the $[-0.02, +0.02mm]$ -range which exhibits the very positive role of the integral action.

2.3.3 Stability of the PI-controller

A linear first-order system with a PI-feedback control is always stable whatever the choice of the positive k_P and k_I gains because its characteristic polynomial is

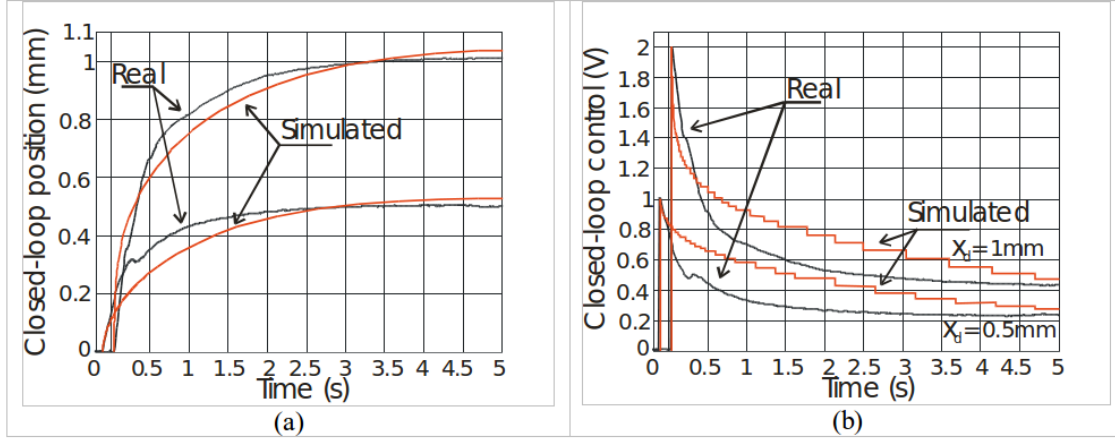


FIGURE 2.8 – Simulation of the closed-loop positioning of the bending actuator by means of a PI-controller with constant (k_P, k_I)-gains : (a) Comparison between real (full line) and simulated (dashed line) step-responses for a desired $+0.5mm$ position and a desired $+1mm$ position, (b) Corresponding real and simulated controls.

TABLE 2.2 – Estimated response time and overshoot for desired steps in the range $[-3mm, +3mm]$

$X_d(mm)$	-3	-2	-1	-0.5	+0.5	+1	+2	+3
Response time(s)95%	24.2	6.71	2.01	2.05	1.99	1.97	7.22	20.05

a second-order one with positive coefficients. At the opposite, the same first order system with a three-term PID-feedback control is unstable for a k_I -gain whose value limit is given by the Runge-Kutta criterion. In the case of our non-linear artificial muscle model, let us assume that the artificial muscle has been put in the equilibrium position x_{equ} by means of a control voltage equal to u_{equ} which must verify the steady-state relationship : $x_{equ} = ku_{equ}$. Let us assume that we move the system from this equilibrium position, briefly and within a short distance, in order that we can assume that the parameters k, r and T keep constant. As a consequence, the PI generates a closed-loop control voltage given by Eq. 2.3 where x_{equ} has to be written instead of x_d . By deriving Eq. 2.2, we get :

$$\dot{x} = k(1 - e^{-\frac{t}{T}})\dot{u} + (\frac{r}{T})t^{r-1}(e^{-\frac{t}{T}})u \quad (2.8)$$

By putting into Eq. 2.8 the expression of resulting from the time derivative of the control equation imposed by the PI as follows : $\dot{u} = -k_P\dot{x} + k_I(x_{equ} - x)$, the following differential equation of the closed-loop system results :

$$\dot{x} \left[1 + kk_P(1 - e^{-\frac{t}{T}}) \right] = kk_I(x_{equ} - x)(1 - e^{-\frac{t}{T}}) + (\frac{kr}{T})t^{r-1}(e^{-\frac{t}{T}})u \quad (2.9)$$

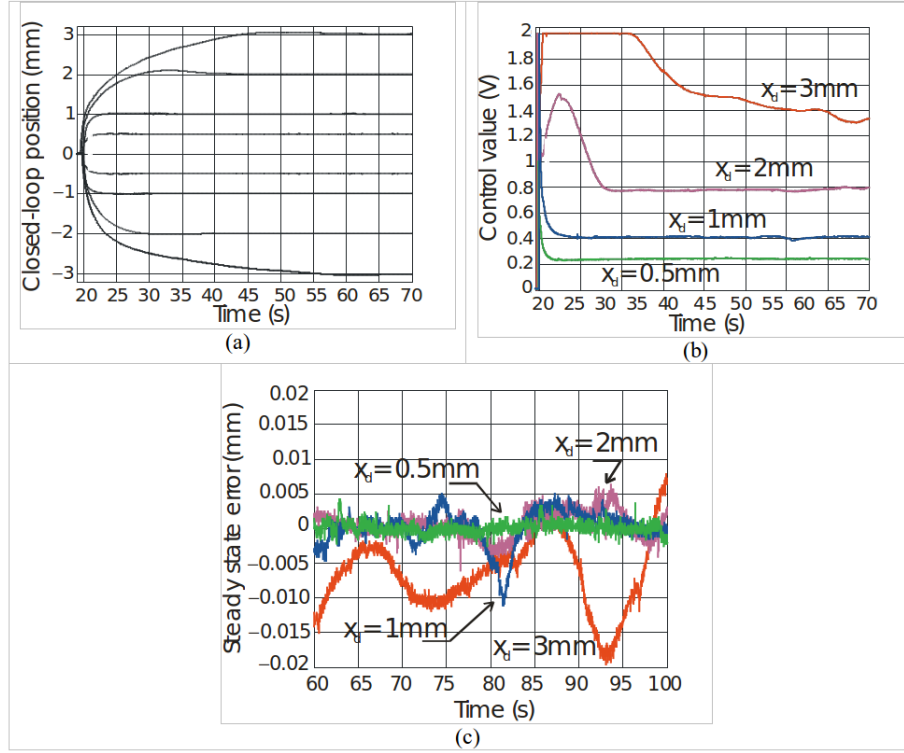


FIGURE 2.9 – Closed-loop positioning of the bending actuator by means of a linear PI control with the same constant (k_P, k_I) -gains : (a) Step responses in the range $[-3mm, +3mm]$, (b) Corresponding variation of control voltage for positive desired positions, (c) Corresponding steady-state errors.

where k, r , and T depend on u according to the relationship expressed in Eq. 2.3. In the neighbourhood of infinite for time t , due to the fact that, for $0 < r \leq 1$, $e^{-\frac{t}{T}}$ and $t^{r-1}e^{-\frac{t}{T}}$ tend to zero when t tends to infinite, Eq. 2.9 is reduced to :

$$\dot{x}(1 + kk_P) = kk_I(x_{equ} - x) \quad (2.10)$$

This last equation is similar to the one resulting from the closed-loop control by a PI of a first-order linear system in the form : $\dot{x} = k(1 - e^{-\frac{t}{T}})u$. We can so conclude from the accurate knowledge of the proposed actuator model that the considered PI-controller makes the closed-loop system stable. A very interesting practical consequence is that any blind tuning of the two considered gains cannot put the closed-loop system into instability, whereas a blind tuning of the three gains of a PID could do it.

2.3.4 Tracking performances

The method for tuning the (k_P, k_I) -gains proposed in section 2.3.2 is not applicable to the choice of a trajectory to be tracked due to the fact that the k_P -gain

cannot be derived from a simple saturation constraint as expressed in Eq. 2.7. An alternative way for tuning the two gains can however be proposed in this case after having remarked that, in steady-state, the considered actuator model behaves like a first order whose only gain k and time constant T are depending on control u . We can indeed write the following equivalence in the neighbourhood of infinite time, for $0 < r \leq 1$ and whatever T :

$$(1 - e^{-\frac{t^r}{T}}) \approx (1 - e^{-\frac{t}{T}}) \quad (2.11)$$

$$t = +\infty \quad (2.12)$$

eq :9 because, when t tends to ∞ , $(1 - e^{-\frac{t^r}{T}})(1 - e^{-\frac{t}{T}})$ tends to 1. As a consequence, and considering mean constant values for k and T , we can deduce, from classical results on tracking errors of first linear order systems in closed-loop with a PI, the following estimation of the tracking error ε_V in response to a constant slope :

$$\varepsilon_V = \frac{V}{k_{mean}k_I} \quad (2.13)$$

where V is the value of the slope, k_{mean} is the mean value for k , either in positive or negative u-range and k_I is the already defined integral gain. We give in Fig. 2.10 tracking results obtained for various sine-waves. In the case of the tracking of a sine-wave of $\pm 2mm$, with a period of $20s$, a near constant tracking error can be observed in a large portion between sinus-wave extrema, as shown in Fig. 2.10f and on the close-up view of the first $\frac{3}{4}$ period of Fig. 2.11a : from time equal to about $8s$ to a time equal to about $12s$, the tracking error $(x_d - x)$ varies, in absolute value, between about $0.06mm$ and $0.08mm$. By estimating the corresponding slope, in absolute value, to about $0.6mm/s$ and considering a mean value k_{mean} roughly equal to about $2.1mm/V$, and because a $k_I = 5$ was considered in the reported experiment, from Eq. 3.13, ε_V can then be estimated, in absolute value, to about $0.57mm$, which is in relative good accordance with the reported experimental values. This emphasizes the relevance of our approach. Another fact is also a direct consequence of the interpretation of the simple dynamic behaviour as a first order system and its PI-control in steady-state : the deviation of the real trajectory from the desired one when curvature is increasing or decreasing. It is indeed well known that, in the case of a first-order system with PI-closed loop, for input time-signals in the form t^r , $r > 1$, the tracking error tends to be infinite with, as a consequence, a maximum tracking error occurring just after each sinus-wave extremum as this can be verified in Figs. 2.10b and 2.10d.

We can now better understand the respective roles of k_P and k_I of our PI-control applied to our bending actuator in trajectory tracking : k_I is the sole gain responsible for the tracking error, when k_P is an additional gain for controlling the transitory state. From conclusion of section 2.3.3, there is no instability risk of increasing k_I to get a better tracking error for constant slope and to limit deviation

increasing during non straight-line parts of the trajectory to be tracked, expect that we are limited by the imposed control range $[-u_{lim}, +u_{lim}]$. We show in Fig. 2.10e, and on the close-up view of Fig. 2.11a, the effect of a control saturation imposed, in our case, to $\pm 2V$. As shown on Fig. 2.11b, the control is saturated just before the system reaches the top of the sine-wave : as a consequence, the system behaves as an open-loop system and cannot continue to efficiently track the sine-wave. At the opposite of the case without saturation, the real trajectory is now below the desired one and the shape of the sine-wave is no more preserved. From all these remarks and because we wanted in this paper to analyze the possibility of a PI-controller with same constant gains for a set of desired trajectories, we considered the following strategy applied to a family of given sine-waves :

- Because k_P is essentially devoted to transitory state dynamics, it is proposed to choose its value equal to this determined in step gain tuning,
- Considering a sine-wave of the maximum desired amplitude k_I is chosen equal to the value in order that $\pm u_{lim}$ is reached at sine-wave top/bottom.

We applied this strategy to sine-wave tracking whose amplitude is between $\pm 0.5mm$ and $\pm 2mm$; three examples are reported for which amplitudes and associated time period were chosen as follows : $\pm 0.5mm$ with a time period of $5s$, $\pm 0.1mm$ with a time period of $10s$ and $\pm 2mm$ with a time period of $20s$. Keeping k_P equal to 2, a k_I equal to 5 was practically chosen from the observation of a control saturated respectively to $+2V$ and $-2V$ when the sine-wave of $\pm 2mm$ reaches respectively the neighbourhood of its maximum and minimum. From the reading of Figs. 2.10a, 2.10b, 2.10d, 2.10f, it can be seen that the tracking errors are respectively in the ranges $[-0.2mm, +0.2mm]$, $[-0.2mm, +0.15mm]$ and $[-0.35mm, +0.3mm]$ for the three considered examples. It is interesting to remark that the error obtained in the third example (amplitude of $\pm 2mm$ at a $0.05Hz$ frequency) is not so far from the result reported by Yao, Alici and Spinks [Yao 2008] with a much faster tri-layer bending actuator — see especially the figure 6 of the mentioned paper.

Conclusion and future work The proposed PI-controller for closed-loop position control of bending actuators was motivated by an original identification of the actuator under the form of a kind of non-linear first-order system as follows : $x(t) = k(1 - e^{-\frac{t}{T}})u$, where the three parameters k , r and T vary with the u-control voltage. This simple non-linear identified model leads us to justify the relevance of a simple PI-controller for an efficient and stable closed-loop control of the actuator. In the case of a step-response, a simple tuning methodology for the two gains is proposed : it is based on the specification of a safe control voltage range $[-u_{lim}, +u_{lim}]$ and on the possibility given to the control to reach such safe working limits. Given a reference position x_{ref} , belonging to the admissible position range derived from the specification of the control voltage-range, the k_P -gain is given by the simple relationship : $k_P = u_{lim}/x_{ref}$; the k_I -gain can then be tuned in order to get the best compromise between no overshoot and quickest response time. As reported, a

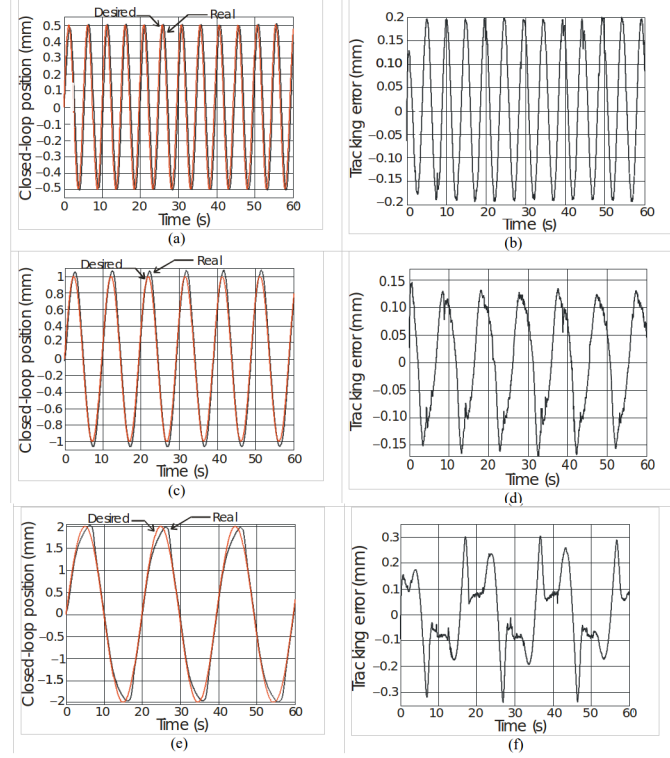


FIGURE 2.10 – Tracking of a sine-wave trajectory by means of a PI closed-loop control with constant gains ($k_P = 2$, $k_I = 5$) : (a), (b) Case of a $[-5mm, +0.5mm]$ -range sine-wave with a time period of 5s and corresponding tracking error, (c), (d) Case of a $[-1mm, +1mm]$ -range sine-wave with a time period of 10 s and corresponding tracking error, (e), (f) Case of a $[-2mm, +2mm]$ -range sine-wave with a time period of 20 s and corresponding tracking error

fine tuning for k_I can be done by simulating the PI-controller with the proposed non-linear bending artificial muscle model. Reported results show the relevance of this approach for getting a same couple of gains in the full position range leading to a maximum overshoot of 5% and a response time taking advantage of the imposed safe voltage limits. The PI-controller is also applied to sine-wave trajectory tracking. In this case, we tried to highlight the analogous behaviour of the studied artificial muscle with a linear first-order system when steady state is established and, as a consequence, the fundamental role of the k_I -gain for limiting the tracking error. Such a similarity also emphasizes the limitation of our PI-control when sharp trajectory curvature changes occur. Future work will focus on improvements in trajectory tracking, especially, with studying the relevance of variable P and I -gains to tackle both with sharp curvature changes and voltage saturation constraints.

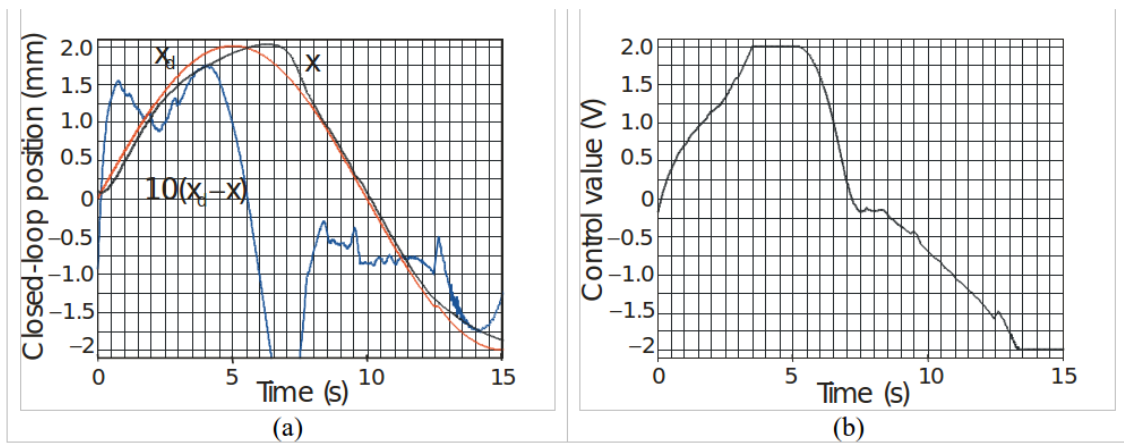


FIGURE 2.11 – Close-up of the tracking performance (a) and associated control (b) in the case of the $\pm 2\text{mm}$ amplitude sine-wave shown on the first $\frac{3}{4}$ period equal to 15s — every gradation in time is equal to 0.5s (see text).

Modeling of the system

Sommaire

3.1	Robotic experimental set-up	53
3.1.1	Kinematic structure of the arm	53
3.1.2	Hardware components	53
3.2	Modeling of the pneumatic system	56
3.2.1	Muscles side dynamics	57
3.2.2	Pressure side dynamics	58
3.2.3	Modeling of Agonistic-antagonistic joint actuator : Symmetric case	60
3.2.4	Modeling of agonistic-antagonistic joint actuator : Generic case	62
3.2.5	Model of the multi Dof pneumatic arm	64
3.3	Conclusion	65

3.1 Robotic experimental set-up

In this chapter we describe the kinematic structure of the 7Dof anthropomorphic arm, a presentation of the hardware on which is based the control architecture, and then we provide a detailed original model of the pneumatic actuation system.

3.1.1 Kinematic structure of the arm

The robot has 7 degrees of freedom (Dof) with three Dofs are at the shoulder and three are at the wrist. One extra Dof is at the elbow. Due to its kinematic structural analogy to human arm, the physiological joint terminology is used rather than the roll-pitch-yaw type mechanical terminology. The External-internal rotation is the rotation of the link along its longest axis. Flexion-extension is the decrease and increase of joint angle. Abduction-adduction is moving away and towards the body sagittal plane. The sequence of Dofs in the arm is described in Fig. 3.1 and Fig. 3.3

3.1.2 Hardware components

Intensity-Pressure converter (IP) : The arm is pressurized by air supply through servo-valves controlled by Intensity-Pressure converter. The product used in our setup is a Samson I/P 6111 manufactured by Samson Corporation, Frankfurt,

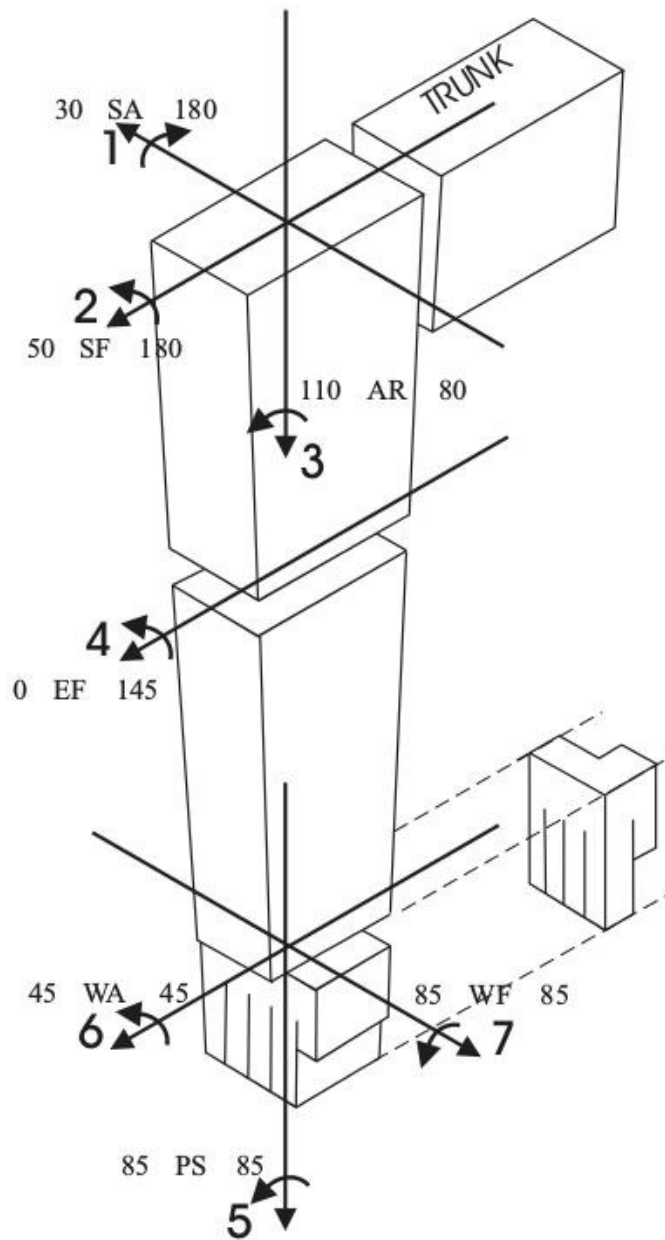


FIGURE 3.1 – Kinematic structure of the robotic arm

Electropneumatic Converter. This IP is rapid in action producing output pressure in range 0 to 5 bar. The bandwidth of IP is volume dependent and can be as high as $5Hz$ for volume of $75cm^3$. There are seven joints and a gripper. Each joint and gripper is actuated by a pair of McKibben muscles and each muscle is controlled by one IP converter and so there are 16 IP converters.

Encoders/Potentiometers : There are seven potentiometers at each joint or Dofs to get the joint angle measurement. These analogue potentiometers could be

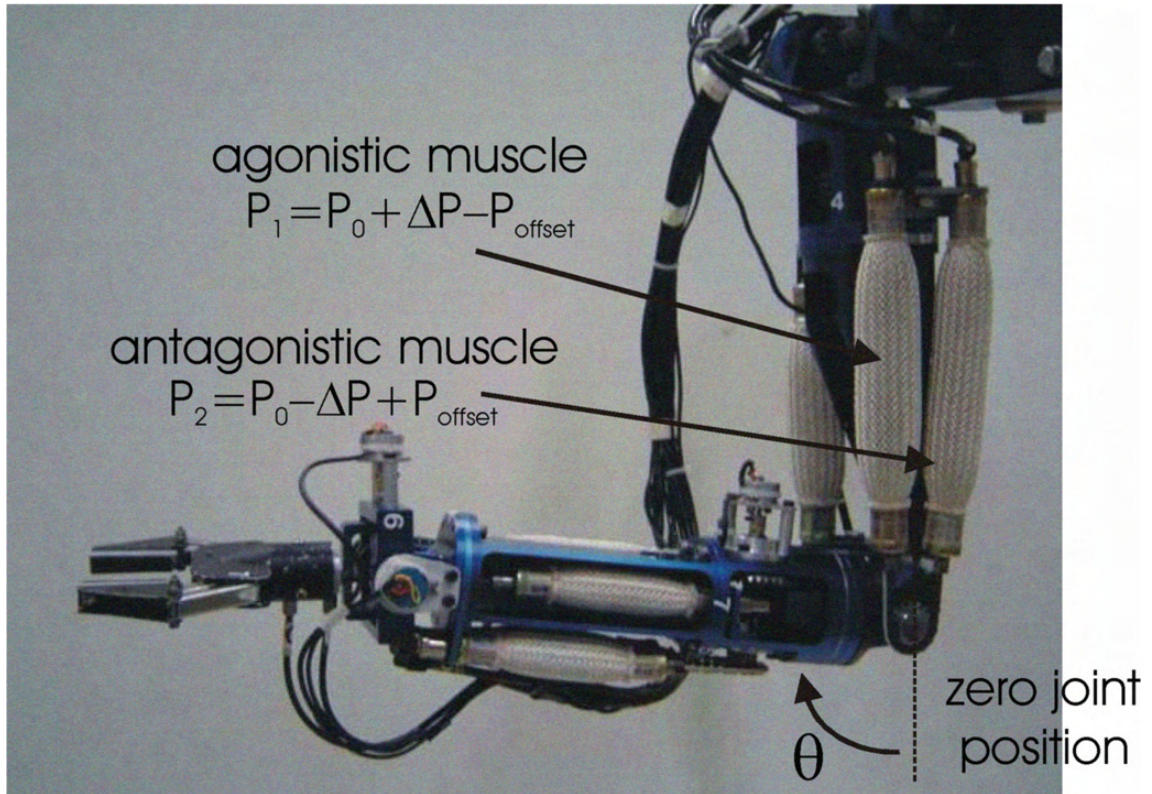


FIGURE 3.2 – The 7 Dofs robotic arm

replaced by digital encoders in near future.

Data Acquisition device : CompactRIO from National Instruments (NI) is used for this purpose. This is a reconfigurable and embeddable chassis, integrating an intelligent real-time controller. According to the customer needs, up to 8 different modules can be plugged into the chassis. Depending on our needs 3 kinds of modules are added :

- NI9205 : It is an Analog-to-Digital-Converter (ADC) with up to 32 channels, selectable acquisition range ($\pm 200mV$, $\pm 1v$, $\pm 5v$ and $0v$) and a max sampling frequency of $250kS/s$. This device will sample the seven potentiometers dedicated to the positioning of the arm.

- NI9265 : There are 3 modules which are Digital-to-Analog-Converters (DAC). They have the particularity to provide analog current outputs. The SAMSON's 6111 electropneumatic converters use this kind of signal. Each module is able to manage up to 4 channels in the 0 to $20mA$ range at $100kS/s$.

- NI9401 : Finally the 4 last modules drive bidirectional digital IOs. These IOs connected to relative quadrature encoders will be able to replace more accurately the current analog potentiometers. Up to 12 quadrature encoders can be acquired. The aim of the CompactRIO is to do the link between the computer managing high level control and the actuators of the 7Dof arm. It means that simple functions such as sampling and encapsulation into standard network protocol (UDP), extraction

from standard network protocol (UDP) and signal generation will be performed.

Development computer : This is the main computer where modeling, simulation and finally control for the robot arm will be implemented. The computer bi-directionally communicates to the NI module via Ethernet cable for sending control command and receives sensory feedback. Figure 5 shows the overall experimental setup at our laboratory.

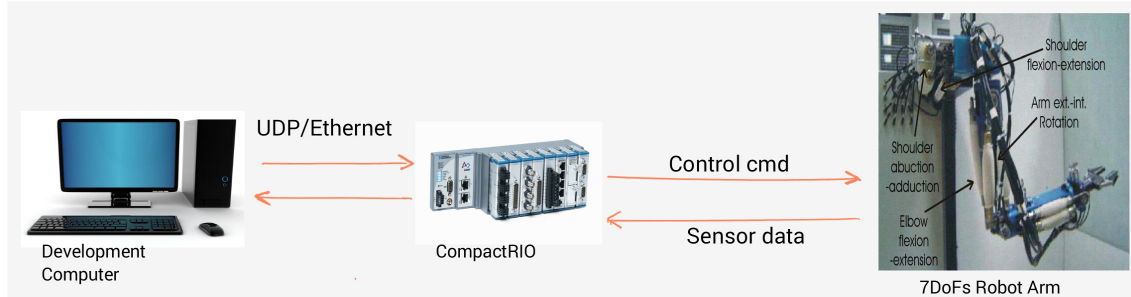


FIGURE 3.3 – Overall experimental setup

Linux kernel : The resulting system is composed of Linux and small co-kernel running side by side on the same hardware. Xenomai co-kernel exclusively controls the real-time applications and real-time interfaces either to kernel-space modules or to user-space applications. These interfaces called skins can mimic pSOS+, VRTX, VxWorks, POSIX, uITRON and RTAI API. Due to this feature, Xenomai is considered as the RTOS chameleon. It is designed to enable smooth migration from a traditional RTOS to Linux without having to rewrite the entire application. Fig. 3.4 illustrates the Xenomai skins architecture. Previously a software was written to control the robot arm manually by using joystick. The software was running under vxworks real time controller. Moving towards open source and linux platform, we have chosen to use Xenomai. Some of the important functions used in previous software have been integrated in the new software architecture by using Xenomai's vxworks skin.

3.2 Modeling of the pneumatic system

There have been several attempts to model the McKibben artificial muscle [Tassa 2013, Tondu 2012, Kothera 2009, Tondu 2006, Daerden 2001]. The difficulty for getting an accurate model is due to a combination of complex phenomena during static and dynamic contraction : shape changing at the muscle tip which lose their initial cylindrical shape for a conical one, mobility and flexibility of the braided sleeve, elasticity of the inner rubber tube, exotic friction in the textile braided sleeve without forgetting, for the pneumatic version of the McKibben muscle, dynamic fluidic phenomena resulting from the artificial muscle volume variation during contraction. When we want to include such a physical model into the closed-loop control of a McKibben muscle actuator, a compromise must be found between the

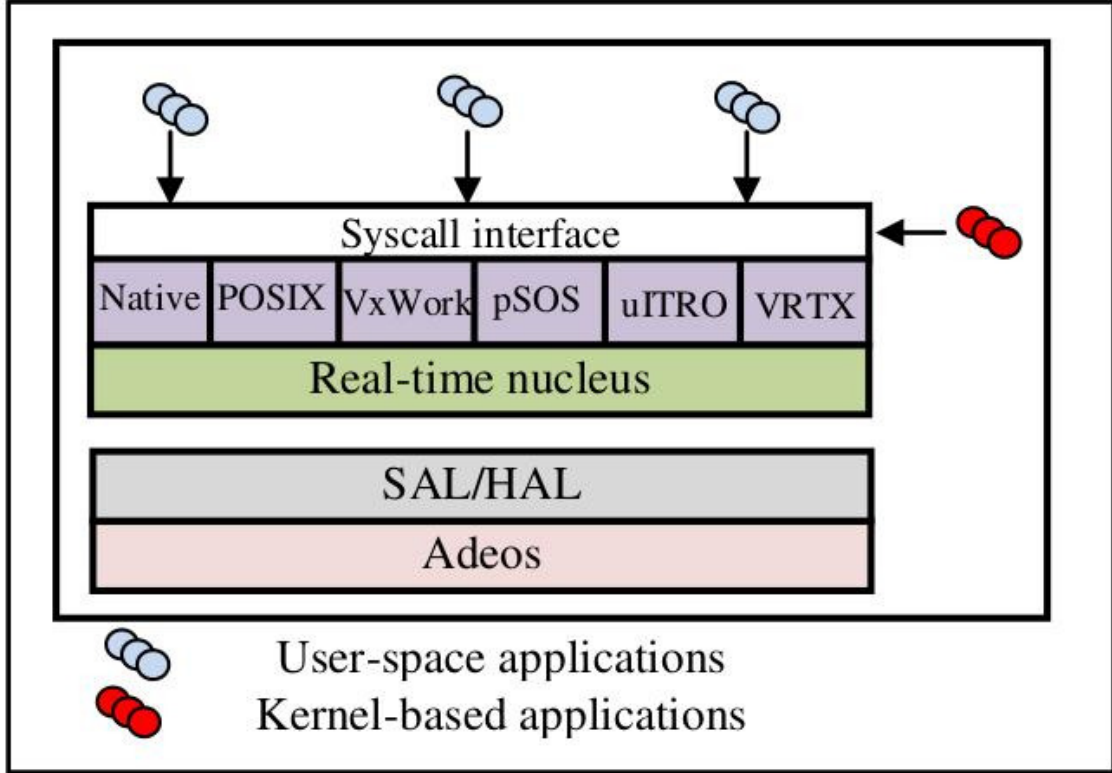


FIGURE 3.4 – The Xenomai skin architecture.

complexity of an accurate model and the time required for its computation. The need for an efficient but not too complex dynamic muscle model is all the more important in the case of artificial muscles for robot arms. Indeed the preservation of the actuator compliance imposes a joint direct-drive mode and so the consideration of a dynamic robot model, linked to the actuator model. The originality of our approach, described in this section, consists in including an original model of real pressure variation inside a simple McKibben muscle dynamic model before proposing a multi-variable pressure control of the actuator made of two similar antagonist muscles.

3.2.1 Muscles side dynamics

The following model was considered for relating the dynamic contraction force F of the artificial muscle to its control pressure P and contraction ratio.

$$F(\varepsilon, P) = (\pi r_0^2) P [a(1 - k\varepsilon)^2 - b] \quad (3.1)$$

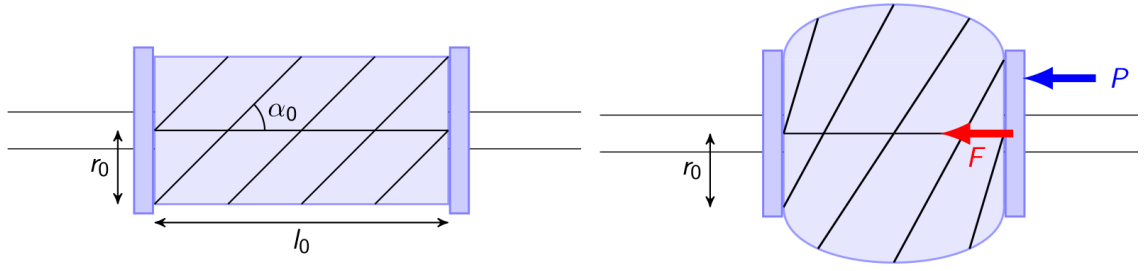


FIGURE 3.5 – Muscle geometric parameters : l_0 initial length, r_0 radius and α_0 braid angle

Where,

$$\begin{aligned}\varepsilon &= \frac{l_o - l}{l_o}, \\ a &= \frac{3}{\tan^2 \alpha_o}, \\ b &= \frac{1}{\sin^2(\alpha_o)},\end{aligned}$$

l being the current muscle length and l_o , r_o , α_o are the muscle geometric parameters corresponding to its initial length, radius and braid angle respectively (see [Tondy 2012] for more details). ε is the contraction ratio. The parameter k , slightly greater than 1, is empirically chosen for taking into account the conic shape at muscle tips. The viscous coefficient is also experimentally estimated for expressing the naturally damped behavior of the artificial muscle contraction due to the complex kinetic friction inside the braided sleeve. Although hysteresis phenomenon due to dry friction is not included in this model, we think it captures most of the static and dynamic behaviour of the artificial muscle.

3.2.2 Pressure side dynamics

As previously introduced, control pressure in a muscle is provided by an Intensity-Pressure (I/P) converter which translates a current value into a desired pressure value that has to be fed to the muscle. In literature, see [Kelasidi 2011] for a survey, there exist several models of pressure generated in a muscle in terms of the mass of air injected, volume of the muscle and some parameters related to servo valves or the I/P converter (for an example see [Vanderborgh 2006]). These models are highly non-linear and eventually become too cumbersome for devising control strategies. We propose a somewhat simpler empirical model to cover the dynamics of the pressure generation from the I/P converter. It is derived from SAMSON I/P converters reported in [Boitier 1996]. Following this model the instantaneous pres-

sure p inside a muscle is represented by a damped second order differential function with a control pressure as input as follows :

$$\ddot{p} + 2w_n\dot{p} + w_n^2p = w_n^2p_{des} \quad (3.2)$$

Note that the input of the intensity converter is a current value which is then scaled to the corresponding pressure control input p_{des} in the pressure unit. The above equation is also non-linear as the natural frequency w_n has been empirically identified as a function of the volume of the muscle, V .

$$w_n = 2\pi f_v(1/V) \quad (3.3)$$

f_v is the empirically found parameter. The volume of a McKibben artificial muscle can be approached by the following cylindrical volume : $V = \pi r^2 l$, where r and l are respectively the current radius and length of the artificial muscle. By using the relationship Eq.(3.4) as reported in [Tondou 1995], we deduce an expression for the volume of the muscle.

$$r/r_0 = (1/\sin(\alpha_0))\sqrt{(1-\varepsilon)^2} \quad (3.4)$$

$$V = \frac{\pi r_0^2 l}{\sin^2(\alpha_0)}(1 - \cos^2(\alpha_0)(1 - \varepsilon)^2) \quad (3.5)$$

For a second order system, the rise time is inversely proportional to its natural frequency and in the case of our pressure dynamic model, the natural frequency is inversely proportional to the volume. It implies that the bigger the muscle, the larger the rise time. Fig. 3.6 depicts a typical variation of w_n with the joint angle at one of the manipulator joints. If the range of operation for a joint is small i.e range of

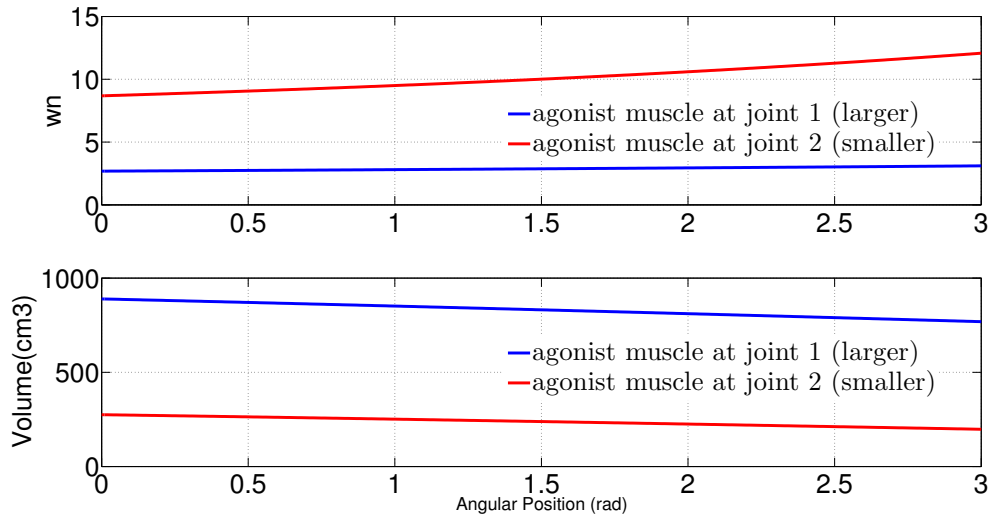


FIGURE 3.6 – Natural frequency and volume of the muscle with the joint angle

θ is small, then the corresponding changes in the volume of the muscles as θ varies,

would be small at that joint. In such case, a constant value for w_n could be chosen for the muscles corresponding to their mean volumes. Here, another interesting point to notice is that for different muscles, pressure dynamics of a larger volume muscle will be slower. The above two points help in trading off between the operating range of the joint and the corresponding easiness of the control strategy.

3.2.3 Modeling of Agonistic-antagonistic joint actuator : Symmetric case

Skeletal artificial muscle usually can generate forces in only one direction i.e. they can only pull and not push. When they are applied to the actuation of anthropomorphic limbs, they cannot work alone and hence configured in agonist-antagonist fashion. The similar attempt had been made by the Washington's Biorobotics Laboratory in the upper limb case [Hannafor 1995] to mimic the complex organization of human musculature. The more recent development in this field using pneumatic muscles can be seen in [B. Verrelst 2005] and [Kurumaya 2016] (Fig. 3.7). However, such an arrangement is not trivial. In order to incorporate a linear skeletal artificial muscle to a revolute joint structure, a basic muscular organization seems to be necessary which is described as follows : the revolute actuator made of two antagonistic artificial muscles illustrated in Figure 9. The two antagonistic muscles are assumed to be identical and attached by means of a non-extensible pulley-chain system, where R denotes the pulley radius. Both muscles are having an initial l_0 active length. In the general case, agonistic muscle is controlled by u_1 and antagonistic muscle is controlled by u_2 , and the resulting actuator angle is θ . The case of

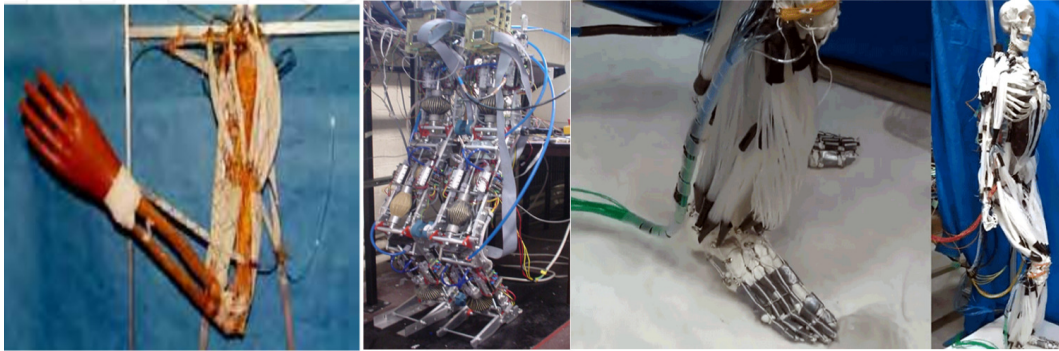


FIGURE 3.7 – From Left to right : Antagonistic biomimetic arm developed at Washington Biorobotic laboratory [Hannafor 1995]. Biped Lucy [B. Verrelst 2005]. Humanoid skeleton powered by artificial muscles [Kurumaya 2016]

symmetric model where both muscles are identical is discussed here first and then the generic model will be presented later. It is assumed that there is no passive tension in the artificial muscles and the joint rest angular position is $\theta = 0$. In this initial state both muscles are equally contracted with a same control u_0 allowing the ε_0 initial contraction. Therefore in any particular joint position θ the agonist

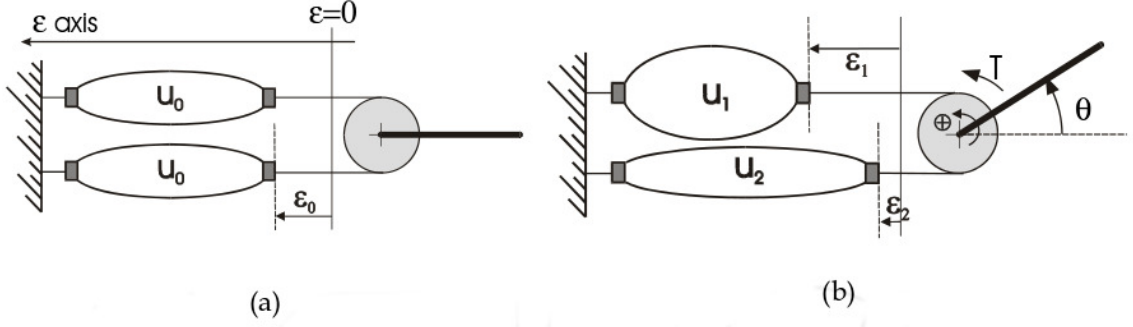


FIGURE 3.8 – Operation principle of the antagonistic muscle actuator, (a) Initial state, (b) Current state

and antagonist contraction ratios are respectively given by

$$\varepsilon_1 = \varepsilon_0 + \frac{R\theta}{l_o} \quad (3.6)$$

$$\varepsilon_2 = \varepsilon_0 - \frac{R\theta}{l_o}, \quad (3.7)$$

where, ε_1 is the contraction ratio for the agonist muscle and ε_2 is that for the antagonist muscle. The actuator torque T can be written as follows

$$T = R(F_1 - F_2) \quad (3.8)$$

where, F_1 is the agonistic force and F_2 is the antagonistic force. The application of the fundamental model of equation (4) leads to the following expression :

$$T = K_1(u_1 - u_2) - K_2(u_1 + u_2)\theta - T_{damp}(u_1, u_2, \theta, \dot{\theta}) \quad (3.9)$$

with

$$K_1 = RF_{max}\left(1 - \frac{\varepsilon_o}{\varepsilon_{max}}\right) \quad (3.10)$$

$$K_2 = \frac{R^2 F_{max}}{l_o \varepsilon_{max}} \quad (3.11)$$

$$T_{damp} = R(F_{1-damp}(u_1, \varepsilon_1, \dot{\varepsilon}_1) - F_{2-damp}(u_2, \varepsilon_2, \dot{\varepsilon}_2)) \quad (3.12)$$

The static component of the actuation torque as expressed in Eq. 3.13

$$T_{stat} = K_1(u_1 - u_2) - K_2(u_1 + u_2)\theta \quad (3.13)$$

has resemblance to the simplified Hogan's model of the biceps/triceps system (Hogan, 1984) [Hogan 1984]. Inspired from this comparison, three fundamental properties of the artificial muscle antagonistic actuator in analogy with the fundamental biceps-triceps natural muscular system can be highlighted.

Stable open loop The equilibrium position θ_{equ} corresponding to a null static torque can be defined as follows :

$$\theta_{equ} = \frac{K_1(u_1 - u_2)}{K_2(u_1 + u_2)} \quad (3.14)$$

In this equilibrium position, the stiffness of the actuator S defined as follows :

$$S = K_2(u_1 + u_2) \quad (3.15)$$

Two output actuator : torque and stiffness The actuator can be considered as a double input-output system whose (u_1, u_2) are the inputs and (T_{stat}, S) are the outputs defined as follows :

$$\begin{bmatrix} T_{stat} \\ S \end{bmatrix} = \begin{bmatrix} K_1 - K_2\theta & -K_1 - K_2\theta \\ K_2 & K_2 \end{bmatrix} \begin{bmatrix} u_1 \\ u_2 \end{bmatrix} \Rightarrow \begin{bmatrix} u_1 \\ u_2 \end{bmatrix} = (1/2K_1K_2) \begin{bmatrix} K_2 & K_1 + K_2\theta \\ -K_2 & K_1 - K_2\theta \end{bmatrix} \begin{bmatrix} T_{stat} \\ S \end{bmatrix} \quad (3.16)$$

Maximum actuator torque decreases continuously from an actuator angle limit to the other one Here we try to establish the actuator angle limit to the maximum contraction of the muscles assuming that each actuator muscle can fully contract to its maximum contraction ratio ε_{max} . If the two muscles are identical, the two actuator angle limits can be defined as follows :

$$[\theta_{min}, \theta_{max}] = [-(\varepsilon_{max} - \varepsilon_o)l_o/R, +(\varepsilon_{max} - \varepsilon_o)l_o/R] \quad (3.17)$$

Assuming that the inputs (u_1, u_2) are the normalized command and so for every actuator angle θ belonging to this range (Eq. 3.17), the following expression of the maximum torque can be obtained, corresponding to a maximum control of the agonistic muscle ($u_1 = 1$) and a null control of the antagonistic muscle ($u_2 = 0$) :

$$T_{max}(\theta) = K_1 - K_2\theta \quad (3.18)$$

As clear from the Eq. 3.18, the maximum torque decreases from θ_{min} to θ_{max} with the $-K_2$ slope. In contrast to the classical actuators, the presence of the restoring torque term ' $K_2(u_1 + u_2)\theta$ ' gives to the biomimetic actuator a natural compliance which can be actively controlled independently from the actuator position. However, this angular position-actuator torque dependence induces a specific sensitivity of the actuator to gravity.

3.2.4 Modeling of agonistic-antagonistic joint actuator : Generic case

Following the human arm model, a pair of artificial muscles can be set up in antagonistic fashion to drive a chained wheel of radius R . According to Fig. 3.9, the

resulting actuator torque T can be written as follows :

$$T = R[F_1(\varepsilon_1, P_1) - F_2(\varepsilon_2, P_2)], \quad (3.19)$$

where F_1 and F_2 are the forces of muscles 1 and 2 respectively, defining the antagonist muscle pair. As illustrated in Fig. 3.9, the relationship between θ , the

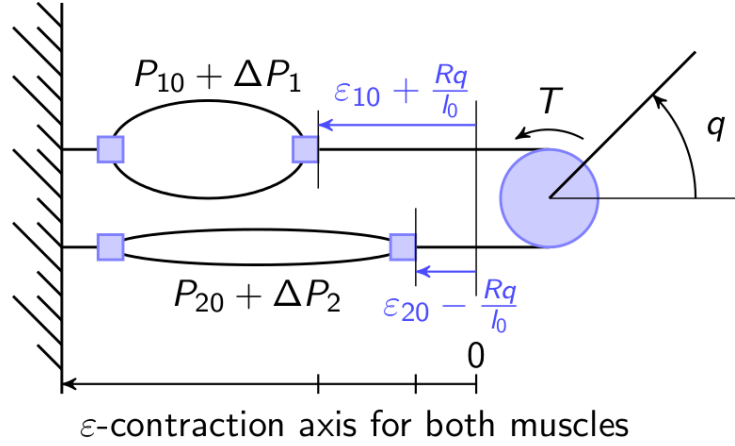


FIGURE 3.9 – Pulley-chain driven antagonist muscle actuator made of two identical McKibben artificial muscles. It has the possibility to adapt initial torque at initial zero θ -position by means of P_{10} , P_{20} , ε_{10} and ε_{20}

actuator angle and the contraction ratios for each muscle can be expressed as follows : $\varepsilon_1 = \varepsilon_{10} + \frac{R\theta}{l_0}$ and $\varepsilon_2 = \varepsilon_{20} - \frac{R\theta}{l_0}$, where ε_{10} and ε_{20} are the initial contraction ratios for muscle 1 and muscle 2 respectively corresponding to the zero-angular position. Moreover, we propose to specify the pressures in muscle 1 and muscle 2 as follows : $P_1 = P_{10} + \Delta P_1$ and $P_2 = P_{20} + \Delta P_2$, where P_{10} and P_{20} are respectively the initial pressure in the agonist-antagonist muscle and related to zero positioning of the joint. ΔP_1 and ΔP_2 , are the control pressures.

Using Eq.(3.1), and neglecting the terms ε_1^2 and ε_2^2 , the torque at the joint can be expressed as

$$T = K_1 \Delta P_1 - K_2 \Delta P_2 - K_3 (P_1 + P_2) \theta - K_4 \dot{\theta} + K_5, \quad (3.20)$$

where,

$$\begin{aligned} K_1 &= (\pi r_o^2) R [a(1 - 2k\varepsilon_{10}) - b], \\ K_2 &= (\pi r_o^2) R [a(1 - 2k\varepsilon_{20}) - b], \\ K_3 &= 2(\pi r_o^2) R^2 ka / l_o, \\ K_4 &= (\pi r_o^2) R^2 f_v / l_o, \\ K_5 &= (\pi r_o^2) R [(a - b)(P_{10} - P_{20}) - 2ka(P_{10}\varepsilon_{10} - P_{20}\varepsilon_{20})]. \end{aligned}$$

If $P_{10} = P_{20}$ and $\varepsilon_{10} = \varepsilon_{20}$, K_5 is equal to zero. The details of our robot-arm including the dimensions of muscles are given in [B.Tondu 2005] and also given in Appendix B. The antagonist muscle actuator is now considered as a MIMO-system whose inputs are the control pressures $\Delta P_1, \Delta P_2$, and outputs are both θ and the actuator stiffness which is defined as the instantaneous ratio between the current torque variation and the current angular position variation (see Eq.(3.22)). When no gravity effect is considered, the static equilibrium position of the actuator can be directly derived from Eq.(3.20) with zero angular velocity.

$$\theta_{equ} = (K_1 \Delta P_1 - K_2 \Delta P_2 + K_5) / (K_3(P_1 + P_2)) \quad (3.21)$$

With associated stiffness σ_{equ} expressed as

$$\sigma_{equ} = -\frac{\partial T}{\partial \theta} = K_3(P_1 + P_2) \quad (3.22)$$

From Eq.(3.21) and Eq.(3.22), it is possible to remark that the equilibrium position can be changed while keeping the same stiffness by modulating ΔP_1 and ΔP_2 with a constant $\Delta P_1 + \Delta P_2$. In the case of a symmetrical pressure variation in both muscles : $\Delta P_1 = -\Delta P_2 = \Delta P$, the actuator becomes a SISO-system whose corresponding torque T_{SISO} , is now given by the following relationship :

$$T = (K_1 + K_2)\Delta P - K_3(P_{10} + P_{20})\theta - K_4\dot{\theta} + K_5 \quad (3.23)$$

where stiffness at equilibrium position is now constant and equal to $K_3(P_{10} + P_{20})$. When the joint angle θ varies, and assuming that the actuator chain is inextensible, the contraction ratio of each muscle is known and, consequently, the pressure dynamic model, proposed in 3.2.2, can be applied to each muscle. It is important to note that, in the case of relatively small joint muscles, the effect of volume variation with joint angle on pressure dynamics could be negligible. If the range of operation is small, a constant w_n could be chosen for that joint. As previously noted, pressure dynamics of a larger volume muscle will be slower which is, especially, the case of the muscles at the shoulder joint compared to the muscles at the elbow joint.

3.2.5 Model of the multi Dof pneumatic arm

This section presents the robot model formally, including the rigid body model of the robot with its pressure dynamics. Let us consider a n degrees of freedom robot with generalized joint angle coordinates $q \in \mathbb{R}^n$. Each joint is actuated by 2 pneumatic muscles, so there will be $2n$ muscles, each one with a pressure $P_i \in \mathbb{R}^{2n}$. The robot dynamics can be represented in standard form as below :

$$M(q)\ddot{q} + C(q, \dot{q}) + G(q) = T(q, P), \quad (3.24)$$

$$\ddot{P} + 2C_p\dot{P} + G_pP = G_pP_{des}, \quad (3.25)$$

where, $M(q) \in \mathbb{R}^{n \times n}$ is the inertia matrix of the robot, $C(q, \dot{q}) \in \mathbb{R}^{n \times 1}$ is the coriolis and centrifugal terms, $G(q) \in \mathbb{R}^n$ is the gravity related terms, $T(q, P) \in \mathbb{R}^n$ is the torque generated by pneumatic muscles as described in Eq.(3.19). $C_p = \text{diag}[w_{n_1}, w_{n_2}, \dots, w_{n_{2n}}]$ and $G_p = \text{diag}[w_{n_1}^2, w_{n_2}^2, \dots, w_{n_{2n}}^2]$ are the collection of coefficients of the pressure dynamics of each muscle and w_{n_i} is the natural frequency of the pressure dynamics at the i^{th} muscle. $P = [P_1, P_2, \dots, P_{2n}]^T \in \mathbb{R}^{2n}$ is the vector of current muscle pressure and $P_{des} = [P_{des_1}, P_{des_2}, \dots, P_{des_{2n}}]^T \in \mathbb{R}^{2n}$, is the vector of desired pressure P_{des_i} , the control input in pressure unit given to the I/P converter of the i^{th} muscle. Any reference trajectory in q given to the robot has to respect the pressure dynamics whose bandwidth depends on w_n . As discussed in the previous section, if the joint is actuated by larger muscles (having smaller bandwidth) and higher rise time, rapidly varying trajectory would be difficult to track and pose a limiting factor in performing explosive tasks. Limits to the operating range of the joints are obviously decided by the maximum contraction of the spanning muscles. In addition to that, w_n could be reasonably considered as constant in a limited operating range, removing in this way the non-linearity in pressure dynamics. Apart from this, due to hardware limitation of I/P converter, the control input P_{des} is bounded as follows :

$$U = P_{des} \in \mathbb{R}^{2n} : P_{des} \in [P_{min}, P_{max}] \quad (3.26)$$

Where, P_{min}, P_{max} are the lower and upper bound on control input P_{des} .

3.3 Conclusion

The problem of modeling a robot manipulator actuated by the pneumatic Mckibben muscles is addressed here. Each module of the actuator and the robot is considered one by one and their behaviour are studied. Based on this studies and empirical experiments, suitable models are proposed. While the model of Mckibben muscles are based on the previous work of B. Tondu [Tondu 1995], the first contribution of this thesis is to propose a model which encapsulates the pressure dynamics in an efficient way. It is done by using a second order differential function whose bandwidth is dependent on the instantaneous volume of the muscles. Even though, the model does not include the effect of dry friction and hysteresis, it covers most of the static and the dynamic behavior. Also a combined model of the entire robotic anthropomorphic manipulator is presented. It is interesting to show the analogy of such kind of robotic manipulators with the conventional electrically driven manipulators. The motor side dynamics are replaced by pressure side dynamics while keeping the structure of the standard manipulator equation (Refer to Eq. 3.24). This model will be used in later chapters for different control strategies while performing different tasks.

Control of the Pneumatic system

Sommaire

4.1	Introduction	67
4.2	PID control of the pneumatic system	69
4.2.1	Model free single Integral action controller	69
4.2.2	Model based PI controller	72
4.3	iLQR control of the anthropomorphic pneumatic arm	76
4.3.1	State space representation	76
4.3.2	Iterative Linear Quadratic Regulator (iLQR)	77
4.4	Conclusion	80

This chapter provides an overview of the control techniques that have been so far applied to control pneumatic systems. Then we describe the approaches that we have developed and applied to control our 7 Dof anthropomorphic arm.

4.1 Introduction

The major advantage of the Mckibben muscles is their inherent compliance but that comes at the cost of complications in control strategies. The force generated or transferred to the load by the muscle depends in a non-linear fashion on the actual muscle length and the supplied pressure. Similarly, the stiffness (variation of the force with respect to the contraction of the muscle) is a non-linear function of the contraction and the input pressure. In addition to this, Mckibben muscles suffer from hysteresis. It is mainly due to the friction between the tube and the braid and between the fibres of the braid. Many researchers had tried to address this problem and proposed several control strategies. A very brief overview of such control strategies is presented here.

Overview of control strategies In a very broad sense, it can be observed that most of the authors had used one of the models presented in [Chou 1996, Tondu 2000, Colbrunn 2001]. Capabilities of controlling the Mckibben muscles are explored by means of neural network control [Hesselroth 1994b, Tian 2014, Thanh 2006], fuzzy logic-based control [Thongchai 2001, Ahn 2011],

adaptive control [Caldwell 1995, Zhu 2008], sliding mode control [Cai 2003, Tondou 2000, Braikia 2011, Jouppila 2014], or nonlinear model-based control [Minh 2009, Xiangrong 2010].

In the work presented in [Pack 1994], a comparison was made between three different control strategies namely PID, PID tuned by a fuzzy supervisor and nonlinear state feedback controller. The Chou-Hannaford ([Chou 1996]) muscle model was chosen for the model and applied to a joint powered by two muscles in an antagonist setup. The conclusion drawn from the simulation results was that the PID controller gives a slow response and the non-linear state feedback controller has the best response. Using the similar experimental set-up, a double loop PI controller is used in [Schroder 2003]. In this work, the torque generated by the muscles, the joint angle and the pressure difference between the muscles were in consideration instead of the force. A double loop of two PI controllers is to control the torque with one loop and the pressure with the other. The torque is estimated by a variation of the classic Chou-Hannaford model by fitting a damping relation.

[Petrovi 2002b] proposed a predictive fuzzy control approach. The predictive fuzzy model is based on their previous work [Petrovi 2002a]. This control approach is applied to a single muscle in simulation. In [van der Smagt 1996], a neural network based feedback controller is used to simulate a robotic arm model. The Chou-Hannaford model was used for the muscle dynamics. Experiments were also performed to verify the control strategy. An adaptive control strategy is proposed by Caldwell [Caldwell 1994], [Caldwell 1995] and verified experimentally. The robot model parameters are embedded in the controller polynomial and the reconstruction of the robot is done by updating an s-domain polynomial in every sample.

[P. Carbonell 2001] has compared the three nonlinear control strategies by simulation in MATLAB. These are robust back-stepping controller, a sliding mode controller and a gain scheduling controller. In this approach, simulation of the controller were performed on a muscle model which was derived by data fitting. Whereas the sliding mode and the back-stepping controller has shown the best error tracking, the sliding mode controller gives a chattered response. Sliding mode controller for tracking has also been used for an antagonist setup [Lilly 2005].

In the literature, one can find some control approaches applied to the multi-link anthropomorphic arm. [Tuijthof 2000] presents the design and control of a 4DoF anthropomorphic arm which is driven by changes in muscle stiffness. Open loop stiffness control is applied on one joint with two muscles. Equilibrium points are derived by a fixed combination of joint angle and rotation stiffness (pressure). The approach was experimentally verified.

Whereas most of the above mentioned experiments used McKibben muscles, [van Ham 1996b] has used a pleated pneumatic artificial muscle. It is done to overcome the hysteresis problem in a more efficient way. This is discussed in the literature review in Chapter 1. The experiments were conducted on a robotic arm driven by pleated artificial muscles. These muscles are fed by binary valves. A bang-bang algorithm which uses the sign of the error as valve signal and a PWM algorithm were used to control the valves. Later such system had also been used in humanoid

walking application [Vanderborght 2006].

Although relevant results were reported from various control approaches, these generally complex strategies need to tune a relatively large number of parameters and their performances in a large class of movements is rarely discussed. Woods et al. [Woods 2013] proved that it is possible to control a McKibben artificial muscle actuator using a fairly simple method that does not require a system model and nor any tuning of parameters.

In our work, we have considered model based PI controller, model free PID controller and more advanced control strategies of iterative LQR. These developments are discussed in detail in the following sections.

4.2 PID control of the pneumatic system

From the review of different control strategies, it is evident that controlling pneumatically actuated anthropomorphic arm is not trivial. However, a simple but reliable model could facilitate the control strategies. Relying on our model presented in Chapter 3, we proposed two control strategies. One is the conventional PID controller while the other method is model-based predictive controller which is comparatively modern. These strategies will be discussed in detail in this section. But before that, we tried to investigate the possibility of model-free control. This approach is based on the work presented in [Tondu 2013] and continued on the same line. The following section presents the discussion and the results of applying a single Integral action on the McKibben muscle.

4.2.1 Model free single Integral action controller

Since modelling the McKibben muscle is difficult, it is desirable to find a fairly simple control method to servo it without the requirement of the exact model and without the need of tuning several control parameters as in [Woods 2013]. In a similar spirit, the relevance of a one-parameter linear integral action is analyzed for accurately controlling in closed-loop the contraction of any artificial muscle characterized by its own stiffness and damping. The motivation behind this approach is to propose that the natural stiffness and natural damping of any artificial muscle could play the role, in its closed-loop positioning control, of the P and D-actions of a classic PID. However, comparing the performance of this I-controller approach with that of a full PID controller is not in the consideration. It is possible that, in some particular case, a PI or a PID controller is able to generate a faster response than the simple proposed I-controller, but the primary goal of this work is to highlight the possibility to control the artificial muscle with a one gain I-action with robustness properties. Although artificial muscles are non-linear complex systems, they globally behave like damped 'active' springs whose stiffness can be controlled by some variable mimicking the neural activation. This is this fundamental non-linear specificity of any artificial muscle which makes possible the use of a single I-action for which it is well known that it cannot be used for closing the loop of a linear

actuator. Now with the assumption that the P and D-actions are now internal to the actuator itself, only an internal I-action is necessary to make equal to zero the steady-state error due to friction and gravity. It is important to note that, as for a classic PID-approach, no dynamic model is required in this approach. It is even expected to manually tune the single integral gain, assuming that increasing it increases the system quickness as long as stability is verified. Our approach, in this framework, is to first analyze the relevance and efficiency of this idea in a theoretical way from a rectilinear artificial muscle model for which we simulate its closed-loop control with a single linear integral action and then report some experimental results performed on the McKibben muscle. Experiments were performed both in step response and sinus-wave tracking, with various embedded load. N. Hogan proposed in his classical 1984's paper [Hogan 1984] a very simple and elegant model of the active tension of the skeletal muscle as a linear relationship with current length muscle, whose constant slope is proportional to a normalized control variable noted u varying between 0 and 1 and representing the neural activation. We consider that a rectilinear artificial muscle deprived of any passive elongation - which will be particularly the case of the McKibben muscle - and let us define its x-contraction length as the always positive difference between its initial length l_0 and its current length l . If we assume that the artificial muscle x-contraction length can vary, independently of u , from 0 to a maximum value denoted x_{max} at which contraction force is equal to zero, we can consider, in Hogan's spirit, the following relationship between the static force F_{stat} and length x :

$$F_{stat} = uF_{max} \left(1 - \frac{x}{x_{max}} \right), \quad (4.1)$$

where F_{max} represents the maximum isometric muscle force corresponding to a zero-contraction and a unit-normalized control value. However, such a model driving a given inertia is not asymptotically stable : a damping-factor is indeed necessary to give stability to the system. Let us call this damping force (F_{damp}) whose nature depends on the artificial muscle physics. The full artificial muscle model force F_{dyn} versus length x can now be defined as follows :

$$F_{dyn} = uF_{max} \left(1 - \frac{x}{x_{max}} \right) - F_{damp}(u, x, \dot{x}) \text{ with } 0 \leq u \leq 1; 0 \leq x \leq x_{max} \quad (4.2)$$

Here, the assumption is made that the artificial muscle drives a given load M against gravity and that during contraction its own mobile weight is equal to m . The following dynamic equation of the artificial muscle with the load can be deduced :

$$uF_{max} \left(1 - \frac{x}{x_{max}} \right) - F_{damp}(u, x, \dot{x}) - Mg = (M + m)\ddot{x} \quad (4.3)$$

This equation can be normalized by dividing all terms by F_{max} ; we deduce the follo-

wing equation in which $r_m = mg/F_{max}$, $r_M = Mg/F_{max}$ and $r_{damp} = F_{damp}/F_{max}$:

$$u \left(1 - \frac{x}{x_{max}} \right) - r_{damp} - r_M = (r_M + r_m)(\ddot{x}/g) \quad (4.4)$$

Specifying the damping force can be particularly complex due to the soft character of the artificial muscle and to shape changing of materials during muscle contraction. In the framework of our study, a simplified model is considered corresponding to a linear viscous friction force whose constant coefficient will be noted by f_v :

$$F_{damp}(\dot{x}) = f_v \dot{x} \quad (4.5)$$

However linear or nonlinear may be the damping component, this dynamic model is essentially nonlinear due to the presence of the term in ' ux '. The fundamental idea of our approach consists in considering this term as a kind of nonlinear proportional action term and to close the positioning loop by a pure integral action term of constant k_I -parameter. Considering a desired x_d -position (constant or variable) and substituting the corresponding closed-loop u -control into Eq. (4.4) leads to :

$$K_I \left[\int_0^t (x_d - x) dt \right] \left[1 - \frac{x}{x_{max}} \right] - r_{damp} - r_M = (r_M + r_m)(\ddot{x}/g) \quad (4.6)$$

Time derivative of this equation (Eq. (4.6)) with respect to time will give :

$$K_I \left[\int_0^t (x_d - x) dt \right] \left(-\frac{\dot{x}}{x_{max}} \right) + K_I (x_d - x) \left(1 - \frac{x}{x_{max}} \right) - \frac{dr_{damp}}{dt} = (r_M + r_m)(\ddot{x}/g) \quad (4.7)$$

Let us assume that the closed-loop system is stable and that, during contraction, u remains lower than 1 and x lower than x_{max} : when t tends to infinite, x tends to some x_∞ - with all derivatives equal to zero - given by following equation :

$$K_I (x_d - x_\infty) \left(1 - \frac{x_\infty}{x_{max}} \right) = 0 \rightarrow x_\infty = x_d \quad (4.8)$$

In order to check the possibility to converge towards the desired x_d -position and to analyze the performances of the I-controller during the transient phase, the artificial muscle model with the linear viscous damping is simulated in response to a desired position step from zero to $x_d = 7cm$, while $x_{max} = 10cm$, by considering a viscous ratio $(f_v/F_{max}) = 0.5s/m$. Moreover, in order to take into account the signal transmission during the initial setting up of the control, a first order term $(1 - e^{-t/T})$ with $T = 0.05s$ was added to it. Fig. 4.1 shows the results obtained for a load/maximum force-ratio $r_M = 0.1$ while $r_m = 0.05$ and various values of the k_I -parameter. The system appears to be largely stable. $k_I = 10m^{-1}s^{-1}$ appears as a good compromise to have a faster response with no overshoot. The stability analysis and the method used for finding proper gains are discussed in the appendix C. Fig. 4.2 shows the effect of load-variation for this imposed k_I -parameter : response time and overshooting depend on the load but no instability appeared.

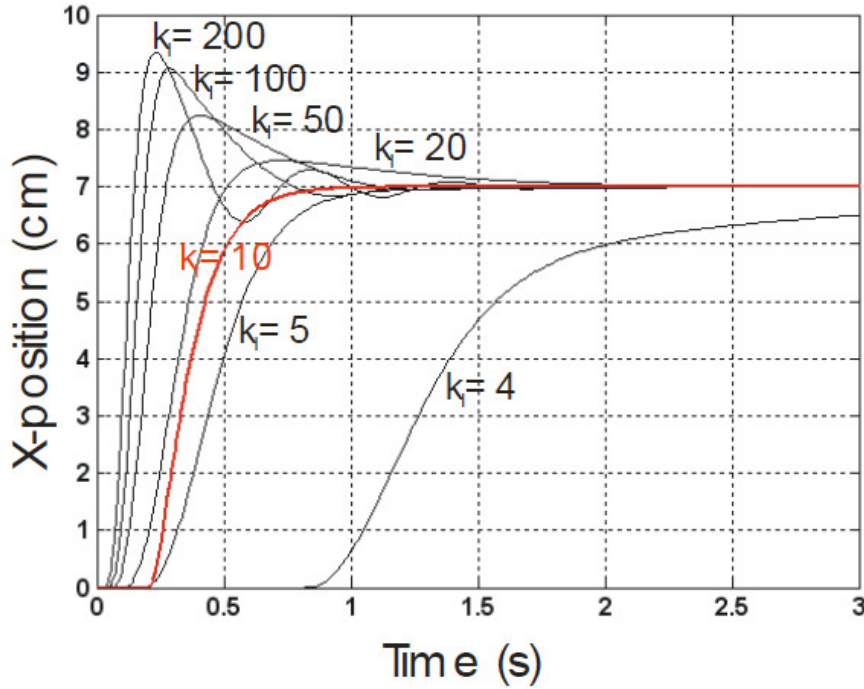


FIGURE 4.1 – Simulation of the closed-loop control of the muscle model with a k_I -single integral action for a 7cm -position step. The plots show the effect of k_I -variation in the case of the linear viscous friction model.

The above experiments and simulations constitute an attempt to see the possibilities of proposing a simple and generic control method for a wide range of McKibben muscles. These experiments were done for demonstration purpose rather than actual implementation on our real robot. It is also important to note that this model cannot be considered as an accurate dynamic model of the McKibben artificial pneumatic muscle, due to the fact that the static relationship of Eq. (4.1) is too far away from the real tension-length curve of a McKibben muscle. But, according to us, this model is sufficient to put into light the dynamic performances of the artificial muscle contraction resulting from the proposed friction model. For the implementation of the controller on our real robot, we have used the model proposed in Chapter 3. In the next section, PID controllers using the model of the muscle and the model of the entire robotic arm are presented.

4.2.2 Model based PI controller

Open loop At any joint, a pressure supply to the muscles (ΔP in the case of SISO model of the joint) generates the torque τ which ultimately actuates the joint. Considering that the pressure increment ΔP is the input and the joint angle q is the output, a simple schematic of an open loop robot model can be shown as in Fig. 4.3. With the knowledge of the model of the muscles and structure of the manipulator, it is possible to express the inverse position-pressure relationship

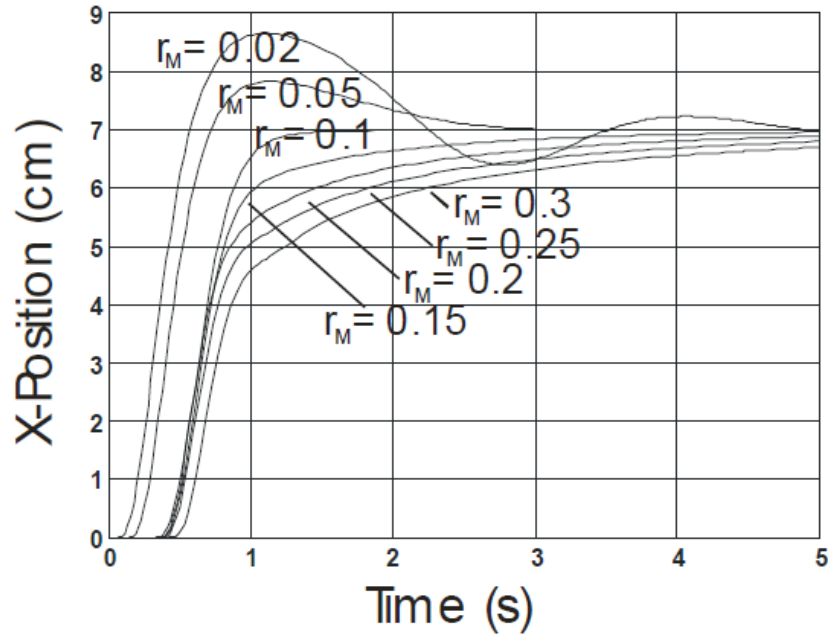


FIGURE 4.2 – The plots show the effect of load variation in the linear viscous friction case for $k_I = 10m^{-1}s^{-1}$.

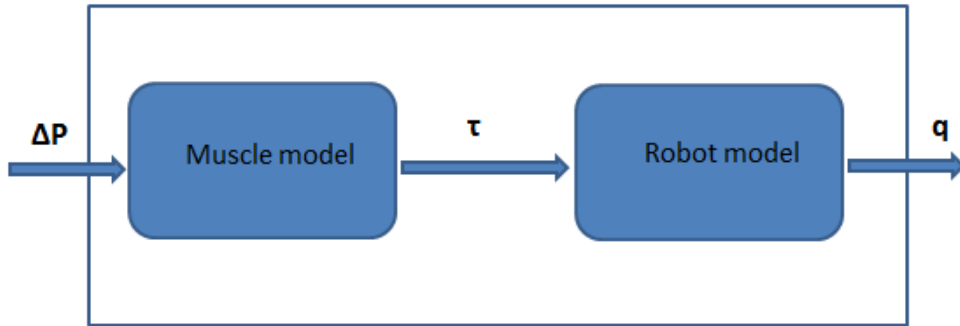


FIGURE 4.3 – Schematic of an open-loop anthropomorphic arm which encapsulates the muscle dynamics and the rigid manipulator dynamics.

which can be schematically presented in Fig. 4.4. In all of our control strategies, position control is preferred. It is well known that a torque control loop with real torque feedback could improve the control quality. In this case, exact modeling describing the behavior of the actuator can be avoided and also the hysteresis and non-linearity could be controlled. But these benefits will come at the cost of the additional torque/force sensors, their IO interfaces with computer and effort of placing wires and sensors into the robotics structure. Therefore, position control is preferred in all our control strategies instead of torque feedback loop. The torque

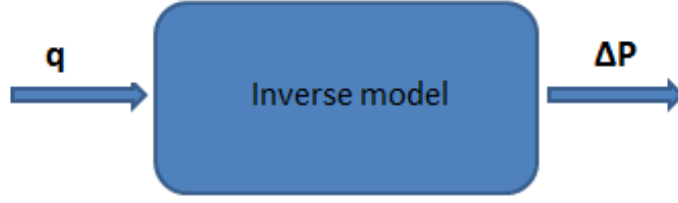


FIGURE 4.4 – Schematic of inverse position-pressure relationship for a joint.

is estimated using our actuator model. In fact, this model-based estimated torque is embedded inside the inverse position-pressure block in Fig. 4.4.

The controller for a robot such as the one used in our work, is expected to be fast and robust. A conventional PI controller is investigated to deploy for this task. The PID controller can be implemented simply by summing the positional error (deviation from of the measured position from the reference), its derivative and integral (See Fig. 4.5). It is observed that this method is able to control the

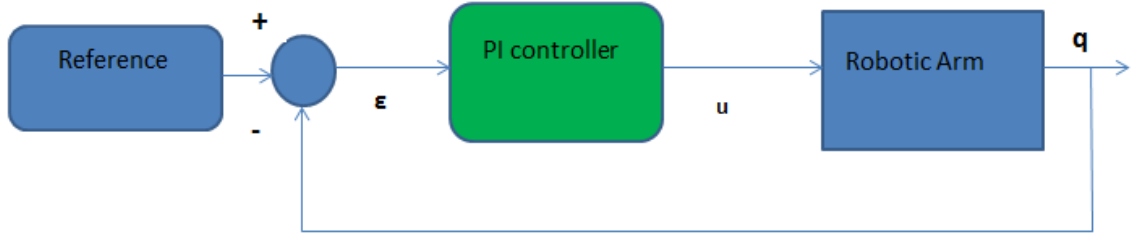


FIGURE 4.5 – Schematic of close loop PI position controller with no feed-forward term.

robot when the motion is very slow, for an example : tracking a ramp with a very small slope. But it is failed to track any rapidly varying trajectories. Moreover, any small disturbance can blow off the system. So, a simple PI controller is not robust and finding a stable controller with good margin is not an easy task. To resolve this problem, a feed-forward PI controller is proposed. The feed-forward term is calculated using the inverse position-pressure block. The block will give a reference pressure with respect to a desired position which is given to the block as an input. The proposed PI controller structure is shown in Fig. 4.7 and expressed mathematically by Eq. 4.9

$$u(t) = \Delta P_{des} + K_p(e(t)) + K_i \int_0^t (e(t))dt, \quad (4.9)$$

where, $e(t) = q_{des} - q(t)$, K_p and K_i are proportional and integral gains respectively.

This method makes use of the knowledge of the model through its feed-forward

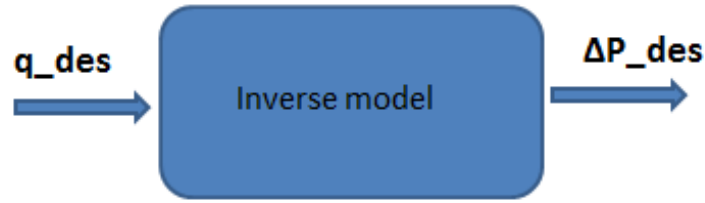


FIGURE 4.6 – This inverse model block generates desired command pressure from the desired joint position for each joint using inverse position-pressure relationship.

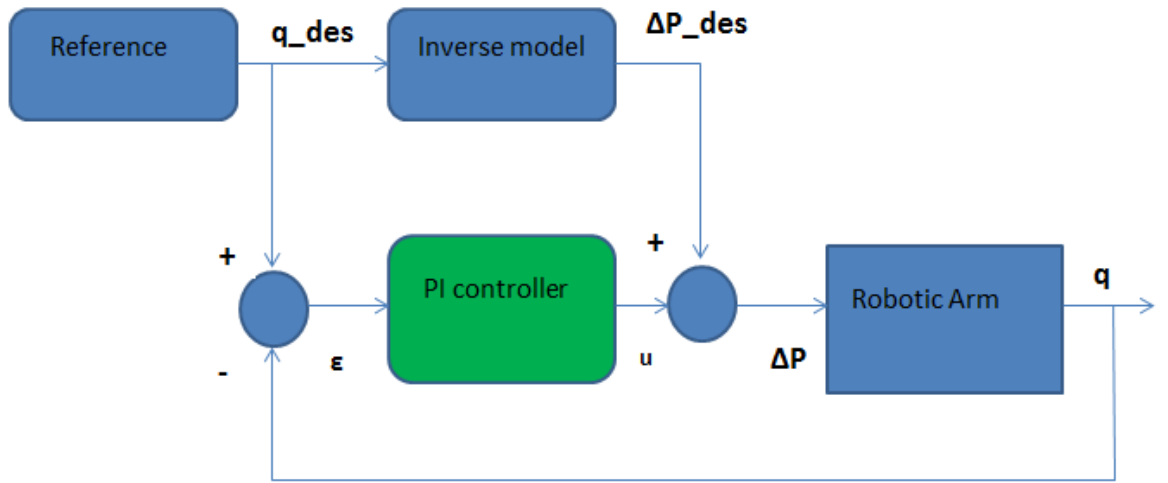


FIGURE 4.7 – Schematic of close loop PI position controller with ΔP_{des} as feedforward term.

block. Then a PID controller designed in this way was found to be much more robust and stable. However, an overshoot can be easily observed in step response. Also the PID controller seems to be stiff and fails to capitalize the benefits of inherent compliance in the muscles.

On the other hand, iLQR approach is known to have the capability to perform predictive control and to tackle the non-linearity in the model [Li 2007], [Tassa 2013]. Moreover, the optimization framework within the iLQR approach could enable the robot to optimize the trajectory in order to make good use of the inherent compliance of the muscles to perform various explosive movements [D.Braun 2013]. Since our goal is to show the capabilities of a pneumatic actuators based robot to perform highly explosive motion like throwing or kicking a ball, the iLQR approach is preferred. The fundamental principle and the basic algorithm is described in the next section. O

4.3 iLQR control of the anthropomorphic pneumatic arm

This section presents the optimal control framework used to find the control sequences to perform a desired task. The optimal control problem is the minimization or maximization of a performance criterion with respect to the control under a set of constraints that arise from the physical limitation of the control action and from the plant dynamics.

4.3.1 State space representation

Let us represent the dynamics stated in Eq.(3.24) and Eq.(3.25) in state space form considering the state vector as $x = [q, \dot{q}, P, \dot{P}]^T$.

$$\dot{x} = f(x, u) = \begin{bmatrix} \dot{q} \\ M^{-1}(-C(q, \dot{q}) - G(q) + T(q, P)) \\ \dot{P} \\ -C_p \dot{P} - G_p P + G_p u, \end{bmatrix} \quad (4.10)$$

where, f is the non-linear function given by Eq.(4.10) in state x and control u that gathers Eq.(3.24) and Eq.(3.25). In the present work, we consider the constraints on the state in the optimal control formulation. There exists a mechanical limit to each degree of freedom of the arm. For the operation to be safe, we have introduced these limits as constraints on the state space inside the cost function of the optimal control formulation. The chosen cost function for the state space constraints is expressed by the following equation :

$$C_s = e^{\lambda * max} + e^{\lambda * min} \quad (4.11)$$

where,

$$\begin{aligned} max &= 1 - \lambda(x_{max} - x), \\ min &= 1 - \lambda(x - x_{min}), \end{aligned}$$

x_{min}, x_{max} are lower and upper limits on the state and λ is a constant. The above consideration for the cost function will ensure that the cost near the limits will be very high and hence the optimal solution will keep the system within the operating limits.

Also, the control action has to be admissible, i.e $u \in U = [P_{min}, P_{max}]$. The control problem formulation is then expressed as determining an open-loop control input $u = u(t, x) \in U$ which can minimize or maximize a cost function along a given time interval $t \in [0, T]$ and with initial state $x(0) = x_0$. For a non-linear dynamics and non-quadratic cost, optimal control solution can be obtained using full DDP. However, as DDP is computationally expensive, an iterative LQR (iLQR) approach is considered [Li 2007]. The iLQR method relies on linearizing the dynamics and

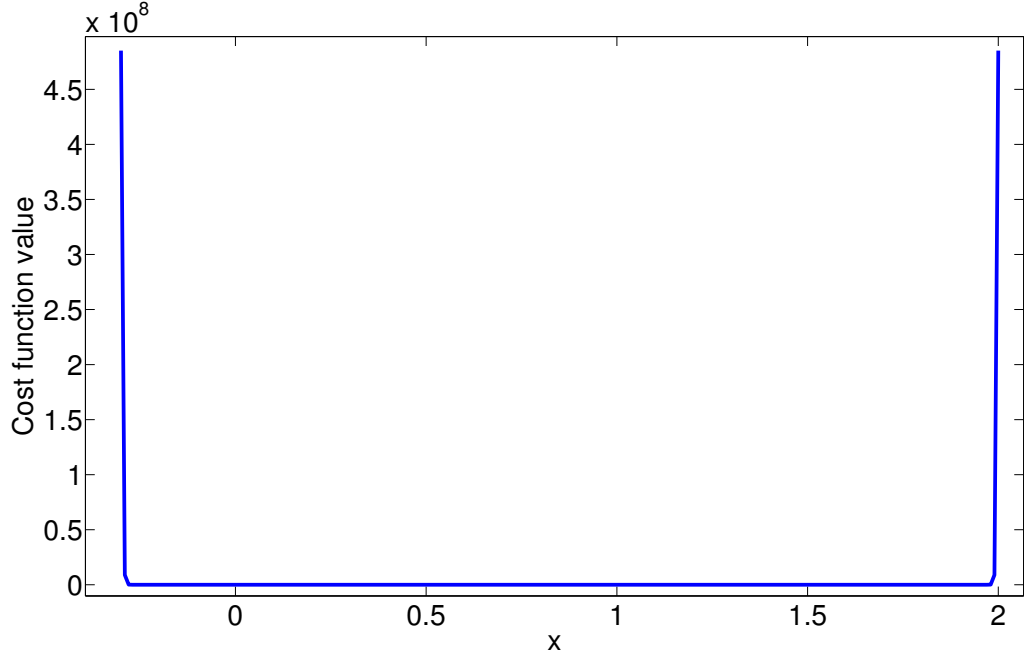


FIGURE 4.8 – State constraints function

approximating the cost function to quadratic form along the x trajectory. This control approach is briefly summarized in the next section.

4.3.2 Iterative Linear Quadratic Regulator (iLQR)

The iterative Linear Quadratic Regulator method (iLQR) is an extension of LQR control. Here, the basic idea is to optimize a whole control sequence starting from any initial state unlike the LQR approach where the optimal control signal is found for the current point in time without any consideration of the future steps. There are basically four steps in this algorithm : Initialization, forward pass, backward pass and control updating. These steps are described in detail after formally defining a generic discrete time dynamical model.

$$x_{t+1} = f(x_t, u_t), \quad (4.12)$$

where $x_t \in X = (x_0, x_1, x_2, \dots, x_N)$ and $u_t \in U = (u_0, u_1, u_2, \dots, u_{N-1})$. The trajectory X is obtained by the application of U on the system with initial state x_0 . In order to consider the future consequences, the total cost function (J) is defined by taking into account the sum of the immediate cost (l) from each state in the trajectory plus the final cost (l_f),

$$J(x_0, U) = \sum_{t=0}^{N-1} l(x_t, u_t) + l_f(x_N) \quad (4.13)$$

The cost-to go function is the sum of the costs from time t to N and is defined as :

$$J_t(x, U_t) = \sum_{i=t}^{N-1} l(x_i, u_i) + l_f(x_N) \quad (4.14)$$

The value function V at time t is the optimal cost-to-go from a given state :

$$V_t(X) = \min_{U_t} J_t(x, U_t) \quad (4.15)$$

From the above equation, it can be said that the optimal cost-to-go is found by using the control sequence U_t that minimizes J_t .

The value function V at the final step is actually the final cost.

$$V(x_N) = l_f(x_N) \quad (4.16)$$

At any previous steps, the value function can be splited and expressed as a function of the current cost and the value function at the next time step :

$$V(X) = \min_u [l(x, u) + V(f(x, u))] \quad (4.17)$$

Having established the definition of various terms used in the algorithm, we can now elaborate the four steps of it.

Forward pass Forward pass means simulating the system from an initial state x_0 by applying the control sequence U to obtain the trajectory (X) through state space. From the trajectory (X, U) , the overall cost of the trajectory can be evaluated. Also in this pass, partial derivatives of the system and the cost function are calculated in order to linearize the dynamics and quadratize the cost function. At each point (x_t, u_t) on the trajectory (X, U) , the partial derivation of the function $f(x_t, u_t)$ is performed with respect to x_t and u_t . Similarly, the first and second partial derivatives of the value functions $l(x_t, u_t)$ and $l_f(x_t, u_t)$ are obtained with respect to x_t and u_t . All of these partial derivative terms are obtained to facilitate the next step of backward pass.

Backward pass Backward pass computes a local solution to the value function Eq. (4.15) using a quadratic Taylor expansion. Let's assume that $(\delta x, \delta u)$ is the perturbation given to the system at (x, u) which results into $Q(\delta x, \delta u)$ as a change in the value function. Thus $Q(\delta x, \delta u)$ can be expressed as in (4.18).

$$Q(\delta x, \delta u) = l(x + \delta x, u + \delta u) + V(f(x + \delta x, u + \delta u)) \quad (4.18)$$

So the second order taylor expansion of Q written as :

$$\begin{aligned} Q_x &= l_x + f_x^T V'_x, \\ Q_u &= l_u + f_u^T V'_x, \\ Q_{xx} &= l_{xx} + f_x^T V'_{xx} f_x + V'_x f_{xx}, \\ Q_{ux} &= l_{ux} + f_u^T V'_{xx} f_x + V'_x f_{ux}, \\ Q_{uu} &= l_{uu} + f_u^T V'_{xx} f_u + V'_x f_{uu}. \end{aligned} \quad (4.19)$$

V' is the value function at the next time step. With the given taylor expansion of Q , the optimal control modification δu^* for the state perturbation δx is obtained by minimizing the quadratic model :

$$\delta u^*(\delta x) = \min_{\delta u} Q(\delta x, \delta u) = k + K \delta x. \quad (4.20)$$

This results into a local linear feedback policy with two terms. The first term k is the feed-forward term and the second term $K \delta x$ is the state feedback whose gains are expressed in (4.21).

$$k = -Q_{uu}^{-1} Q_u \text{ and } K = -Q_{uu}^{-1} Q_{ux} \quad (4.21)$$

Substituting this policy back into Eq. (4.19) with some mathematical manipulation will give the quadratic model of V , which can be expressed in Eq. (4.22) as follows :

$$\begin{aligned} V_x &= Q_x - K^T Q_{uu} k, \\ V_{xx} &= Q_{xx} - K^T Q_{uu} K. \end{aligned} \quad (4.22)$$

The backward pass proceeds with the initialization of the Value function with the terminal cost and its derivatives $V(x_N) = l_f(x_N)$ and then Eq. (4.20) and Eq. (4.22) are recursively computed.

Updating the control signal After the backward pass, k and K can be obtained which will give the optimal control value. Whether this update will be accepted, rejected or modified depends on the evaluation of the resulting new trajectory denoted by (\hat{X}, \hat{U}) . So a forward pass is done and the cost is recorded.

$$\begin{aligned} \hat{x} &= x_0 \\ \hat{u}_t &= u_t + \alpha k_t + K_t(\hat{x}_t - x_t) \\ x_{t+1} &= f(\hat{x}_t, \hat{u}_t). \end{aligned} \quad (4.23)$$

where α is a backtracking search parameter. It is set to 1 initially and then iteratively reduced. If the cost of the new trajectory (\hat{X}, \hat{U}) is less than that of the previous trajectory (X, U) then the control is updated to $U = \hat{U}$. The backward-forward process is repeated until the new cost is below a certain threshold and then it will be assumed that the final trajectory converges to the locally optimal trajectory. Also

in order to ensure a good descent direction in all cases even while inverting Q_{uu} , a regularization term is usually embedded. This regularization and backtracking terms are determined by the Levenberg-Marquardt heuristic. The summary of this algorithm is presented in Algorithm. 1

Algorithm 1 ILQR ($u_t, x_i, x_N, Q_N, Q, R, dt, n_{Iter}$)

```

 $cost_{curr} \leftarrow \text{ILQRCost}(u_t, x_i, x_N, Q_N, Q, R, dt)$ 
for  $j = 1, \dots, n_{Iter}$  do
     $\delta u \leftarrow \text{ILQRIterate}(u_t, x_i, x_N, Q_N, Q, R, dt)$ 
     $u'_t \leftarrow u_t + \alpha \delta u_t$ 
     $cost_{new} \leftarrow \text{ILQRCost}(u'_t, x_i, x_N, Q_N, Q, R, dt)$ 
    if  $cost_{new} - cost_{curr} < cost_{threshold}$  then
        TerminateIteration
    end if
     $cost_{curr} \leftarrow cost_{new}$ 
     $u_t \leftarrow u'_t$ 
end for
return  $(u_t^{opt}, cost^{opt})$ 

```

4.4 Conclusion

In this chapter, our goal was to introduce the relevant control strategies that are considered in our work. We have presented a very brief review of several methods to control pneumatic systems and the difficulty faced by all of those methods due to the highly nonlinear nature of the system. It was then interesting to see the possibility of a generic control method independent of the model, so that it can be used for a wide range of the Mckibben muscles. The proposed method using a single Integral action is appealing theoretically and can even be verified experimentally on a single Mckibben muscle but the response is comparatively slower when it is compared with a full three gains PID controller. We then come up with a PI controller with a feed-forward term which encapsulates the model of the muscles and the robotic arm. This approach, so far, gives the better result but it comes at the cost of overshooting and stiff movement. Finally, the iLQR approach is presented which is known to deal with the non-linear model by linearizing the dynamics and cost function along the trajectory. In Chapter 5, various simulation and experimentation results using these control strategies will be presented.

Simulation and Experiments

Sommaire

5.1	Open loop simulation of the robot	81
5.2	Close loop control with PI controller	83
5.2.1	Trapezoidal trajectory tracking	83
5.2.2	Sine wave trajectory tracking	84
5.3	Application of iLQR in performing explosive motion	85
5.3.1	Task 1 : Position control	86
5.3.2	Task 2 : Maximizing the link speed	88
5.3.3	Task 3 : Maximizing the end effector speed	88
5.3.4	Task 4 : Ball throwing and kicking	89
5.4	Conclusion	92

The experimental set up considered here is the manipulator of LAAS CNRS which is an anthropomorphic arm of seven degrees of freedom (DoF), where each joint is pneumatically actuated by a pair of McKibben muscles. In the experiment presented in this paper, only two joints are controlled. These joints are the flexion θ_1 at the shoulder and the flexion θ_2 at the elbow (see Fig. 5.1). So, for the experiments, the robot can be viewed as a 2 DoF manipulator with state defined by $x = [\theta_1, \dot{\theta}_1, \theta_2, \dot{\theta}_2]^T$. Each muscle is pressurized by an I/P converter which converts a current command to a reference pressure value. The chapter is dedicated to report various results obtained by performing several experiments on the real robot and simulations using the robot model. These experiments are carried out to understand the robot behavior, evaluating the accuracy and the significance of the proposed model and evaluating different control strategies used to control the system.

5.1 Open loop simulation of the robot

The first experiment is done by supplying a constant pressure as a step input. It is tested on the robot with only one link (the elbow joint). The typical response of the joint is shown in Fig. 5.2

The step response of the robot is then compared with the step response of the proposed model. There are no force and torque sensors on the robot. The validation mainly relies on the encoder measurements. The torque generated by the muscles spanning over the joint is coming from our proposed model of muscle dynamics and

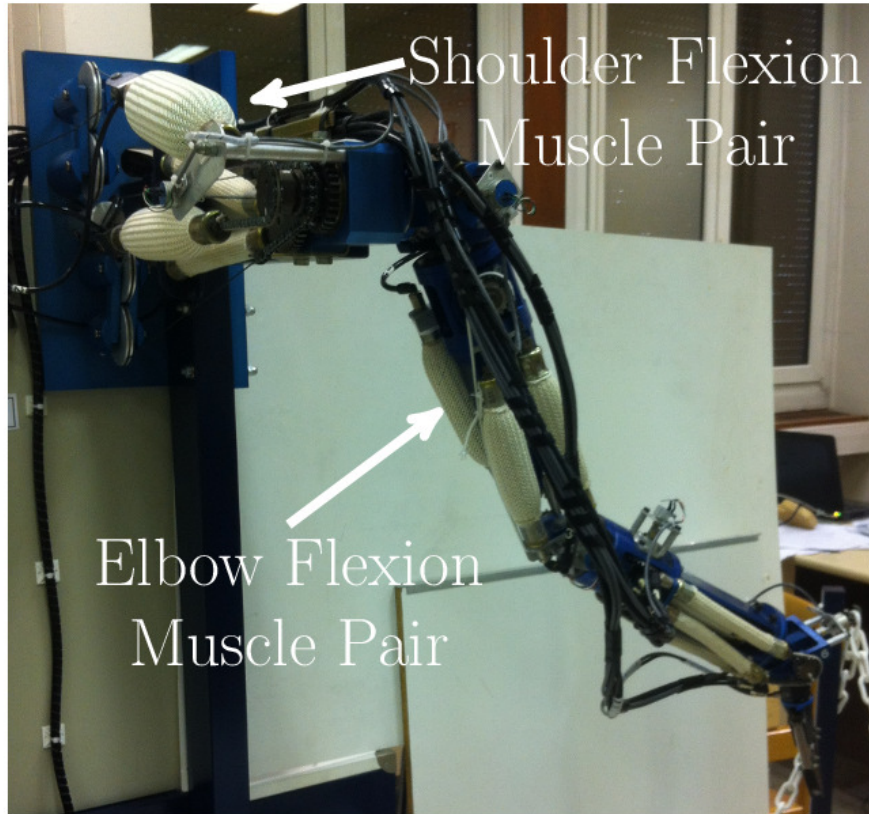


FIGURE 5.1 – Picture of the robot-arm showing the two pairs of muscles, in shoulder and elbow flexion.

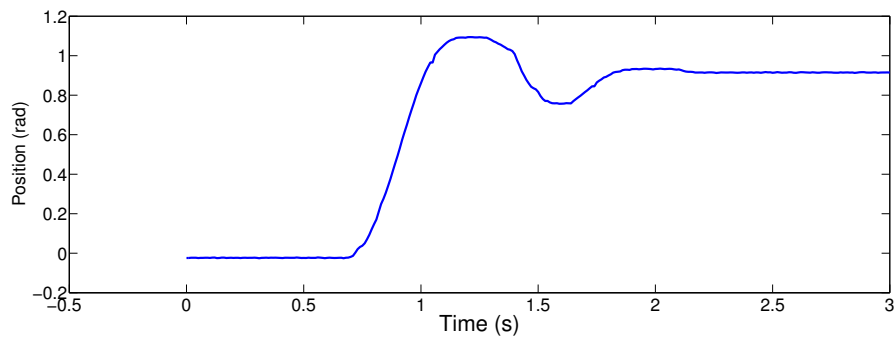


FIGURE 5.2 – A typical step response of a joint when both agonist-antagonist muscles actuating this joint are fed with $\Delta P = 1.5bar$ pressure as a step input.

the pressure dynamics as mentioned in the modelling chapter. The model used here for a single link can be expressed as :

$$\tau_{ext} - f_v \dot{\theta} - G(\theta) = I_M \ddot{\theta} \quad (5.1)$$

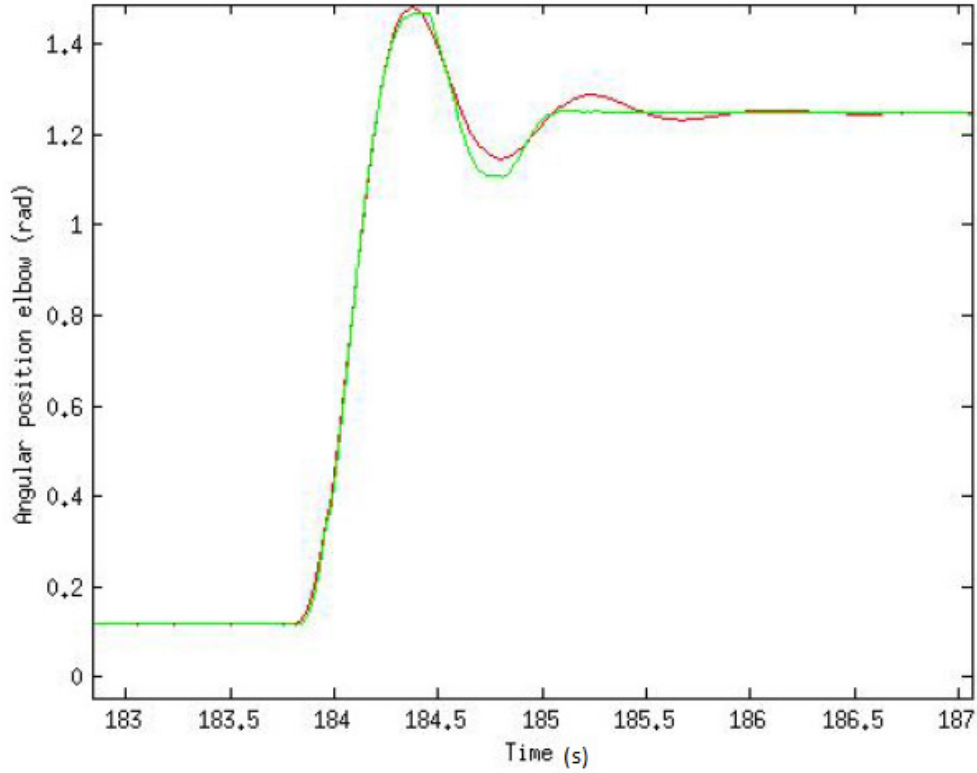


FIGURE 5.3 – Step response of the elbow joint (Green) and response of the model of the elbow joint (Red) at 2 bar.

The parameters used in the experiments are either estimated or measured. For the elbow joint, f_v is found to be 0.8. The estimation of the inertia of the link and viscous parameters are obtained through CAD model and least square estimation.

5.2 Close loop control with PI controller

In this section, some important results are reported to show the effectiveness of a feed-forward PI controller. The experiments are done on the elbow joint of the robot. The joint is subjected to track two different trajectories : Trapezoidal trajectory and sine wave trajectory.

5.2.1 Trapezoidal trajectory tracking

A reference trajectory in the form of a trapezoid (in a position-time plot) is given to the joint. Based on the model of the actuator, feed-forward term generates a desired ΔP pressure trajectory corresponding to the reference position trajectory. The PI controller then uses the position feedback to compensate the model error. We have got a very good results with this approach as shown in Fig. 5.4

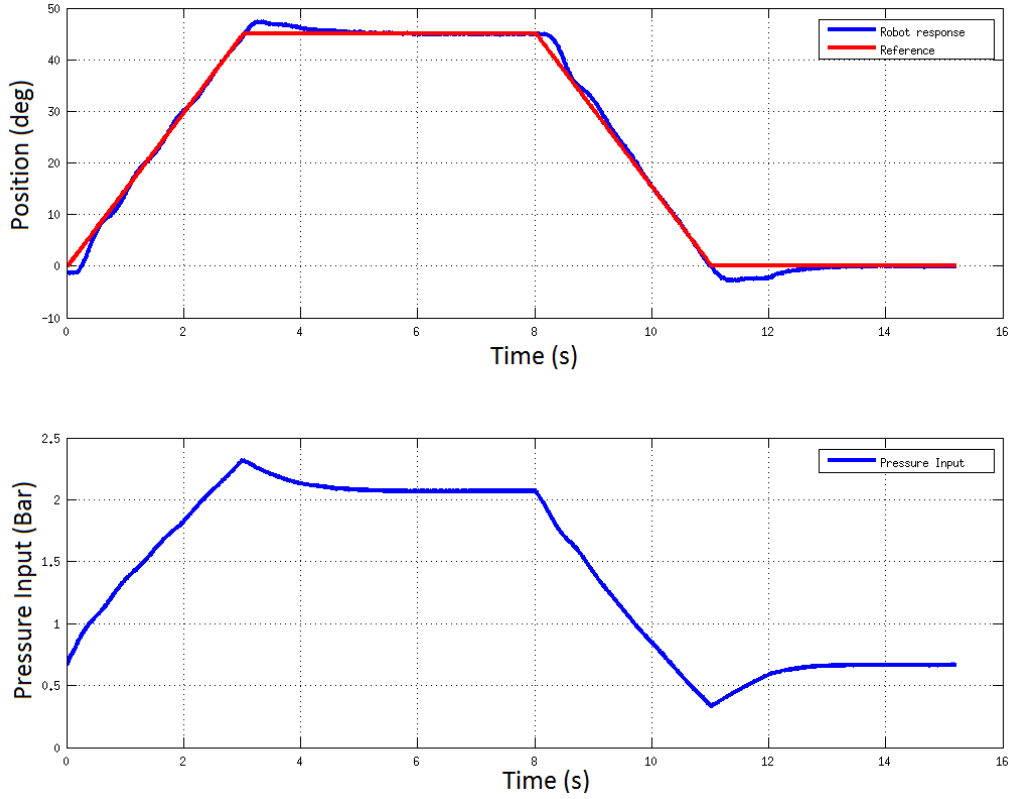


FIGURE 5.4 – Close loop response of the elbow joint (Green) while tracking a reference trajectory (Red).

5.2.2 Sine wave trajectory tracking

A sine wave trajectory is given as a reference to be followed by the elbow joint. Since this joint cannot move backward i.e. the angular position θ cannot be negative, the proposed sine trajectory is $30 + 20\sin(2\pi ft)$ with amplitude of 20 deg and $0.1Hz$ frequency.

It is evident from Fig. 5.5 that the tracking result is quite promising at this frequency. However, it is observed that the tracking performance deteriorates with high frequency. It is probably due to the effect of hysteresis which is not considered in the model. So, as long as the frequency is low and the trajectory is slowly varying (less velocity), the effect of hysteresis would be less and the model would be more accurate. The hysteresis effect will be dealt in detail in the future work. But for now, we are able to track a slowly varying trajectory (up to $0.5Hz$) very well using feed-forward PI controller. Having a simple model of the pneumatic arm which provides us the capability of predicting the future steps, a local optimal control framework (iLQR) is investigated. iLQR control is then used to perform several tasks which are usually embedded in the cost function of the optimal problem. The method is described in detail in Chapter 4. In the next section, various experiments to perform different tasks and their results are presented.

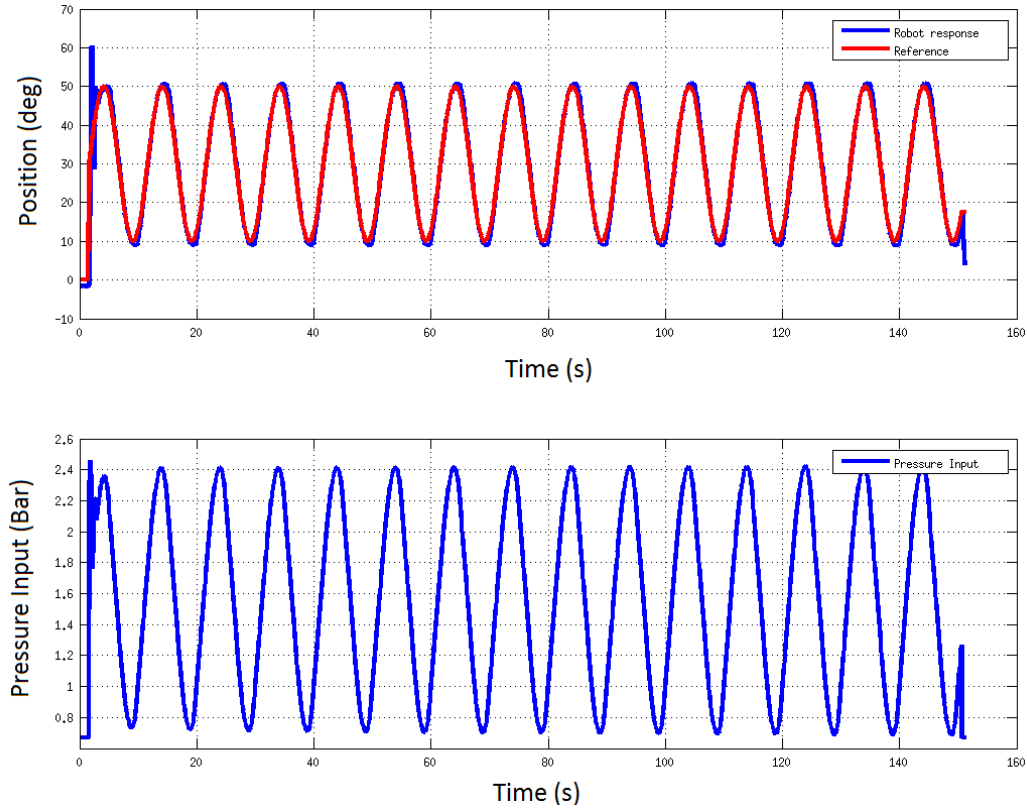


FIGURE 5.5 – Close loop response of the elbow joint (Green) while tracking a reference trajectory(Red).

5.3 Application of iLQR in performing explosive motion

The objective of the experiments is to evaluate the performance of the iLQR control to achieve the following tasks with our multi-link pneumatic robot.

1) Final position control : We aim to compare the quality of the positioning control in the presence of different loads with the iLQR approach and with the feed-forward proportional control. 2) Capability to execute explosive movements by maximizing the link speed at a given time. For this second task we compare simulation results with the results of experiment executed with the real robot. For each task, we analyze the stiffness modulation and we show that the optimal control approach enhances the explosive motion capabilities by simultaneous modulation of position and stiffness. In order to do that, two cases of simulations and experiments are considered :

1) Case-I : When the sum of the pressure in the agonist-antagonist pair of muscles at each joint is kept constant, i.e. $P_1 + P_2 = \text{Constant}$.

2) Case-II : When P_1 and P_2 are left independent. In this case, there will be two inputs for each joint.

It is important to mention here that the experiments on the real robot are done in open loop. It is possible that the iLQR framework could be used to generate a reference trajectory in position and control and then a feed-forward PI controller could be used to close the loop. However, in order to understand and validate our proposed model, we have preferred to continue the experiments by directly feeding the control generated by the iLQR controller.

5.3.1 Task 1 : Position control

The manipulator is given a final position with a load mass of $m_l = 0.1kg$ at the end effector. iLQR is used here to find the optimal path to reach the final goal $(\theta_1, \theta_2) = (28.8, 57.6)$ degrees. The same task is repeated with different load masses of $m_l = 0.1kg$ and $m_l = 1.0kg$ which is shown in Fig. 5.6.

The following cost function is considered for this task.

$$\begin{aligned} C_f &= Q_f(x_{ref}(T) - x(t))^2, \\ C_r &= Q \int_0^T ((x_{ref}(T) - x(t))^2 + u^2(t))dt, \end{aligned} \quad (5.2)$$

where, x_{ref} is the final position for the two joints. The iLQR control uses Eq. 3.10 and Eq.(5.2) to solve for the optimal control sequence u^* . This optimal control sequence in forward application to Eq. 3.10 will yield the needed trajectory. To compare the effectiveness of the iLQR approach, the task is executed using a Proportional-Integral controller with a feed-forward term. The feed-forward term gives a desired pressure for each muscle at the joint needed to maintain a desired joint angle. Thus, the control action of the feed-forward PI controller can be defined as follows :

$$u(t) = P_{feed} + K_p(e(t)) + K_i \int_0^t (e(t))dt \quad (5.3)$$

where, $e(t) = x_{ref} - x(t)$, and K_p and K_i are proportional and integral gains respectively. The simulation results are shown in Fig. 5.7. The response of the feed-forward PI controller is shown in black dashed line is compared with the responses of optimal position control in Case-I when $P_1 + P_2 = Constant$ (blue lines) and in Case-II when P_1 and P_2 are independent (magenta lines)(See Fig. 5.7).

From the position plots in Fig. 5.7, it appears that the iLQR approach gives a good compromise between keeping the stiffness low and minimizing the oscillations which results into a smooth motion. However, the feed-forward PI controller makes joint 1 very stiff and joint 2 very flexible leading to an overshoot and oscillations.

As discussed in section Chapter 3, the stiffness can be adjusted for the same equilibrium position by changing the sum of pressures in the agonist-antagonist pair of muscles. As the sum increases, stiffness at the equilibrium increases which can be observed at each joint (blue and brown lines in stiffness plots).

In order to find the most compliant position trajectory, i.e to find the best sum of pressure in the agonist-antagonist pair, P_1, P_2 are left independent and Eq.(3.20) has two independent inputs for each joint. In this case, the optimal solution gives

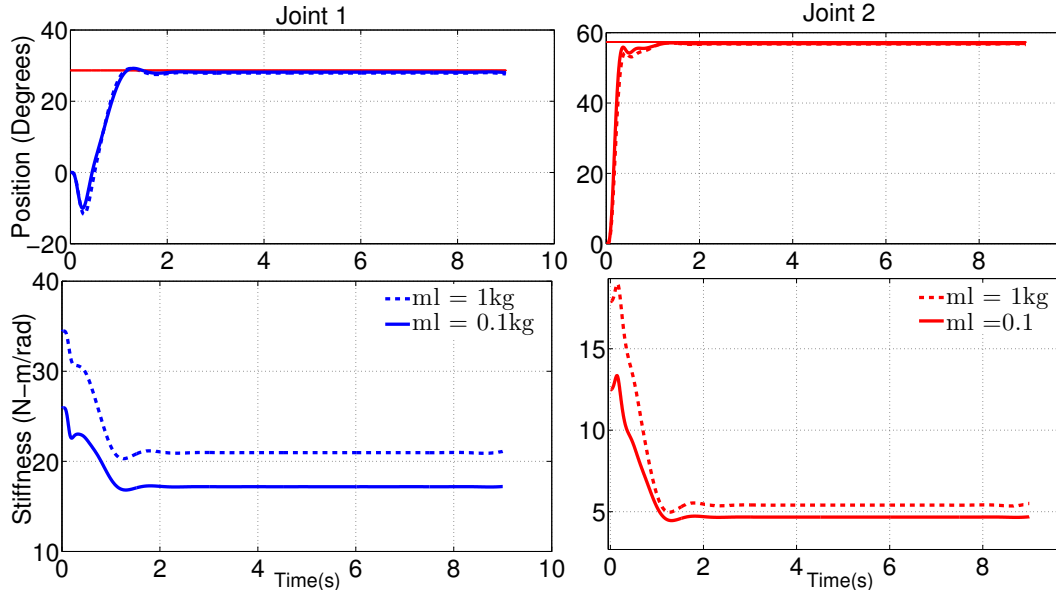


FIGURE 5.6 – Figures on the left side represent the position response and stiffness variation at joint 1 and figures on the right side represent the same for joint 2 in order to reach the target $(\theta_1, \theta_2) = (28.8^\circ, 57.6^\circ)$. The plots compare the response of the joints and the stiffness profile when the end effector is loaded with mass 0.1kg (solid line) and 1.0kg (dashed line). For the heavier load, optimal control gives a stiffer stiffness profile.

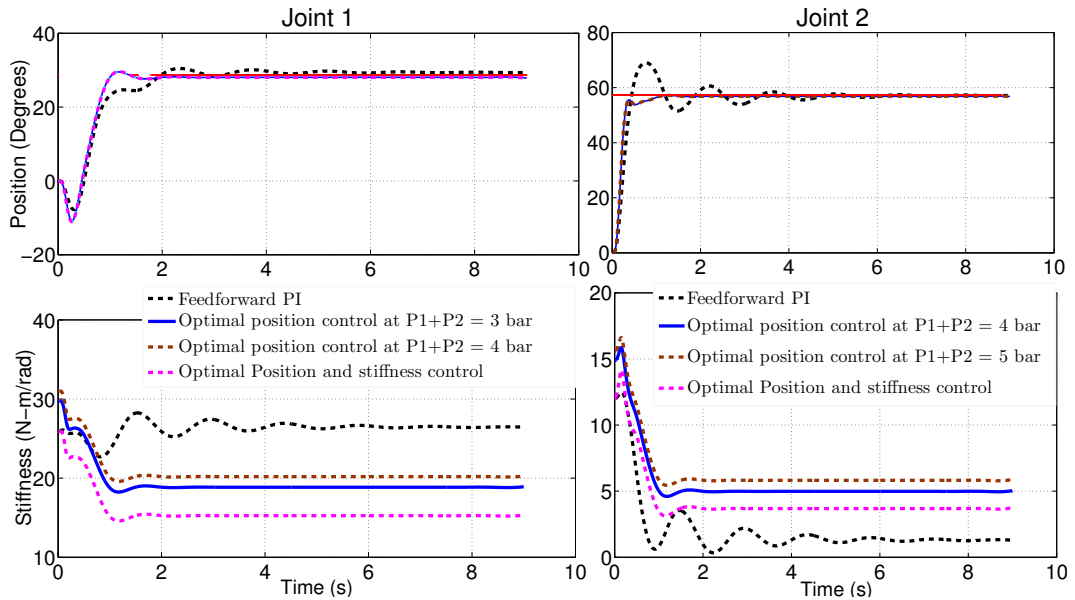


FIGURE 5.7 – Figures on the left side represent the position response and stiffness variation at joint 1 and figures on the right side represent the same for joint 2.

the similar optimal position trajectory but with better stiffness profile (magenta line in stiffness plot in Fig. 5.7). Here, the better stiffness profile is not too stiff to loose the inherent compliance nature of the Mckibben muscle actuated joint and not too highly compliant in order to avoid oscillation and poor position control.

5.3.2 Task 2 : Maximizing the link speed

The objective is to execute some explosive motions with the aim to perform, in the future, tasks such as ball throwing, kicking or hammering a nail. Such motions would require either maximizing the joint/link speed or end-effector speed [Garabini 2011], [D.Braun 2013]. Here, two sub-tasks are presented :

1) Maximizing the angular speed of the elbow joint. The task is first simulated and then executed by the real robot. A comparison between simulation and the experimental results are shown in Fig. 5.8.

2) Maximizing the end effector speed : The objective of this task is to achieve maximum end-effector speed at terminal time T . Simulations are done for both Case-I ($P_1 + P_2 = \text{Constant}$) and Case-II (P_1 and P_2 are independent).

5.3.2.1 Maximizing the angular speed

For maximizing the elbow joint's angular speed at final time $T = 1$, the task requires only the terminal cost, C_f . But to minimize the control effort, a running cost C_r involving only control pressures is used.

$$\begin{aligned} C_f &= -Q_f(x_4(T))^2, \\ C_r &= Q_u \int_0^T u^2(t)dt, \end{aligned} \tag{5.4}$$

where, $x_4 = \dot{\theta}_2$ is the angular velocity of the elbow joint which constitutes the fourth state variable. Q_f and Q_u are weights for the terminal cost and the running cost respectively. The simulation results are shown in Fig. 5.8

In simulation, the maximum joint velocity which is around -15 rad/sec, is reached at terminal time (See Fig. 5.8). The robot response and the simulation response in position and speed show a good match. However, some discrepancies can be observed. Apart from some modeling error, this difference is probably due to the fact that the constraints on the state vector are not considered in the optimal control problem formulation. This is an improvement that we implemented in the subsequent experiments. Snapshots of the video of the experiment are presented in Fig. 5.9

5.3.3 Task 3 : Maximizing the end effector speed

The objective is to maximize the end-effector speed of the manipulator at terminal time. The cost function, thus, comprises the terminal cost C_f involving the

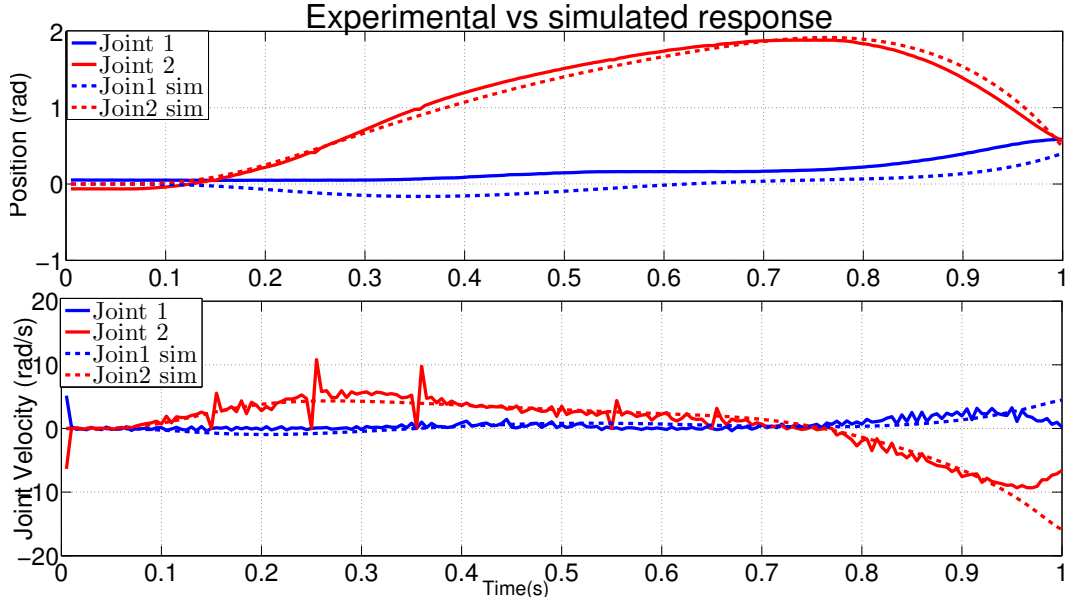


FIGURE 5.8 – Plots on the top compare the robot response (solid lines) with simulated response (dashed lines) at joint 1 (blue line) and joint 2 (red line). Bottom plots compare the velocity response of the robot and the simulation.

end-effector velocity and the running cost C_r involving only control efforts.

$$\begin{aligned} C_f &= -Q_f(f_{vel}(x(T)))^2, \\ C_r &= Q_u \int_0^T u^2(t)dt, \end{aligned} \quad (5.5)$$

where, $f_{vel}(x(t))$ is the function which computes end effector velocity from the robot kinematics. Simulations are done for the following two cases. In Case-I, the sum of pressures in the agonist-antagonistic pair is kept constant. This value is equal to 3 bars at joint 1 and to 4 bars at joint 2 (Fig. 5.10).

In this second simulation (Case-II), we let P_1, P_2 independent (Fig. 5.11).

Comparing the velocity plots and the corresponding stiffness plots in Fig. 5.12, it can be seen that the maximum end-effector velocity has increased from $3.8m/s$ in Case-I to $4.1m/s$ in Case-II. This is due to the fact that in Case-II, the optimal control has the freedom to modulate the compliance with two inputs at each joint and hence it was able to achieve higher speed.

5.3.4 Task 4 : Ball throwing and kicking

The objective is to throw a ball to a maximum distance. The distance to be reached is related to the kinematics of the arm and hence is a function of the state of the arm. The cost function, thus, comprises the terminal cost C_f involving the distance and the running cost C_r involving only control efforts. Also the final time

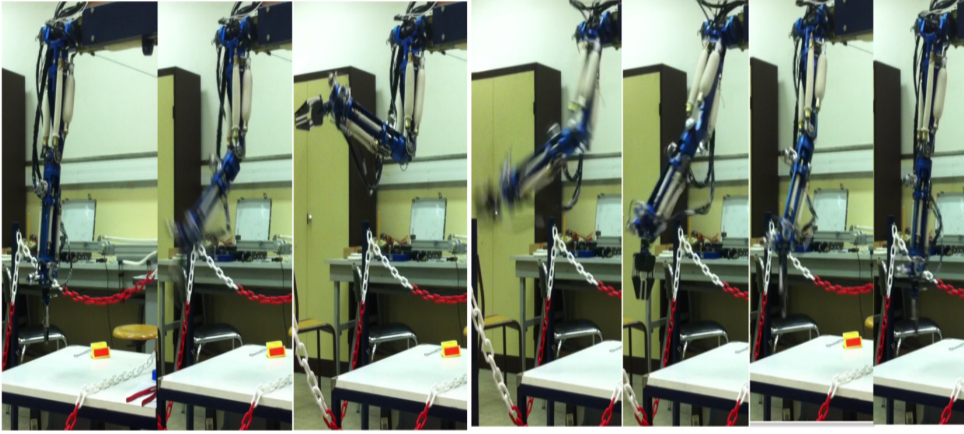


FIGURE 5.9 – The pneumatic manipulator arm executing the task of maximizing the angular speed of the elbow.

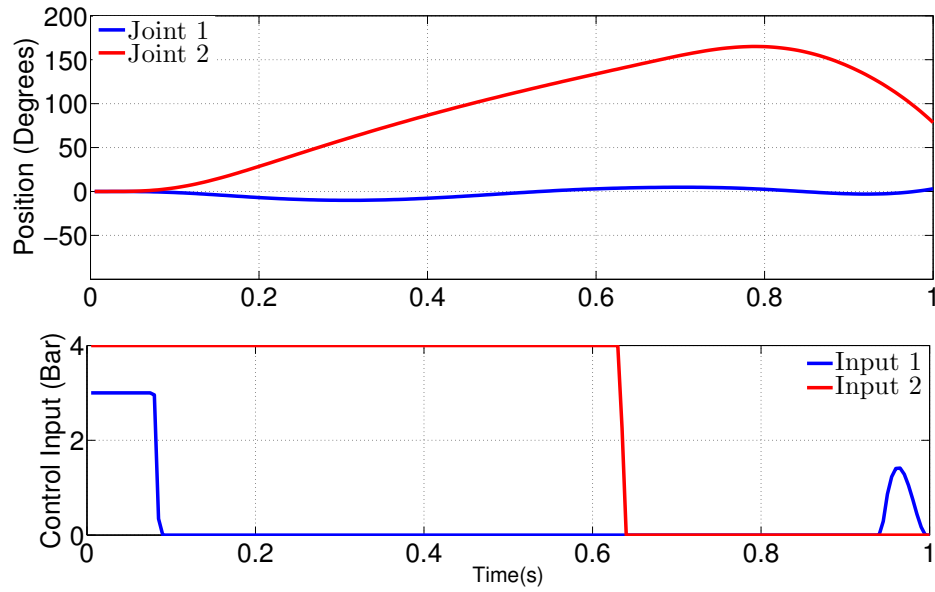


FIGURE 5.10 – Case-I : $P_1 + P_2 = \text{Const.}$ Plots on the top show the simulated position response of joint 1 (blue line) and Joint 2 (black line). Control effort is shown in the bottom plots. The control inputs, Input 1 and Input 2 are applied on joint 1 and joint 2 respectively.

of the motion is fixed at $T = 4$ seconds.

$$\begin{aligned} C_f &= d = kf(x) \\ C_r &= Q_u \int_0^T u^2(t)dt, \end{aligned} \tag{5.6}$$

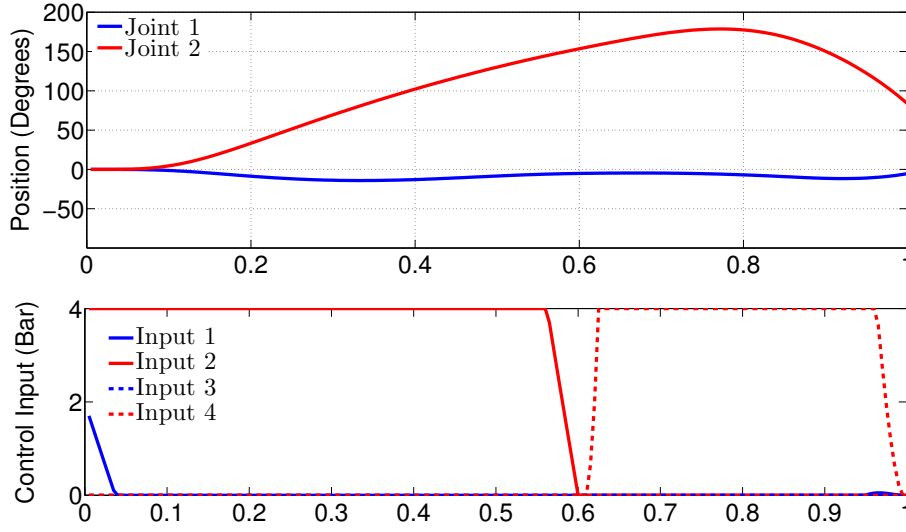


FIGURE 5.11 – Case-II : P_1, P_2 are independent. Plots on the top show the simulated position response of joint 1 (blue line) and joint 2 (black line). Control effort is shown in the bottom plots. The control inputs, Input 1 and Input 3 are inputs to the agonist-antagonist pair at joint 1. The control inputs, Input 2 and Input 4 are inputs to the agonist-antagonist pair at joint 2.

where, $kf(x(t))$ is the function which computes the maximum distance to which the ball will be thrown. This function relates the motion of the ball with the robot kinematics. We used the same cost function in a second experiment for the task of kicking a ball stationed at a point. Snapshots of the video of both the experiments are presented in Fig. 5.13.

Simulations are done for the case where the sum of pressures in the agonist-antagonistic pair is kept equal to 4 bars at the joint 1 and to 4 bars at the joint 2. We present the simulation results when there are no constraints on the state of the robot (Fig. 5.14). However, the robot has limits at its joints which is typically between $[-28.5^\circ, 114.6^\circ]$ in degrees. It is evident from Fig. 5.14 that it is necessary to include the constraints in order to make the real robot execute the task.

Plots in Fig. 5.15 compare the response of the real robot with the simulated response of the model when optimal control inputs are applied in the open-loop. It is interesting to note that the optimal solution given by the iLQR control is somewhat intuitive to the human behaviour. It takes few swings to attain the maximum speed of the end effector before launching the ball. The maximum distance achieved by the ball was 2.3m against 3m predicted by the simulation. The observed discrepancies between simulated and real robot response can be justified by the fact that the system is controlled in open-loop without feedback. Also we have no model of the various effects of hysteresis and dry friction. Moreover, the model of the gripper is not available, so the exact time of opening of the gripper is not known. It has

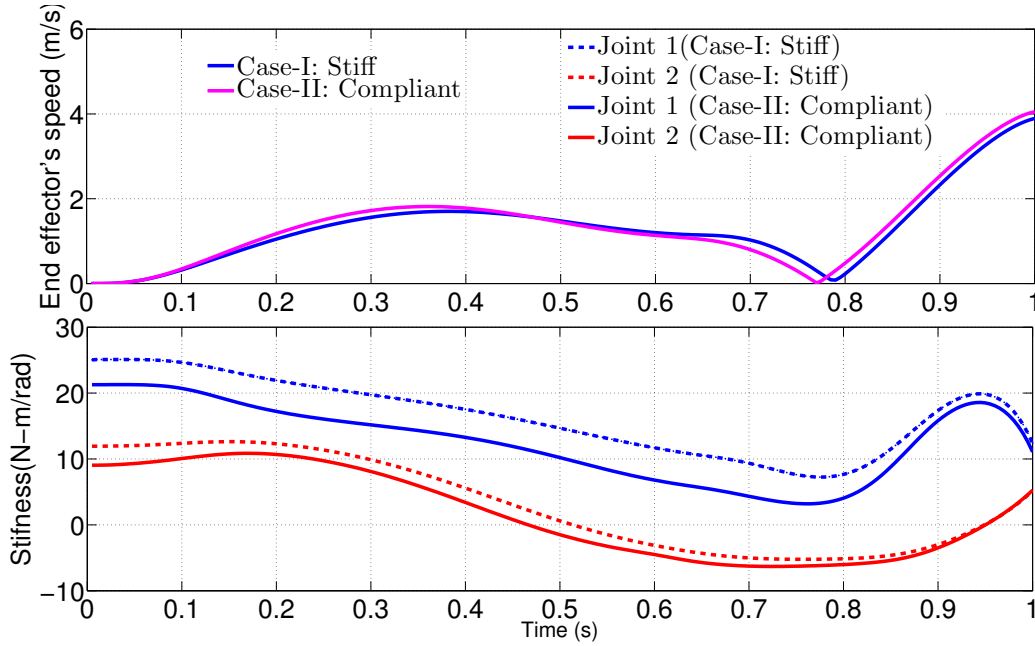


FIGURE 5.12 – Comparison of the stiffness profile of each joint (joint 1 : blue lines, Joint 2 : red lines) in Case-I when $P_1 + P_2 = Const$ (dashed lines) and Case-II when P_1, P_2 are independent (solid lines). It is evident from the plots that the motion in Case-II is indeed slightly more compliant than the motion in Case-I.

been roughly estimated by observation for the ball throwing experiment. Since modeling all the aspects of pneumatic muscles actuators seem to be difficult, it will be interesting in the future to rely on close loop control.

5.4 Conclusion

The various simulations and experiments are carried out in open loop and then in closed loop. From the open loop simulation and its comparison with the real experiment, it can be said that the model is good enough to capture the static and the dynamic behaviour of the actuator. Based on this model, an inverse mapping leads to a feed-forward term. A PI controller with this feed-forward term is very effective in tracking trajectories like line, trapezoid or sine wave. Though, the tracking performance could be enhanced with a better understanding of the physical phenomenon occurring inside the McKibben muscles and the pressure generating valves. Specially, hysteresis modelling is crucial to track trajectories with high velocities. The simplified model, however, makes the iLQR approach feasible for application on the robot. In view of the experiments with the real robot and the comparison with the simulation results, it can be claimed that the model is reliable enough to predict the future steps to be used in the iLQR kind of controllers. This results into smoother tracking and enable the anthropomorphic arm to execute high per-



FIGURE 5.13 – Two experiments have been performed. Left picture is the set-up for the task of kicking the ball while the picture in right is the set-up for throwing the ball.

formance motion which would be very difficult otherwise (with PI controller). Also, experiments are done with both SISO system (ΔP input) and MIMO system (independent P_1 , P_2). Simulations have shown that the iLQR approach has utilized the two inputs to generate a better optimized trajectory with respect to energy and hence is capable to improve the performance of the explosive motion by increasing the throwing speed.

It can be concluded from this chapter that our proposed model is valid enough and can be used in the control of the anthropomorphic arm actuated by the Mckibben muscles. The robot can thus be controlled either by feed-forward control or by means of a more sophisticated receding horizon model predictive controller can also be used.

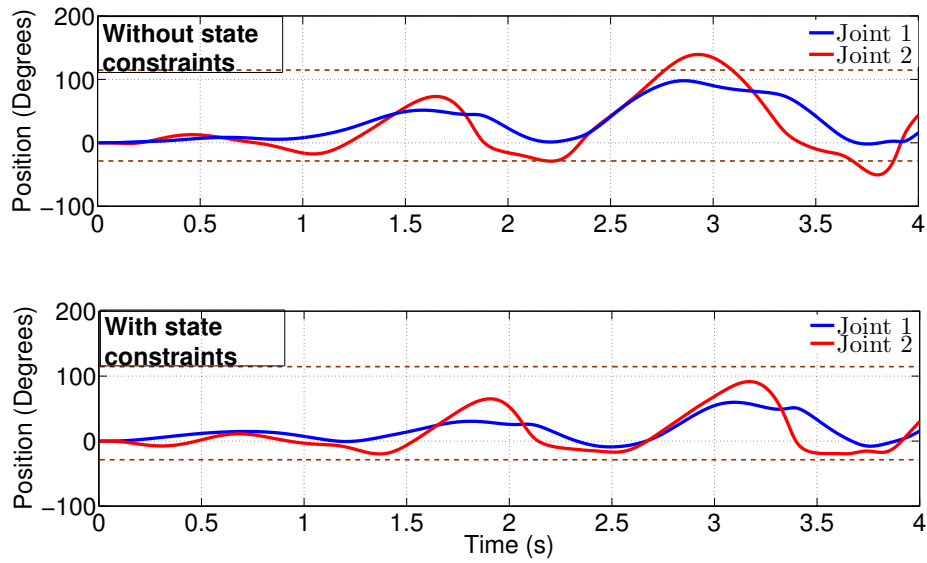


FIGURE 5.14 – Plots on the top show the simulated position response of joint 1 (blue line) and Joint 2 (red line) under no constraints and the plot below presents the same after applying the state constraints. Brown lines are the limits on the state

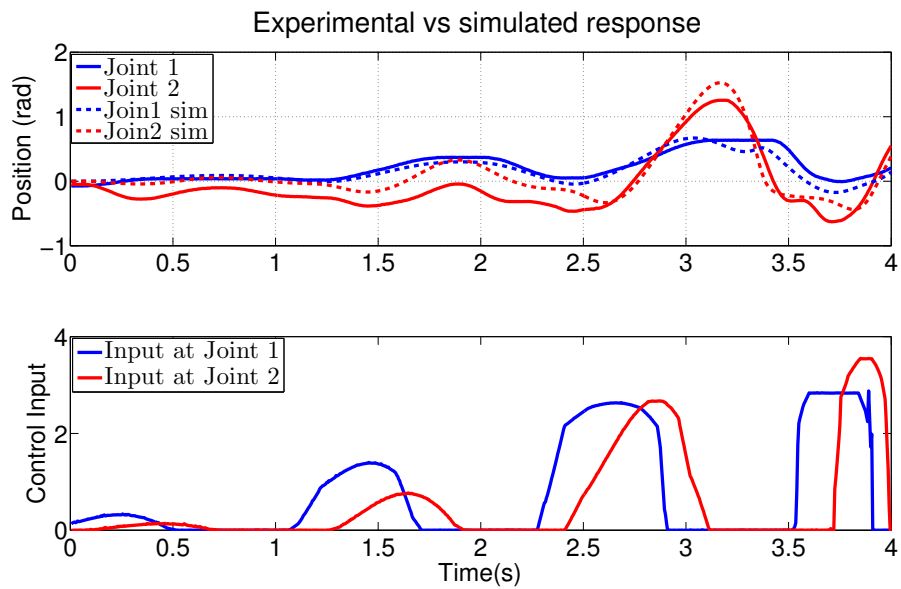


FIGURE 5.15 – Plots on the top show the simulated position response of joint 1 (blue line) and Joint 2 (red line). Control effort is shown in the bottom plots. The control inputs, Input 1 and Input 2 are applied on joint 1 and joint 2 respectively.

Conclusion

Our interest in the scope of this thesis was to explore the potential of alternative actuators than the traditional electric motors. This is in particular inspired from the human musculoskeletal design. It is well known that human utilize the inherent elasticity in the muscle-tendon linking to store energy for later use or optimize the energy to perform tasks efficiently. Also this energy storing capability makes such system shock absorber. From robotics perspective, all of these properties are very interesting. On one hand, energy storage capability will make the robot safe for both the human, the environment and the robot itself while on the other hand it empowers the robot with the capability to perform extreme movements which would be impossible for a rigid robot to do. In the literature various electro-mechanical designs are proposed to acquire such a behaviour. Several different designs have been presented in the state of the art of this thesis. Usually this is achieved by placing an elastic component between the links and the motors. Moreover, in order to even actively control the level of stiffness, additional motors are deployed. These class of actuators (VSAs and AWAS, AMSC etc.), though capable of controlling position and compliance simultaneously, are usually very bulky and complex to be integrated in a full size robot. Its a challenging task to find a best compromise in terms of having variable compliance actuator with simpler and lighter design. The scope of our study also covered a futuristic electroactive polymers based actuator which bends on the application of voltage and thus generates motion. These are very light and may be best suited for micro or nano robots. Finally, the Mckibben muscle based pneumatic actuator is considered in the study due to its similarity with the human muscles and having a very good power to weight ratio. The Mckibben muscles actuate each joint of our anthropomorphic arm in agonist-antagonist set-up. However, modelling such system is not trivial. In fact, this is the problem which has been addressed in depth in our work. A mathematical model was proposed to encompass all the different components of a pneumatic actuator based robots. Simulations and experiments were used to validate the proposed model. The main points that can be concluded from this modeling as the following ones :

- It is possible to model such a non-linear system with quite simple model.
- Pressure generation inside the muscle is approximated by second order differential equation. However, the non-linearity in this model which arises as the natural frequency of the second order differential function is dependent on the instantaneous volume of the muscle, which in turn depends on the instantaneous joint angle.
- The model does not include hysteresis effects due to dry friction in the present study but still, it covers most of the static and the dynamic behavior.

Some of the parameters in the model (usually coefficients in the torque function) are identified using gray box modeling with the knowledge of the dynamics of the system. A combined model of the entire anthropomorphic manipulator is presented as an analogy to the robotic manipulators with conventional electrical motors. The

motor side dynamics are replaced by pressure side dynamics while keeping the structure of the standard manipulator equation (Refer to Eq. 3.24).

A generic model free single-I controller is tested in simulation. Though the results were promising, it is not relevant for practical purposes because of the over simplification of the McKibben system. Moreover, it results into very slower response in comparison to a full three gains PID controller. A PI controller with a feed-forward term which encapsulates the model of the muscles and the robotic arm is used. Although, it has shown overshoot and stiff response, it can be considered as the better option for tracking a reference trajectory (specially when the trajectory is slowly varying). The iLQR controller is used to enable the robot to perform various tasks while utilizing the inherent compliance and energy storing capabilities.

One of the objective of our work was to empower the robot with the capability of performing high performance motion. In order to do so, various simulation and experiments are carried out in open loop and then in closed loop. Following points can be clearly deduced from these experiments :

- Comparison of the simulation of the model and the real robot response confirm that the model is good enough to capture the static and the dynamic behaviour of the actuator.

- A PI controller with this feed-forward term is very effective in tracking trajectories like line, trapezoid or sine wave.

- The iLQR controller application on the robot is made possible by the simplified model. It results into smoother tracking and enable the anthropomorphic arm to execute high performance motions like kicking or throwing a ball. The solution given by iLQR in ball kicking or throwing experiments is very interesting because the kind of trajectory given by the iLQR is quite intuitive to human. A human would most probably chose the similar trajectory for his arm to throw a ball to a maximum distance if he is constrained to optimize the energy as in the case of our robot.

Encouraged by these successful experiments, we are planning to continue our experiments to perform more difficult task like hammering a nail. Also it will be of our interest to consider an improvement of the model by including an hysteresis effect. All of the experiments have been done in open loop. The iLQR generates an optimal control sequence that is fed directly to the robot. In the near future, an MPC scheme would be engaged to use the real time feedback from the robot.

The thesis also present our proposed non-linear model for the dynamic behaviour of the ionic polymer bending actuator. The model is based on the identification of the actuator under the form of a kind of non-linear first-order system with parameters varying with the control voltage. A PI controller was found to be efficient and stable to control the system. The tuning for the two gains of the PI controller was also proposed based on the specification of a safe control voltage range and on the possibility given to the control to reach such safe working limits. Reported results show the relevance of this approach for getting a same couple of gains in the full position range leading to a maximum overshoot of 5% and a response time taking advantage of the imposed safe voltage limits. The limitation of our PI-control

are reached when sharp trajectory curvature changes occur. Future work will focus on improvements in trajectory tracking, especially, with studying the relevance of variable P and I -gains to tackle both with sharp curvature changes and voltage saturation constraints.

I would like to write my thesis in English. The work done in my research could be interesting for various other institutions working on similar topics. In order to reach wider and international audience, this thesis is considered to be written in English. Also, We are inviting jury from different country (Belgium). In addition to that, my french level is not fluent yet and I may not be able to express all my arguments very well in French.

Characterization of PEDOT :PSS Ionic actuator actuators

One can refer the thesis of Simate [Simaite 2015a] in which fabrication and characterization of PEDOT :PSS Ionic actuator is reported in very much detail. Here is presented the different sensors and the experimental set-up used in characterization of the actuator.

The **thickness** of dry and soaked actuators was measured by digimatic indicator (Mitutoyo Absolute) and also estimated from the SEM pictures. SEM images of membranes and actuators were obtained using a Hitachi *S* – 4800 field emission scanning electron microscope (acceleration voltage 800 *V*, working distance of about 5 *mm*).

Resistance and conductivity of PEDOT :PSS was measured between two extremities of each electrode and between two electrodes, by applying 0.1 – 0.5 *V* voltage (with 0.01 *V* increment) and measuring current, using Suss PA200 probe station and Agilent 4142B tester. Conductivity was then calculated assuming dimensions of 2 *mm* x 1.5 *cm* and the thickness measured by SEM not taking into account the PEDOT :PSS in the membrane.

For all **bending characterization** measurements, actuators were placed between two copper electrodes clamped at 1 – 2 *mm* from one end of the actuator. For bending measurements actuators were placed under Leica MZ-12 microscope (Leica Microsystems) with Digital Sight camera system (Nikon) as shown in Fig. A.1. The square voltage wave with various amplitudes and frequencies was generated with Keithley 2450 sourcemeter. Bending was recorded at 100 frames per second, 640x480 resolution. After recording it was converted from raw to 5 frames per second 'mpeg4' encoded video in order to reduce its size. Videos there processed using Matlab Image processing toolbox to track the displacement of actuators tip. The strain was then calculated from tip displacement using formulas proposed by Sugino *et al* [Sugino 2009] :

$$\varepsilon = \frac{2hd}{L^2 + d^2} \times 100\% \quad (\text{A.1})$$

where ε is strain in %, h , L and d are thickness, free length and displacement of the actuator respectively. Thickness of dry actuator, estimated by SEM, was used for calculations.

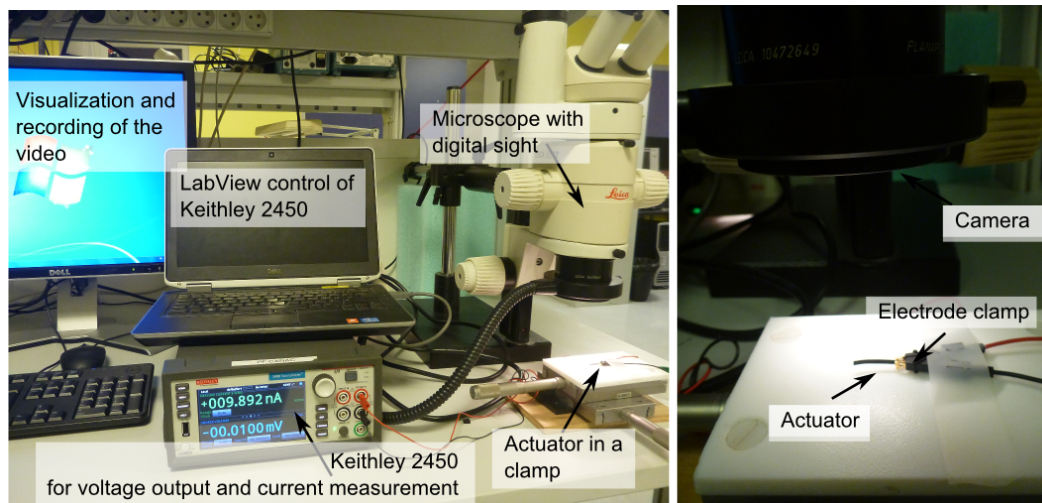


FIGURE A.1 – Picture of the experimental set-up used for bending characterization by recording the bending and tracking the position of the tip

Cyclic voltammetry (CV) measurements were performed using Autolab potentiostat PGSTAT30 (Metrohm Autolab) coupled with NOVA 1.8 Software at room temperature (23 ± 1). Two electrode configuration was adopted (equivalent to the one used for bending characterization), in which two surfaces of PEDOT :PSS were working and reference electrodes. CV measurements were performed at various voltages and scan rates as indicated in the labels of the figures.

Actuator bending for **lifetime measurements** was recorded by laser displacement sensor (optoNCDT 1302, MicroEpsilon) at the position of about 2 mm from the end of the actuator. All measurements were performed in the room temperature and humidity that were slightly varying. Actuation voltage was generated by Keithley 6221 waveform generator.

For bending characterization, laser displacement sensor (optoNCDT 1700, MicroEpsilon) was used connected to Ni-DAQmx card as shown in Fig. A.2. Ni-DAQmx was also used for signal generation and current measurements. Displacement measured by laser was used as a feed-back in order to switch actuators position to 1 mm above or below the initial by changing polarity of applied voltage (± 1.5 V). The time needed to reach the set position was calculated for each cycle.

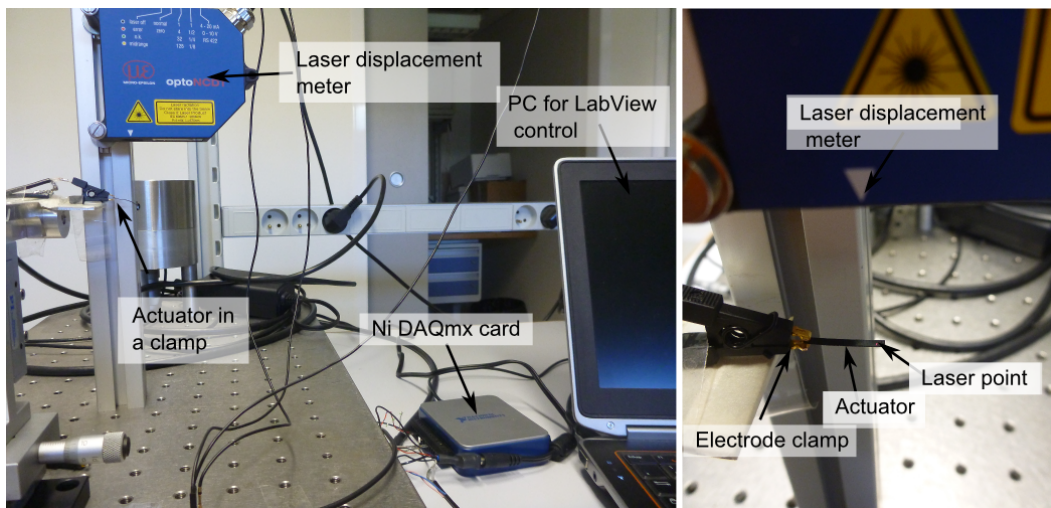


FIGURE A.2 –

FIGURE A.3 – Tracking bending using laser displacement meter.

Geometrical parameter of the robot

B.1 Kinematics of of the robot

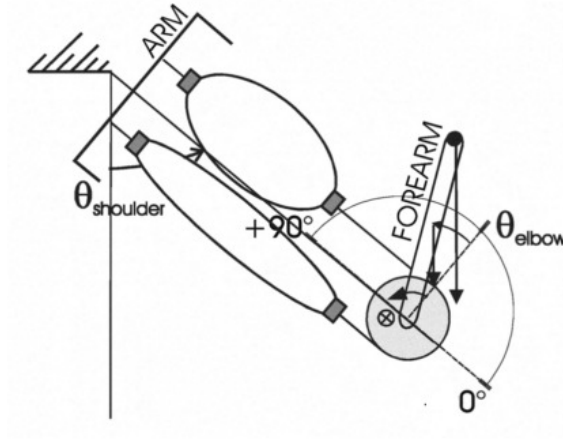


FIGURE B.1 – Two Dof set-up of the robotic arm with its initial zero position. For this thesis, we have actuated only two joints (the elbow and the shoulder).

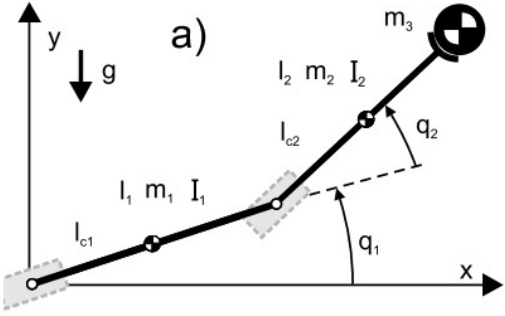
For this thesis, we have actuated only two joints (the elbow and the shoulder). So for all the kinematic equations, we have used the 2 Dof model and did all the calculation manually similar to the work presented in [D.Braun 2013].

B.2 Cad model of the robot

The total mass of the mobile part of the arm is $m_1 + m_2 + m_3 + m_4 = 5.138kg$. This does not include mass of the shoulder joint and mass of the muscles, chains, wires and air tubes.

TABLE B.1 – Muscle parameters at the actuating Joints

<i>Joints</i>	$l_o(cm)$	$\alpha_o(degrees)$	k	$r_o(cm)$
<i>ShoulderJoint</i>	23	20	1.1	1.2
<i>ElbowJoint</i>	18.5	20	1.2	0.85



a)

$$\mathbf{M} = \begin{bmatrix} I_1 + m_1 l_{c1}^2 + I_2 + m_2(l_1^2 + 2l_1 l_{c2} \cos(q_2) + l_{c2}^2) + m_3(l_1^2 + 2l_1 l_2 \cos(q_2) + l_2^2) & \times \\ I_2 + m_2(l_{c2}^2 + l_1 l_{c2} \cos(q_2)) + m_3(l_2^2 + l_1 l_2 \cos(q_2)) & I_2 + m_2 l_{c2}^2 + m_3 l_2^2 \end{bmatrix},$$

$$\mathbf{C} = \begin{bmatrix} -(m_2 l_{c2} + m_3 l_2) l_1 \sin(q_2) (2\dot{q}_1 \dot{q}_2 + \dot{q}_2^2) \\ (m_2 l_{c2} + m_3 l_2) l_1 \sin(q_2) \dot{q}_1^2 \end{bmatrix}, \quad \mathbf{D} = \begin{bmatrix} b_1 \dot{q}_1 \\ b_2 \dot{q}_2 \end{bmatrix},$$

$$\mathbf{G} = \begin{bmatrix} g(m_1 l_{c1} + m_2 l_1 + m_3 l_1) \cos(q_1) + g(m_2 l_{c2} + m_3 l_2) \cos(q_1 + q_2) \\ g(m_2 l_{c2} + m_3 l_2) \cos(q_1 + q_2) \end{bmatrix}.$$

FIGURE B.2 – Kinematic diagram and calculation for parameters in dynamical equation of the manipulator).

TABLE B.2 – Joint parameters

Joints	$R(m)$	$m(kg)$	$l(cm)$	$l_c(cm)$	$I(kgm^2)$	f_v
ShoulderJoint	0.009	2.7	351	125	0.02	3.0
ElbowJoint	0.015	2.6	307	178	0.0144	0.8

Inertial property of the arm in G-frame (center of gravity frame with 1, 2 and 3 as principal axes as shown in the Fig. B.4) :

$$\mathbf{I}_G = \begin{bmatrix} 4.93593 & 0 & 0 \\ 0 & 328.749 & 0 \\ 0 & 0 & 330.924 \end{bmatrix} \quad \& \quad \overrightarrow{OG} = \begin{bmatrix} 1.58 \\ -0.84 \\ -309 \end{bmatrix} \quad (\text{B.1})$$

Distances are in mm and so the inertia is in $kg - mm^2$.

Dimensions and mechanical charecteristics of the arm

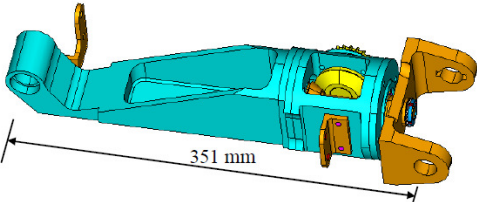
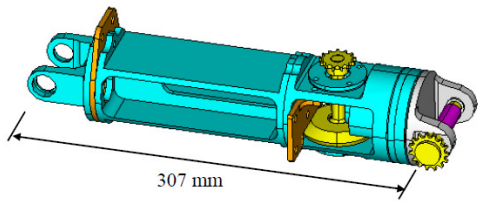
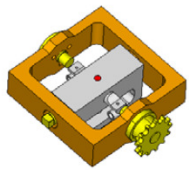
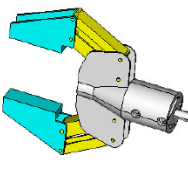
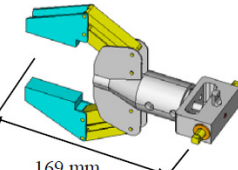
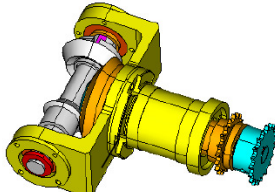
			
Mass of back arm $m_1 = 2,655 \text{ kg}$		Mass of fore-arm $m_2 = 1,689 \text{ kg}$	
			
Mass of Wrist $m_3 = 0,261 \text{ kg}$	Mass of tool $m_{4a} = 0,532 \text{ kg}$	Mass of tool + rudder $m_{4b} = 0,627 \text{ kg}$	Mass of shoulder $m_5 = 2,596 \text{ kg}$

FIGURE B.3 – Different parts of the robot arm

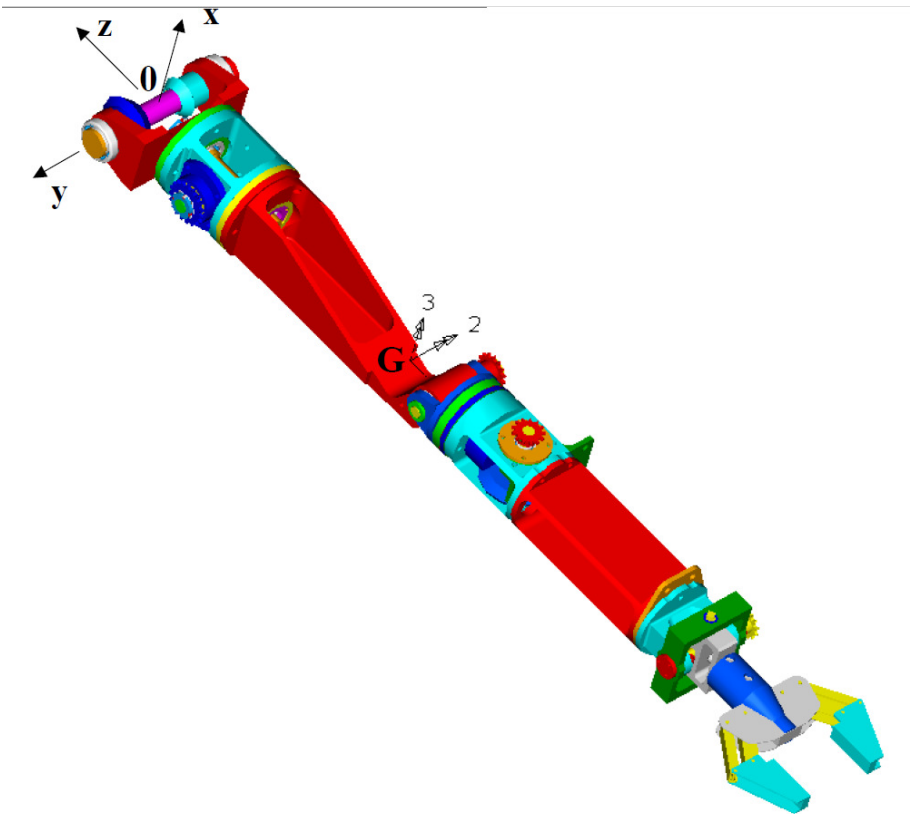


FIGURE B.4 – Solid model of the entire integrated robot arm

Closed-loop stability analysis of single-I controller

In order to better understand closed-loop stability, we propose to apply to our nonlinear system a classic linearization around the desired position considered as system's equilibrium point. We will limit, in a first step, our analysis to the linear viscous friction case. From Eqn. (3) Eq. (4.3) we derive :

$$\dot{u}F_{max} \left[1 - \frac{x}{x_{max}} \right] - uF_{max} \left(\frac{\dot{x}}{x_{max}} \right) - f_v \ddot{x} = (M + m) \ddot{x} \quad (\text{C.1})$$

Let us define the state variables as follows $x_1 = \ddot{x}$, $x_2 = \dot{x}$ and $x_3 = x - x_d$. As a consequence, the linearization will be realized around a zero-equilibrium point $x_{1d} = x_{2d} = x_{3d} = 0$ in such a way that $x_1 = x_{1d} + \varepsilon_1$, $x_2 = x_{2d} + \varepsilon_2$, $x_3 = x_{3d} + \varepsilon_3$. Let us define the following integral term $Int(x_3)$:

$$Int(x_3) = \int_0^t (x_d - x) dt = - \int_0^t x_3 dt \quad (\text{C.2})$$

From Eq. (C.1) Eqn. (10) the following state representation is deduced in which the term in x_3^2 corresponding to a ε_3^2 -term was neglected :

$$\begin{aligned} \dot{x}_1 &= \left(\frac{1}{m + M} \right) \left[-f_v x_1 - \frac{k_I Int(x_3) F_{max}}{(m + M) x_{max}} x_2 - k_I F_{max} \left(1 - \frac{x_d}{x_{max}} \right) x_3 \right] \\ \dot{x}_2 &= x_1 \\ \dot{x}_3 &= x_2 \end{aligned} \quad (\text{C.3})$$

In a classic way, we can deduce the matrix relationship $\dot{\varepsilon} = \mathbf{J} \varepsilon$ in which $\varepsilon = [\varepsilon_1, \varepsilon_2, \varepsilon_3]^T$ and the characteristic polynomial corresponding to $\det(\mathbf{J} - \lambda \mathbf{I}_3)$ where \mathbf{I}_3 is the 3×3 unit-matrix and λ a complex variable. We get :

$$\lambda^3 + \frac{f_v}{(m + M)} \lambda^2 + \frac{k_I Int(x_3) F_{max}}{(m + M) x_{max}} \lambda + k_I \frac{F_{max}}{(m + M)} \left(1 - \frac{x_d}{x_{max}} \right) = 0 \quad (\text{C.4})$$

Analyzing the system stability from this equation has however a meaning only if all coefficients are constant. This can be made from a simple physical interpretation of $Int(x_3)$: let us assume that the system transitory state takes a finite time to put the system from its initial position to the neighborhood of x_d with the ε -accuracy, and that this time is long enough in order that its change resulting from the ε -vector is

negligible. In this case we can write :

$$Int(x_3) \approx u_d/k_I, \quad (C.5)$$

where u_d is the unique closed-loop control value corresponding to the equilibrium x_d -position and given by :

$$u_d F_{max} \left(1 - \frac{x_d}{x_{max}}\right) = Mg \quad (C.6)$$

By reporting Eq. (C.5)Eqn. (14) and Eq. (C.6)(15) into Eq. (C.4)(13) we get :

$$\lambda^3 + \frac{f_v}{(m+M)}\lambda^2 + \frac{Mg}{(m+M)(x_{max}-x_d)}\lambda + k_I \frac{F_{max}}{(m+M)}\left(1 - \frac{x_d}{x_{max}}\right) = 0 \quad (C.7)$$

It is now possible to apply the classic Routh-Hurwitz stability criterion peculiar to a third order system in the form $\lambda^3 + A\lambda^2 + B\lambda + C = 0$: the system is stable if and only if $A > 0, B > 0, C > 0$ and $AB > C$. In our case these conditions can be gathered in the following relationship :

$$k_I < \frac{f_v g x_{max}}{(1 + m/M)F_{max}(x_{max} - x_d)^2} \quad (C.8)$$

Two important facts can be deduced from this stability condition : the higher the load M is, the more stable the system is and the closer the desired position is to x_{max} , the more stable the system is. If we apply this formula to the numerical values used in previous simulations, a limit k_I -value of about $363m^{-1}s^{-1}$ is deduced ; in fact this parameter induces some intermediate x -values exceeding the maximum of 10 cm, leading to saturate the muscle contraction position, which is not taken into account in our model. Moreover, it is also possible to underestimate this stability condition to get one k_I -parameter bound value which is now independent on load and desired position. On the one hand, we can write $(x_{max} - x_d) < x_{max}$ and, on the other hand, we can consider that $m < M$ i.e. the mobile muscle mass is low and so $(1 + m/M) < 2$; as a consequence, we derive the following expression of k_I -bound parameter now independent on load and desired position :

$$k_{I_{lim}} < \frac{f_v g}{2F_{max}x_{max}} \quad (C.9)$$

Its value, in the case of our simulations, is equal to about $24.5m^{-1}s^{-1}$ and is still greater than the chosen value of 10 associated to a load Mg equal to 10% the maximum force. It is possible to apply such analysis to our non-linear kinetic friction model if we assume that, when the system is removed from its equilibrium position, its restoring velocity can be considered to be constant and equal to the initial slope of the kinetic friction versus speed relationship i.e. in accordance with our previously

introduced notations :

$$k_{Lim} < \frac{f_v g}{2F_{max}x_{max}} \frac{dF_{damp}}{d\dot{x}}(u_d, \dot{x} = 0) = u_d \frac{(F_k - F_s)}{\dot{x}_k} \quad (C.10)$$

where u_d is now the control value corresponding to the following equilibrium positioning equation :

$$u_d F_{max} \left(1 - \frac{x_d}{x_{max}}\right) = Mg + F_s \quad (C.11)$$

By using this new expression of u_d in Eq. (C.4)Eqn. (13) and substituting initial slope of Eq. (C.10)Eqn. (19) for f_v , we get the following stability condition for k_I -parameter :

$$k_I < \frac{(Mg + F_s)^2 x_{max}^2 (F_k - F_s)}{(m + M) F_{max}^2 (x_{max} - x_d)^3 \dot{x}_k} \quad (C.12)$$

As earlier, increasing load or desired position are stability factors but also a large difference $(F_k - F_s)$ which, according to us, is particularly well realized in the case of the double helix braided sleeve used in McKibben artificial muscle technology. To derive from Eq. (C.13)Eqn. (21) a bound-value independent of load and desired position can be made if we assume, as previously, that $(x_{max} - x_d) < x_{max}$ and $m < M$; we get the following bound-expression for k_I :

$$k_{Lim} < \left(\frac{mg}{F_{max}}\right) \left(\frac{F_k - F_s}{F_{max}}\right) \frac{g}{2x_{max}\dot{x}_k} \quad (C.13)$$

which is equal to about to $9.8m^{-1}s^{-1}$ in the case of numerical values used for our simulation, very close to the empirically chosen $10m^{-1}s^{-1}$. Although questionable due to its very simplifying assumptions, this stability analysis suggests that a closed-loop stable control by means of a single linear integral action is feasible for the McKibben muscle without adding any supplementary damping device, as experimentally checked in further reported experiments.

Electronics of the robot

Sommaire

D.1 Intensity-Pressure converter	111
D.2 NI module	112
D.2.1 From Host computer to NI module	112
D.2.2 From NI module to Host computer	114

D.1 Intensity-Pressure converter

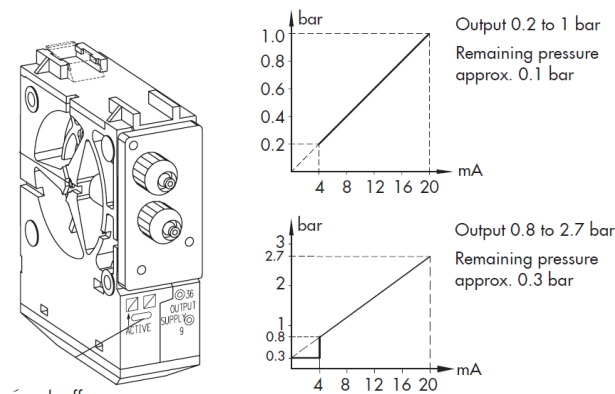


FIGURE D.1 – Mechanical design and the operational characteristic of the pneumatic valves [IPd 2014]

To provide pressure to the muscles, Intensity-Pressure converters are used on our robot. It is a Samson I/P 6111 manufactured by Samson Corporation, Frankfurt, Electropneumatic Converter. The current to pressure conversion done by the IP converter is shown in its datasheet.

This IP is rapid in action producing output pressure in the range 0 to 5 bar. The bandwidth of IP is volume dependent and can be as high as 5Hz for a volume of 75cm^3 . There are seven joints and a gripper. Each joint and gripper is actuated by a pair of McKibben muscles and each muscle is controlled by one IP converter and so there are 16 IP converters.

D.2 NI module

The electronics of the 7 Dofs anthropomorphic arm is upgraded. Previous solutions based on the old and obsolete ISA bus were not adapted to these new evolutions. Finally, CompactRIO from National Instruments was selected. This is a reconfigurable and embeddable chassis, integrating an intelligent real-time controller. According to the customer needs, up to 8 different modules can be plugged into the chassis. Depending of our needs 3 kinds of modules are added :

- 1x NI9205. It is an Analog-to-Digital-Converter (ADC) with up to 32 channels, selectable acquisition range ($\pm 200mV, \pm 1V, \pm 5V \pm 0V$) and a max sampling frequency of $250kS/s$. This device will sample the potentiometers (7 in numbers) dedicated to the positioning of the arm.

- 3x NI9265. These 3 modules are Digital-to-Analog-Converters (DAC). They have the particularity to provide analog current outputs. The SAMSON's 6111 electropneumatic converters use this kind of signal. Each module is able to manage up to 4 channels in the 0 to $20mA$ range at $100kS/s$.

- 4x NI9401. Finally the 4 last modules drive bidirectional digital IOs. These IOs connected to relatives quadrature encoders will be able to replace more accurately the current analog potentiometers. Up to 12 quadrature encoders can be acquired. The aim of the CompactRIO is to make the link between the computer managing high level control and the actuators of the 7DOF arm. It means that simple functions such as sampling and encapsulation into standard network protocol (UDP), extraction from standard network protocol (UDP) and signal generation will be performed.

D.2.1 From Host computer to NI module

Initialization of the communication Before broadcasting data, NI module requests that a host initialize the communication, defining numbers of useful data in all the others messages :

- "ADC channels to be transmitted" : Between $0x00$ and $0x20$ on an unsigned char. It corresponds to the total of analog-to-digital inputs transmitted by the NI 9205 converter. Up to 32 channels are available.

- "Counters to be transmitted" : Between $0x00$ and $0x0C$ on an unsigned char. It corresponds to the number of counters transmitted on the 3 NI9401 digital IO controllers. Up to 12 counters can be acquired.

- "Errors to be transmitted" : Between $0x00$ and $0x04$ on an unsigned char. It corresponds to the errors broad casted by the four NI 9265 digital-to-analog currents converters. As the four modules are connected, all of them can send its status.

- "Sampling Period" : Between $0x0001$ and $0xFFFF$ on an unsigned short. It corresponds to the sampling period expressed in milliseconds. Every N sampling period ADC values and NI9401 status errors are sampled and send to the host computer.

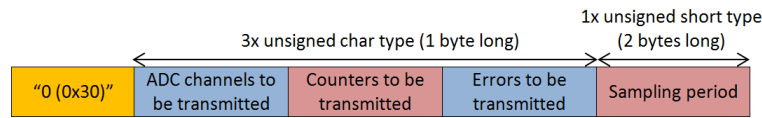


FIGURE D.2 – Data frame for initialization of the communication

Electrical current commands for the electropneumatic converters A 1D array composed of 16 unsigned shorts words (24 bytes or 16 bits long) is sent up to one millisecond.

- "0" corresponds to a $4mA$

- "216-1 = 65535" to a $20.6mA$ on the output of the NI module. According to the datasheet of the SAMSON's 6111 electropneumatic converter, $4/20mA$ signal is used, it has to be confirmed. Likewise, pressure to current conversion will have to be evaluated. Endianness will have to be verified too. The frame is composed as shown in Fig. D.3 :

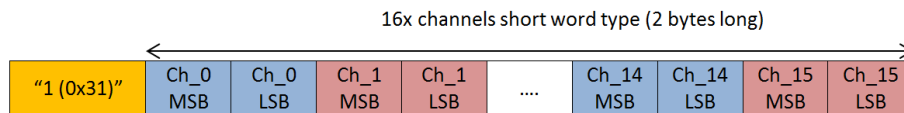


FIGURE D.3 – Data frame for Electrical current commands

Counters Reset A 2 states unsigned byte (0x00 or 0x01) can be sent to reset synchronously the values of the 12 counters recording the encoders. Take care, that an "enable" command as to be performed after a "reset" in order to start counting otherwise counters will be maintained in reset state. The frame is shown in Fig. D.4 :

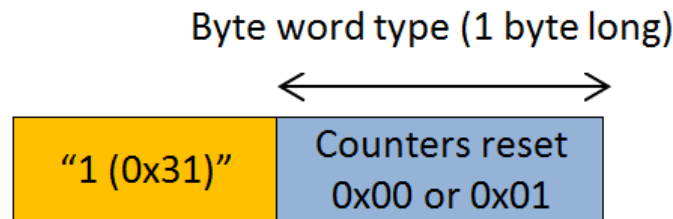


FIGURE D.4 – Data frame for Counters Reset

Digital output control A digital output is available on the NI9205 module. A 2 states unsigned byte (0x00 or 0x01) can be sent to set or reset the output. The frame is shown in Fig. D.5 :

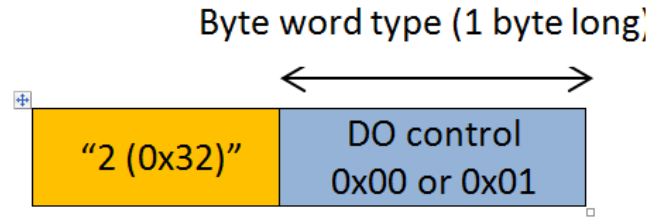


FIGURE D.5 – Data frame for Digital output control

D.2.2 From NI module to Host computer

Potentiometers values A 1D array of single float words (4 bytes or 32 bits long) + 1 unsigned long word (4 bytes or 32 bits long) of label (increased every millisecond) is sent every millisecond. The number of elements contained into the 1D array is initialized at start-up (varying from 0 up to 32). The 7 first values correspond to the tension available on the potentiometers, others inputs are free and can be used in future. Conversions have to be done between tensions and positions. Endianness will have to be verified. The frame is shown in Fig. D.6 (in case all 32 ADC channels are requested) :

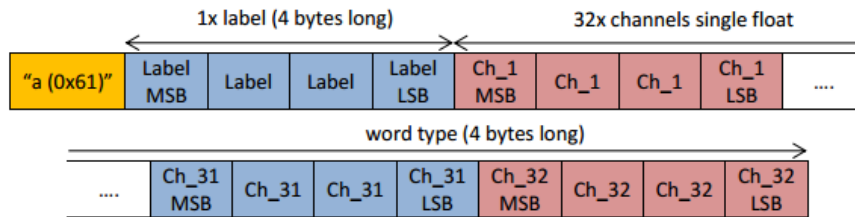


FIGURE D.6 – Data frame for Potentiometers

Counters values A 1D array of 12 signed integer words (4 bytes or 32 bits long) + 1 unsigned long word (4 bytes or 32 bits long) of label (increased every millisecond) is sent every millisecond. The number of elements contained into the 1D array is initialized at start-up (varying from 0 up to 12). The values correspond to counters associated to incremental encoders. Endianness will have to be verified. The frame is composed as in Fig. D.7 (in case all 12 counters are requested) :

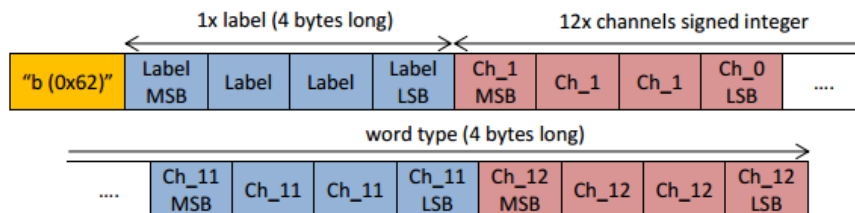


FIGURE D.7 – Data frame for Counters values

Current module error Each NI9265 Digital-to-Analog-Converter can provide a diagnostic of its state. 4 bytes (because of the 4 stacked modules) + 1 identification byte + 1 unsigned long word (4 bytes or 32 bits long) of label (increased every millisecond) are sent every millisecond. Each of the 4 bytes is a bits field.

- Bit 0 : NI9265 module is working normally or is in fault state.
- Bit 1 : NI9265 is not supplied externally. In order to provide current, an external supply must be connected in the 9 to 36Vdc range.
- Bit 2 - 5 : Each of the 4 channels cans diagnostic a "current open loop".
- Bit 6 - 7 : '0' padding. The frame is shown in Fig. D.8 :

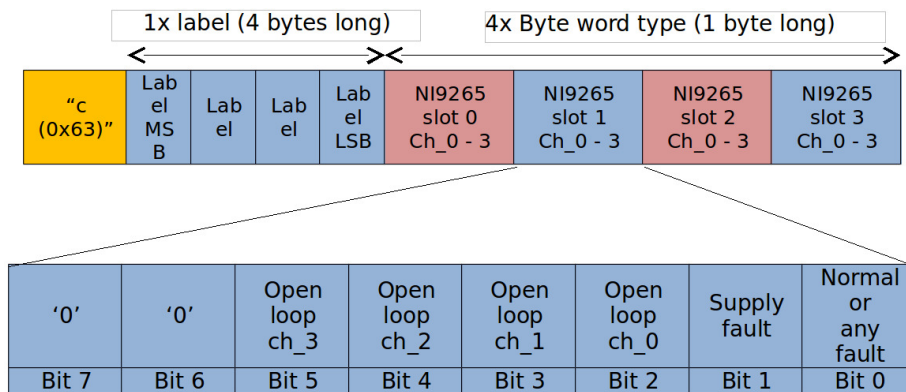


FIGURE D.8 – Data frame for Current module error

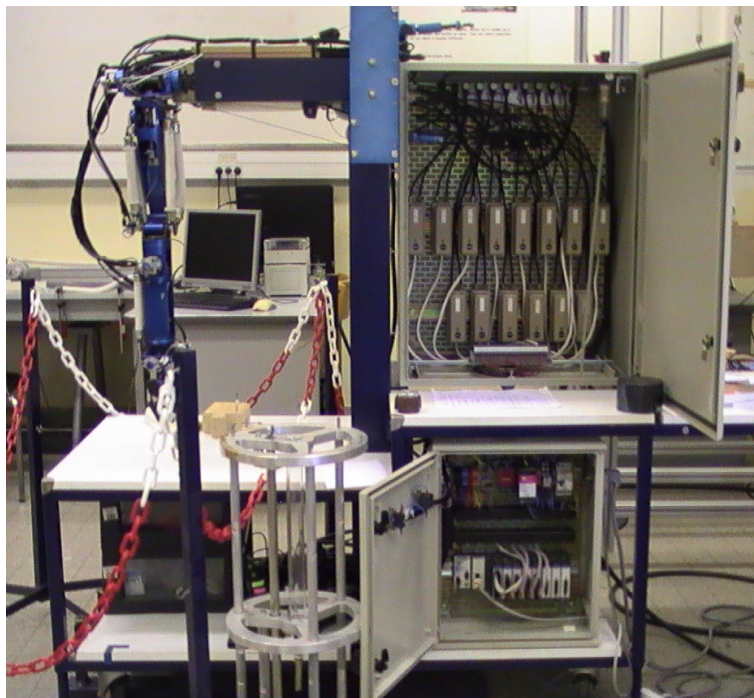


FIGURE D.9 – The complete experimental set-up

Bibliographie

- [Ahn 2011] H.P.H. Ahn et K.K. Ahn. *Hybrid Control of a Pneumatic Artificial Muscle (PAM) Using an Inverse NARX Fuzzy Model*. Eng. Appl. Artif. Intell, vol. 24, pages 697–776, 2011. (Cited on page 67.)
- [Andrikopoulos 2013] G. Andrikopoulos, G.Nikolakopoulos et S. Manesisa. *Pneumatic artificial muscles : A switching Model Predictive Control approach*. Control engineering practice, vol. 21, pages 1653–1664, 2013. (Cited on page 3.)
- [Annabestani 2015] M. Annabestani et N. Naghavi. *Non linear identificatio of ipmc actuators based on anfis-narx paradigm*. Sensors and Actuators A, vol. 209, pages 140–148, 2015. (Cited on pages 4 and 41.)
- [Au 2008] S. Au et H. Herr. *On the design of a powered ankle-foot prosthesis : The importance of series and parallel motor elasticity*. IEEE Robotics and Automation Magazine, 2008. (Cited on page 11.)
- [B. Verrelst 2005] B. Vanderborght F. Daerden B. Verrelst R. Van Ham et D. Lefebvre. *The pneumatic biped lucy actuated with pleated pneumatic artificial muscles*. Autonomous Robots, vol. 13, pages 201–213, 2005. (Not cited.) :AR :2005 :AR :2005 :AR :2005 :AR :2005
- [Barisci 2004] JN Barisci, GG Wallace, DR MacFarlane et RH Baughman. *Investigation of ionic liquids as electrolytes for carbon nanotube electrodes*. Electrochemistry communications, vol. 6, no. 1, pages 22–27, 2004. (Cited on page 27.)
- [Bassil 2014] Maria Bassil, Judy AL Moussawel, Michael Ibrahim, Georges Azzi et Mario El Tahchi. *Electrospinning of highly aligned and covalently cross-linked hydrogel microfibers*. Journal of Applied Polymer Science, vol. 131, no. 22, 2014. (Cited on page 27.)
- [Baughman 1996] RH Baughman. *Conducting polymer artificial muscles*. Synthetic metals, vol. 78, no. 3, pages 339–353, 1996. (Cited on page 26.)
- [Baughman 1999] Ray H Baughman, Changxing Cui, Anvar A Zakhidov, Zafar Iqbal, Joseph N Barisci, Geoff M Spinks, Gordon G Wallace, Alberto Mazzoldi, Danilo De Rossi et Andrew G Rinzler. *Carbon nanotube actuators*. Science, vol. 284, no. 5418, pages 1340–1344, 1999. (Cited on pages 26 and 27.)
- [Bawa 2009] Priya Bawa, Viness Pillay, Yahya E Choonara et Lisa C du Toit. *Stimuli-responsive polymers and their applications in drug delivery*. Bio-medical Materials, vol. 4, no. 2, page 022001, 2009. (Cited on page 26.)
- [Behl 2013] Marc Behl, Karl Kratz, Ulrich Noechel, Tilman Sauter et Andreas Lendlein. *Temperature-memory polymer actuators*. Proceedings of the National Academy of Sciences, vol. 110, no. 31, pages 12555–12559, 2013. (Cited on page 25.)

- [Bennett 2004] M. Bennett et D. Leo. *Ionic liquids as stable solvents for ionic polymer transducers*. Sensors and Actuators A, vol. 115, 2004. (Cited on pages 4 and 40.)
- [Boitier 1996] V. Boitier. *Design and control of a 2-DOF SCARA-type robot actuated by pneumatic McKibben artificial muscles*. Ph.D thesis, INSA-Toulouse, France, 1996. (Cited on page 58.)
- [Braikia 2011] K. Braikia, M. Chettouh, B. Tondou, P. Acco et M. Hamerlain. *Improved Control Strategy of 2-Sliding Controls Applied to a Flexible Robot Arm*. Adv. Robot, vol. 25, pages 1515–1538, 2011. (Cited on page 68.)
- [Brochu 2010] Paul Brochu et Qibing Pei. *Advances in dielectric elastomers for actuators and artificial muscles*, 2010. (Cited on page 26.)
- [B.Tondu 2005] B.Tondu, S. Ippolito et J. Guiochet. *A Seven-degrees-of-freedom Robot-arm Driven by Pneumatic Artificial Muscles for Humanoid Robots*. Int. Jour. of Robotics Research, vol. 24, no. 4, 2005. (Cited on pages 3 and 64.)
- [Burdet 2013] E. Burdet, D. Franklin et T. Milner. *Human Robotics : Neuromechanics and Motor Control*. MIT press, London, vol. 4, pages 201–213, 2013. (Cited on page 9.)
- [Cabane 2012] Etienne Cabane, Xiaoyan Zhang, Karolina Langowska, Cornelia G. Palivan et Wolfgang Meier. *Stimuli-Responsive Polymers and Their Applications in Nanomedicine*. Biointerphases, vol. 7, no. 1, pages –, 2012. (Cited on page 26.)
- [Cai 2003] D. Cai et Y. Dai. *A sliding Mode Controller for Manipulator Driven by Artificial Muscle Actuators*. Electron. Commun. Jpn, vol. 86, page 57â64, 2003. (Cited on page 68.)
- [Caldwell 1993] D.G. Caldwell, G.A. Medrano-Cerda et M. J. Goodwin. *Braided pneumatic actuator control of a multi-jointed manipulator*. In In Proceedings of the IEEE International Conference on Systems, Man and Cybernetics, pages 423–428, 1993. (Cited on page 30.)
- [Caldwell 1994] D.G. Caldwell, G.A. Medrano-Cerda et M. Goodwin. *Characteristics and adaptive control of pneumatic muscle actuators for a robotic elbow*. In IEEE international conference on robotics and automation, volume 4, pages 3558–3563, 1994. (Cited on page 68.)
- [Caldwell 1995] D.G. Caldwell, G.A. Medrano-Cerda et M. Goodwin. *Control of pneumatic muscle actuators*. IEEE control systems magazine, vol. 15(1), pages 550–558, 1995. (Cited on page 68.)
- [Catalano 2010a] M.g. Catalano, G. Grioli, F. Bonomo, R. Schiavi et A. Bicchi. *On joint design with intrinsic variable compliance : Derivation of the DLR QA-joint*. In In Proc. IEEE Int. Conf. on Robotics and Automation, 2010. (Cited on page 10.)

- [Catalano 2010b] M.g. Catalano, G. Grioli, F. Bonomo, R. Schiavi et A. Bicchi. *VSA-HD : From the enumeration analysis to the prototypical implementation*. In In IEEE/RSJ International Conference on Intelligent RObots and Systems, 2010. (Cited on page 10.)
- [Chen 2011] Zheng Chen, Tae I Um et Hilary Bart-Smith. *A novel fabrication of ionic polymer-metal composite membrane actuator capable of 3-dimensional kinematic motions*. Sensors and Actuators A : Physical, vol. 168, no. 1, pages 131–139, 2011. (Cited on page 27.)
- [Cheung 2004] J. T.-M. Cheung, M. Zhang et K. An. *Effects of plantar fascia stiffness on the biomechanical responses of the ankle-foot complex*. Clinical Biomechanics, vol. 19, 2004. (Cited on page 12.)
- [Choi 2007] HR Choi, KM Jung, JC Koo et JD Nam. *Robotic applications of artificial muscle actuators*. In Electroactive Polymers for Robotic Applications, pages 49–90. Springer, 2007. (Cited on page 24.)
- [Choi 2011] Seung Tae Choi, Jeong Yub Lee, Jong Oh Kwon, Seungwan Lee et Woonbae Kim. *Varifocal liquid-filled microlens operated by an electroactive polymer actuator*. Optics letters, vol. 36, no. 10, pages 1920–1922, 2011. (Cited on page 26.)
- [Chou 1996] C.-P. Chou et B. Hannaford. *Measurement and Modeling of McKibben Pneumatic Artificial Muscles*. IEEE Trans. on Robotics and Automation, vol. 12, no. 1, pages 90–102, 1996. (Cited on pages 31, 32, 67 and 68.)
- [Colbrunn 2001] R.W. Colbrunn, G.M. Nelson et R.D. Quinn. *Modeling of braided pneumatic actuators for robotic control*. In IEEE/RSJ international conference on intelligent robots and systems, pages 1964–1970, 2001. (Cited on pages 31 and 67.)
- [D. G. Caldwell 1995] G. A. Medrano-Cerda D. G. Caldwell et M. J. Goodwin. *Control of Pneumatic Muscle Actuators*. IEEE Control Systems Magazine, vol. 15, no. 1, pages 40–48, 1995. (Not cited.) :csm :1995 :csm :1995 :csm :1995 :csm :1995
- [Daerdan 1998] F. Daerdan, D. Lefeber et P. Kool. *Using free radial expansion pneumatic artificial muscles to control a 1dof robot arm*. In In Proceedings of the First International Symposium on Climbing and Walking Robots, pages 209–214, 1998. (Cited on pages 29 and 30.)
- [Daerdan 1999] F. Daerdan. *Conception and realization of pleated pneumatic artificial muscles and their use as compliant actuation elements*. PhD Thesis, Vrije Universiteit Brussel, 1999. (Cited on pages 28, 29 and 30.)
- [Daerdan 2001] F. Daerdan et D. Lefeber. *The concept and design of pleated pneumatic artificial muscles*. International Journal of Fluid Power, vol. 2, pages 41–50, 2001. (Cited on pages 28 and 29.)
- [Daerden 2001] F. Daerden et D. Lefeber. *The concept and design of pleated pneumatic artificial muscles*. International Journal of

- Fluid Power, vol. 2, no. 3, pages 41–50, 2001. (Not cited.)
:IJFP :2001 :IJFP :2001 :IJFP :2001 :IJFP :2001
- [Daerden 2002] Frank Daerden et Dirk Lefeber. *Pneumatic artificial muscles : actuators for robotics and automation*. European journal of mechanical and environmental engineering, vol. 47, no. 1, pages 11–21, 2002. (Cited on pages 24, 28, 29 and 30.)
- [Daneshvar 2014] E.D. Daneshvar et E. Smela. *Characterization of conjugated polymer actuation under cerebral physiological conditions*. Advanced healthcare materials 3, vol. 7, pages 1026–1035, 2014. (Cited on page 35.)
- [D.Braun 2013] D.Braun, F. Petit, F. Huber, S. Haddadin, P.Van Der Smagt, A. Albu-Schaffer et S.Vijayakumar. *Robots driven by compliant actuators : Optimal control under actuation constraints*. In IEEE Transactions on Robotics, volume 29, 2013. (Not cited.)
:ieee :2013 :ieee :2013 :ieee :2013 :ieee :2013
- [De Volder 2010] Michaël De Volder et Dominiek Reynaerts. *Pneumatic and hydraulic microactuators : a review*. Journal of Micromechanics and microengineering, vol. 20, no. 4, page 043001, 2010. (Cited on page 24.)
- [Doring 2013] Artjom Doring, Wolfgang Birnbaum et Dirk Kuckling. *Responsive hydrogels—structurally and dimensionally optimized smart frameworks for applications in catalysis, micro-system technology and material science*. Chemical Society reviews, vol. 42, no. 17, page 7391â7420, 2013. (Cited on page 26.)
- [Druitt 2014] C.M. Druitt. *Intelligent control of electroactive polymer actuators based on fuzzy and neurofuzzy methodologies*. IEEE/ASME Transactions on Mechatronics, vol. 19, 2014. (Cited on pages 40 and 44.)
- [F. 2011] Flacco F., A. Luca, I. Sardellitti et Tsagarakis. *Robust estimation of variable stiffness in flexible joints.n*. In In Proc. IEEE/RSJ Int. Conf. Intell. Robots Syst, 2011. (Cited on page 8.)
- [Feng 2014] Guo-Hua Feng et Wei-Lun Huang. *A self-strain feedback tuning-fork-shaped ionic polymer metal composite clamping actuator with soft matter elasticity-detecting capability for biomedical applications*. Materials Science and Engineering : C, vol. 45, pages 241–249, 2014. (Cited on page 27.)
- [Flacco 2011] F. Flacco, A. Luca, I. Sardellitti et N. Tsagarakis. *Robust estimation of variable stiffness in flexible joints*. In In Proc. IEEE/RSJ Int. Conf. Intell. Robots Syst, 2011. (Cited on pages 15 and 16.)
- [Ford 2015] Stefan Ford, Gary Macias et Ron Lumia. *Single active finger IPMC microgripper*. Smart Materials and Structures, vol. 24, no. 2, page 025015, 2015. (Cited on page 27.)
- [Fruehauf 1994] P. Fruehauf, I. Chien et M. Laurister. *Simplified imc-pid tuning rules*. ISA Transactions, vol. 33, pages 43–59, 1994. (Cited on page 40.)

- [Gaihare 2013] B. Gaihare, S. Ashraf, G.M. Spinks, P.C. Innis et G.G. Wallace. *Comparative displacement study of bilayer actuators comprising of conducting polymers, fabricated from polypyrrole, poly (3, 4- ethylenedioxythiophene) or poly (3, 4-propylenedioxythiophene)*. Sensors and Actuators A : Physical, vol. 193, pages 48–53, 2013. (Cited on page 36.)
- [Garabini 2011] M. Garabini, A. Passagliaand, F.A.W Belo, P. Salaris et A. Bicchi. *Optimality principles in variable stiffness control : VSA hammer*. In IROS, 2011. (Not cited.) :iee :2011 :iee :2011 :iee :2011 :iee :2011
- [Gorissen 2011] Benjamin Gorissen, Radu Donose, Dominiek Reynaerts et Michaël De Volder. *Flexible pneumatic micro-actuators : analysis and production*. Procedia Engineering, vol. 25, pages 681–684, 2011. (Cited on page 24.)
- [Gorissen 2014] Benjamin Gorissen, Takuya Chishiro, Shuhei Shimomura, Dominiek Reynaerts, Michael De Volder et Satoshi Konishi. *Flexible pneumatic twisting actuators and their application to tilting micromirrors*. Sensors and Actuators A : Physical, vol. 216, pages 426–431, 2014. (Cited on page 24.)
- [Grioli 2011] G. Grioli et Bicchi A. *A real-time parametric stiffness observer for usa devices*. In In Proc. IEEE Int. Conf. on Robotics and Automation, Shanghai, 2011. (Cited on page 8.)
- [Groothuis 2013] S. Groothuis, G. Rusticelli, A. Zucchelli, S. Stramigioli et R. Carloni. *The variable stiffness actuator vsaut-ii : Mechanical design, modeling, and identification*. In In Proc. IEEE/ASME transaction on Mechatronics, 2013. (Cited on pages 11 and 19.)
- [Guimard 2007] Nathalie K Guimard, Natalia Gomez et Christine E Schmidt. *Conducting polymers in biomedical engineering*. Progress in Polymer Science, vol. 32, no. 8, pages 876–921, 2007. (Cited on page 24.)
- [Haines 2014] Carter S Haines, Márcio D Lima, Na Li, Geoffrey M Spinks, Javad Foroughi, John DW Madden, Shi Hyeong Kim, Shaoli Fang, Mônica Jung de Andrade et Fatma Göktepe. *Artificial muscles from fishing line and sewing thread*. science, vol. 343, no. 6173, pages 868–872, 2014. (Cited on pages 25 and 26.)
- [Hannaford 1995] B. Hannaford, J.M. Winters, C.P. Chou et P. Marbot. *The Anthroform Biorobotic Arm : A System for the Study of Spinal Circuits*. Ann. Biomed. Eng., vol. 23, pages 399–408, 1995. (Cited on page 60.)
- [Hara 2004] S. Hara, T. Zama, W. Takashima et K. Kaneto. *Artificial muscles based on polypyrrole actuators with large strain and stress induced electrically*. Polymer journal 36, 2004. (Cited on page 36.)
- [Hara 2005] S. Hara, T. Zama, W. Takashima et K. Kaneto. *Free-standing gel-like polypyrrole actuators doped with bis (perfluoroalkylsulfonyle) imide exhibiting extremely large strain*. Smart Materials and Structures 14, vol. 6, 2005. (Cited on page 36.)

- [Hara 2011] S. Hara, T. Zama, W. Takashima et K. Kaneto. *Electro-chemical creeping and actuation of polypyrrole in ionic liquid*. Journal of Applied Physics 50, vol. 6, page 091601, 2011. (Cited on page 36.)
- [Harlotte 2002] I. Harlotte, K. K. Holmgren-Peterson, K. E. Magnusson et al. *Conjugated-polymer micro-and milliactuators for biological applications*. MRS bulletin 27, vol. 06, pages 461–464, 2002. (Cited on page 35.)
- [Hesselroth 1994a] T. Hesselroth, K. Sarkar, P. van der Smagt et K. Schulten. *Neural network control of a pneumatic robot arm*. IEEE Transactions on Systems, Man and Cybernetics 24, vol. 1, pages 28–38, 1994. (Cited on page 30.)
- [Hesselroth 1994b] T. Hesselroth, P. Sarkar, P. Smagt et K. Schulten. *Neural Network Control of a Pneumatic Robot Arm*. IEEE Trans. Syst. Man Cybern, vol. 24, pages 28–37, 1994. (Cited on page 67.)
- [Hirzinger 2001] G. Hirzinger, N. Sporer, A. Albu-Schaeffer, H. Maehnle et A. Pasucci. *DLR's torque-controlled light weight robot III—are we reaching the technological limits now?* In In IEEE International Conference on Robotics and Automation, 2001. (Cited on page 11.)
- [Hirzinger 2008] G. Hirzinger et S. Wolf. *A new variable stiffness design : matching requirements of the next robot generation*. In In IEEE International Conference on Robotics and Automation, 2008. (Cited on page 12.)
- [Hogan 1984] N. Hogan. *Adaptive Control of Mechanical Impedance by Coactivation of Antagonistic Muscles*. IEEE Trans. Automatic Control, pages 681–690, 1984. (Cited on pages 61 and 70.)
- [Hogan 1985] N. Hogan. *An approach to manipulation : Partial theory*. J. Dyn. Syst., Meas., Control, vol. 107, pages 1–7, 1985. (Cited on page 8.)
- [Hollander 2005] K. Hollander, T. Sugar et D. Herring. *Adjustable robotics tendon using a 'jack spring'*. In In Proc. Int. Conf. Rehabil. Robot, 2005. (Cited on pages 10 and 16.)
- [Hurst 2004] J. Hurst, J. Chestnutt et A. Rizzi. *An actuator with mechanically adjustable series compliance*. In Technical Report CMU-RI-TR-04-24, Carnegie Mellon University, 2004. (Cited on page 10.)
- [Ilievski 2011] Filip Ilievski, Aaron D Mazzeo, Robert F Shepherd, Xin Chen et George M Whitesides. *Soft robotics for chemists*. Angewandte Chemie, vol. 123, no. 8, pages 1930–1935, 2011. (Cited on page 24.)
- [Imran 2010] Abu Bin Imran, Takahiro Seki et Yukikazu Takeoka. *Recent advances in hydrogels in terms of fast stimuli responsiveness and superior mechanical performance*. Polymer journal, vol. 42, no. 11, pages 839–851, 2010. (Cited on page 27.)
- [Inoue 1987] K. Inoue. *Rubbertuators and applications for robotics*. In In Proceedings of the 4th International Symposium on Robotics Research, pages 57–63, 1987. (Cited on page 30.)

- [IPd 2014] *Electropneumatic converters type 6111 i/p converter*, Samson Corporation, Frankfurt, 2014. (Cited on page 111.)
- [Ishikawa 2005] M. Ishikawa, P. Komi, M. Grey, V. Lepola et G. Bruggemann. *Muscle-tendon interaction and elastic energy usage in human walking*. Journal of applied physiology, vol. 99, 2005. (Cited on page 12.)
- [Jafari 2010] A. Jafari, B. Vanderborght N. Tsagarakis et D. Caldwell. *A novel actuator with adjustable stiffness (awas)*. In In Proc. IEEE/RSJ Int. Conf. Intell. Robots Syst, 2010. (Cited on pages 10 and 13.)
- [Jafari 2011] A. Jafari, B. Vanderborght N. Tsagarakis et D. Caldwell. *Awas-ii : A new actuator with adjustable stiffness based on the novel principle of adaptable pivot point and variable lever ratio*. In In Proc. IEEE Int. Conf. Robot. Autom, 2011. (Cited on pages 10, 13, 14 and 15.)
- [Jo 2013] Choonghee Jo, David Pugal, Il-Kwon Oh, Kwang J Kim et Kinji Asaka. *Recent advances in ionic polymer-metal composite actuators and their modeling and applications*. Progress in Polymer Science, vol. 38, no. 7, pages 1037–1066, 2013. (Cited on page 26.)
- [John 2010] S. John, G. Alici et C. Cook. *Inversion-based feedforward control of polypyrrole trilayer bender actuators*. IEEE/ASME Transactions on Mechatronics, vol. 15, 2010. (Cited on pages 40 and 41.)
- [Jouppila 2014] V.T. Jouppila, S.A. Gadsden, G.M. Bone, A.U. Ellman et S.R. Habibi. *Sliding Mode Control of a Pneumatic Muscle Actuator System with a PWM Strategy*. Int. J. Fluid Power, vol. 15, pages 19–31, 2014. (Cited on page 68.)
- [Kelasidi 2011] E. Kelasidi, G. Andrikopoulos, G. Nikolakopoulos et S. Manesis. *A Survey on Pneumatic Muscle Actuators Modeling*. Journal of Energy and Power Engineering, vol. 6, pages 1442–1452, 2011. (Not cited.)
:jepe :2012 :jepe :2012 :jepe :2012 :jepe :2012
- [Kheirikhah 2011] Mohammad Mahdi Kheirikhah, Samaneh Rabiee et Mohammad Ehsan Edalat. *A review of shape memory alloy actuators in robotics*. In RoboCup 2010 : Robot Soccer World Cup XIV, pages 206–217. Springer, 2011. (Cited on page 24.)
- [Kim 2005] Byungkyu Kim, Deok-Ho Kim, Jaehoon Jung et Jong-Oh Park. *A biomimetic undulatory tadpole robot using ionic polymer-metal composite actuators*. Smart Materials and Structures, vol. 14, no. 6, page 1579, 2005. (Cited on page 27.)
- [Kim 2010a] B. S. Kim, J. B. Song, et J.J Park. *A serial-type dual actuator unit with planetary gear train : Basic design and applications*. In In IEEE Trans. on Mechatronics, 2010. (Cited on pages 10 and 11.)
- [Kim 2010b] B. S. Kim et J. B. Song. *Hybrid dual actuator unit : A design of a variable stiffness actuator based on an adjustable moment arm mechanism*. In In Proc. IEEE Int. Conf. Robot. Autom, 2010. (Cited on page 11.)

- [Klute 1999] G. Klute, J. Czerniecki et B. Hannaford. *McKibben artificial muscles : pneumatic actuators with biomechanical intelligence*. In In International conference on advanced intelligent mechatronics, 1999. (Cited on page 32.)
- [Koerner 2004] Hilmar Koerner, Gary Price, Nathan A Pearce, Max Alexander et Richard A Vaia. *Remotely actuated polymer nanocompositesâstress-recovery of carbon-nanotube-filled thermoplastic elastomers*. Nature materials, vol. 3, no. 2, pages 115–120, 2004. (Cited on page 25.)
- [Kong 2014] Lirong Kong et Wei Chen. *Carbon Nanotube and Graphene-based Bioinspired Electrochemical Actuators*. Advanced Materials, vol. 26, no. 7, pages 1025–1043, 2014. (Cited on page 26.)
- [Kornbluh 2013] Roy D Kornbluh, Ron Pelrine, Harsha Prahla, Annjoe Wong-Foy, Brian McCoy, Susan Kim, Joseph Eckerle et Tom Low. *Stretching the Capabilities of Energy Harvesting : Electroactive Polymers Based on Dielectric Elastomers*. In Advances in Energy Harvesting Methods, pages 399–415. Springer, 2013. (Cited on page 26.)
- [Kothera 2009] C.S. Kothera, M. Jangid, J. Sirohi et N.M. Wereley. *Experimental Characterization and Static Modeling of McKibben Actuators*. Transactions of the ASME, Journal of Mechanical Design, vol. 131, 2009. (Cited on page 56.)
- [Kumar 2013] V. Kumar, Z. Xu et E. Todorov. *Fast, strong and compliant pneumatic actuation for dexterous tendon-driven hands*. In ICRA, 2013. (Not cited.) :ICRA :2013 :ICRA :2013 :ICRA :2013 :ICRA :2013
- [Kumar 2014] V. Kumar, Y. Tassa, T. Erez et E. Todorov. *Real-time behaviour synthesis for dynamic Hand-Manipulation*. In ICRA, 2014. (Not cited.) :ICRA :2014 :ICRA :2014 :ICRA :2014 :ICRA :2014
- [Kurumaya 2016] S. Kurumaya, K. Suzumori, H. Nabae et S. Wakimoto. *Musculoskeletal lower-limb robot driven by multifilament muscles*. ROBOMECH journal, pages 3–18, 2016. (Cited on page 60.)
- [Li 2007] W. Li et E. Todorov. *Iterative linearisation methods for approximately optimal control and estimation of non-linear stochastic system*. Int. Jour. of Control, vol. 80, no. 9, pages 1439–1453, 2007. (Not cited.) :IJC :2007 :IJC :2007 :IJC :2007 :IJC :2007
- [Li 2008] Chunyu Li, Erik T. Thostenson et Tsu-Wei Chou. *Sensors and actuators based on carbon nanotubes and their composites : A review*. Composites Science and Technology, vol. 68, no. 6, pages 1227–1249, Mai 2008. (Cited on page 27.)
- [Lilly 2005] J.H. Lilly et L. Yang. *Sliding mode tracking for pneumatic muscle actuators in opposing pair configuration*. IEEE transactions on control systems technology, vol. 13(4), pages 550–558, 2005. (Cited on page 68.)
- [Lima 2012] Márcio D Lima, Na Li, Monica Jung De Andrade, Shaoli Fang, Jiyoung Oh, Geoffrey M Spinks, Mikhail E Kozlov, Carter S Haines, Dongseok Suh

- et Javad Foroughi. *Electrically, chemically, and photonically powered torsional and tensile actuation of hybrid carbon nanotube yarn muscles*. Science, vol. 338, no. 6109, pages 928–932, 2012. (Cited on page 25.)
- [Lu 2002] W. Lu, A. Fadeev, B. Qi et al. *Use of ionic liquids for conjugated polymer electrochemical devices*. Science, vol. 297, pages 983–987, 2002. (Cited on page 40.)
- [Madden 2004a] Peter GA Madden, John DW Madden, Patrick Anquetil, Nathan Vandesteeg et Ian W Hunter. *The relation of conducting polymer actuator material properties to performance*. Oceanic Engineering, IEEE Journal of, vol. 29, no. 3, pages 696–705, 2004. (Cited on page 26.)
- [Madden 2004b] P.G. Madden, J.D Madden, P. Anquetil, N. Vandesteeg et I.W. Hunter. *The relation of conducting polymer actuator material properties to performance*. Oceanic Engineering, IEEE Journal, vol. 29, pages 696–705, 2004. (Cited on pages 38 and 39.)
- [Maeda 2010] Shingo Maeda, Yusuke Hara, Ryo Yoshida et Shuji Hashimoto. *Active polymer gel actuators*. International journal of molecular sciences, vol. 11, no. 1, pages 52–66, 2010. (Cited on page 26.)
- [Marcincin 1993] J. Marcincin et A. Palko. *Negative pressure artificial muscle—An unconventional drive of robotic and handling systems*. In Transactions of the University of Kosice, pages 350–354, 1993. (Cited on page 28.)
- [Martinez 2014] Ramses V Martinez, Ana C Glavan, Christoph Keplinger, Alexis I Oyetibo et George M Whitesides. *Soft actuators and robots that are resistant to mechanical damage*. Advanced Functional Materials, vol. 24, no. 20, pages 3003–3010, 2014. (Cited on page 24.)
- [Meller 2014] Michael A Meller, Matthew Bryant et Ephraim Garcia. *Reconsidering the McKibben muscle : Energetics, operating fluid, and bladder material*. Journal of Intelligent Material Systems and Structures, vol. 25, no. 18, pages 2276–2293, 2014. (Cited on page 24.)
- [Melling 2002] Wilson S. Melling D. et E. W Jager. *The effect of film thickness on polypyrrole actuation assessed using novel non-contact strain measurements*. Smart Materials and Structures 22, vol. 10, 2002. (Cited on pages 35 and 39.)
- [Mengistie 2014] D.A. Mengistie, M.A. Ibrahem, P.C. Wang et C.W. Chu. *Highly conductive PEDOT : Pss treated with formic acid for ito-free polymer solar cell*. ACS applied materials and interfaces, vol. 6, pages 2292–2299, 2014. (Cited on page 36.)
- [Migliore 2005] S.A. Migliore, E. Brown et S. DeWeerth. *Biologically inspired joint stiffness control*. In In IEEE International Conference on Robotics and Automation, 2005. (Cited on page 19.)
- [Milner] T. Milner, C. Cloutier, A.B. Leger et D.W.Franklin. *Inability to maximally activate muscles during co-contraction and the effect on joint stiffness*. Experiment Brain Research, vol. 107, pages 293–303. (Cited on page 10.)

- [Minh 2009] T.V. Minh, T. Tjahjowidodo, H. Ramon et H. Brussel. *Control of Pneumatic Artificial Muscle (PAM) with Model-based Hysteresis Compensation*. In In Proceedings of the IEEE/Adv. International Conference on Mechatronics, Singapore, volume 4, pages 1082–1087, 2009. (Cited on page 68.)
- [Mirfakhrai 2007] Tissaphern Mirfakhrai, John DW Madden et Ray H Baughman. *Polymer artificial muscles*. Materials today, vol. 10, no. 4, pages 30–38, 2007. (Cited on page 26.)
- [Mirvakili 2013] Seyed M Mirvakili, Alexey Pazukha, William Sikkema, Chad W Sinclair, Geoffrey M Spinks, Ray H Baughman et John DW Madden. *Niobium nanowire yarns and their application as artificial muscles*. Advanced Functional Materials, vol. 23, no. 35, pages 4311–4316, 2013. (Cited on pages 24, 25 and 26.)
- [Morin 1953] A.H. Morin. *Elastic diaphragm*. US Patent No. 2 642 091, 1953. (Cited on page 28.)
- [Morin 2014] Stephen A Morin, Yanina Shevchenko, Joshua Lessing, Sen Wai Kwok, Robert F Shepherd, Adam A Stokes et George M Whitesides. *Using Click-Bricks to Make 3D Elastomeric Structures*. Advanced Materials, vol. 26, no. 34, pages 5991–5999, 2014. (Cited on page 24.)
- [Morita 1995] T. Morita et S. Sugano. *Development of a new robot joint using a mechanical impedance adjuster*. In In Proc. IEEE Int. Conf. Robotics and Automation, 1995. (Cited on page 10.)
- [Mosadegh 2014] Bobak Mosadegh, Panagiotis Polygerinos, Christoph Keplinger, Sophia Wennstedt, Robert F Shepherd, Unmukt Gupta, Jongmin Shim, Katia Bertoldi, Conor J Walsh et George M Whitesides. *Pneumatic networks for soft robotics that actuate rapidly*. Advanced Functional Materials, vol. 24, no. 15, pages 2163–2170, 2014. (Cited on page 24.)
- [Otero 2003] T. Otero et I. Boyano. *Comparative study of conducting polymers by the escr model*. The Journal of Physical Chemistry B, vol. 107, pages 6730–6738, 2003. (Cited on page 36.)
- [Ozawa 2002] R. Ozawa et H. Kobayashi. *Response characteristics of elastic joint robots driven by various types of controllers against external disturbances*. In In Proc. 6th Int. Conf. on Motion and Vibration Control, 2002. (Cited on page 8.)
- [P. Carbonell 2001] Z. Jiang P. Carbonell et D. W. Repperger. *Nonlinear control of a pneumatic muscle actuator system*. Control Applications, pages 167–172, 2001. (Cited on page 68.)
- [Pack 1994] R.T. Pack, M. Iskarous et K. Kawamura. *Comparison of fuzzy and nonlinear control techniques for a flexible rubberuator-based robot joint*. In International Fuzzy Systems and Intelligent Control Conference, pages 361–370, 1994. (Cited on page 68.)

- [Palmre 2013] Viljar Palmre, Joel J Hubbard, Maxwell Fleming, David Pugal, Sungjun Kim, Kwang J Kim et Kam K Leang. *An IPMC-enabled bio-inspired bending/twisting fin for underwater applications*. Smart Materials and Structures, vol. 22, no. 1, page 014003, Janvier 2013. (Cited on page 27.)
- [Petrovi 2002a] P. B. Petrovi. *Modeling and control of an artificial muscle, part one : Model building*. In X-th conference on mechanical vibrations, volume 47, 2002. (Cited on page 68.)
- [Petrovi 2002b] P. B. Petrovi. *Modeling and control of an artificial muscle, part one : Model verification*. In X-th conference on mechanical vibrations, volume 47, 2002. (Cited on page 68.)
- [Pratt 1995] G. A. Pratt et M. M. Williamson. *Series elastic actuators*. In In Proc. IEEE/RSJ Int. Conf. on Intelligent Robots and Systems, 1995. (Cited on pages 10 and 11.)
- [Pytel 2007] R.Z. Pytel. *Artificial muscle morphology : structure/property relationships in polypyrrole actuators*. Massachusetts Institute of Technology, USA, 2007. (Cited on page 39.)
- [Ruiz 2015] Siul Ruiz, Benjamin Mead, Viljar Palmre, Kwang J Kim et Woosoon Yim. *A cylindrical ionic polymer-metal composite-based robotic catheter platform : modeling, design and control*. Smart Materials and Structures, vol. 24, no. 1, page 015007, 2015. (Cited on pages 24 and 27.)
- [Schiavi 2008] R. Schiavi, G. Grioli, S. Sen et A. Bicchi. *VSA-II : A novel prototype of variable stiffness actuator for safe and performing robots interacting with humans*. In In IEEE Int. Conf. Robot. Autom., 2008. (Cited on pages 10 and 21.)
- [Schroder 2003] J. Schroder, D. Erol, K. Kawamura et R. Dillmann. *Dynamic pneumatic actuator model for a model-based torque controller*. IEEE international symposium on computational intelligence in robotics and automation, pages 342–347, 2003. (Cited on pages 31 and 68.)
- [Shepherd 2013] Robert F Shepherd, Adam A Stokes, Rui Nunes et George M Whitesides. *Soft machines that are resistant to puncture and that self seal*. Advanced Materials, vol. 25, no. 46, pages 6709–6713, 2013. (Cited on page 24.)
- [Simaite 2015a] A. Simaite. *Development of ionic electroactive actuators with improved interfacial adhesion : towards the fabrication of inkjet printable artificial muscles*. PhD thesis. LAAS-CNRS, Toulouse, 2015. (Cited on pages 36, 38, 39 and 99.)
- [Simaite 2015b] A. Simaite, B. Tondou, P. Soeres et C. Bergaud. *Hybrid pvdf/pvdfgraft-pegma membranes for improved interface strength and lifetime of pedot :pss/pvdf/ionic liquid actuators*. In ACS Applied Materials and Interfaces, 2015. (Cited on page 40.)
- [Simaite 2016] A. Simaite, F. Mesnilgrete, B. Tondou, P. Soeres et C. Bergaud. *Towards inkjet printable conducting polymer artificial muscle*. Sensors and Actuators B : Chemical, pages 425–433, 2016. (Cited on page 40.)

- [Sugino 2009] T. Sugino, K. Kiyohara, I. Takeuchi, K. Mukai et K. Asaka. *Actuator properties of the complexes composed by carbon nanotube and ionic liquid : the effects of additives*. Sensors and Actuators B : Chemical, vol. 141, pages 179–18, 2009. (Cited on pages 38 and 99.)
- [Sun 2014] L Sun, WM Huang, CC Wang, Z Ding, Y Zhao, C Tang et XY Gao. *Polymeric shape memory materials and actuators*. Liquid Crystals, vol. 41, no. 3, pages 277–289, 2014. (Cited on page 25.)
- [Surana 2015] Karan Surana, Pramod K Singh, B Bhattacharya, CS Verma et RM Mehra. *Synthesis of graphene oxide coated Nafion membrane for actuator application*. Ceramics International, vol. 41, no. 3, pages 5093–5099, 2015. (Cited on page 27.)
- [Tassa 2013] Y. Tassa, T. Wu, J. Movellan et E. Todorov. *Modeling and identification of pneumatic actuators*. In Int. Conf. on Mechatronics and Automation (ICMA), pages 437–443, 2013. (Cited on pages 3, 56 and 75.)
- [Temmer 2013] R. Temmer, A. Maziz, C. Plesse et et al. *In search of better electroactive polymer actuator materials : Ppy versus pedot versus pedot-ppy composites*. Smart Materials and Structures 22, vol. 10, page 104006, 2013. (Cited on page 36.)
- [Terasawa 2014] Naohiro Terasawa et Ichiroh Takeuchi. *Electrochemical and electromechanical properties of carbon black/carbon fiber composite polymer actuator with higher performance than single-walled carbon nanotube polymer actuator*. Electrochimica Acta, vol. 123, pages 340–345, Mars 2014. (Cited on page 27.)
- [Thanh 2006] TU.D.C. Thanh et K.K. Ahn. *Nonlinear PID Control to Improve the Control Performance of 2 Axes Pneumatic Artificial Muscle manipulator Using Neural Network*. Mechatronics, vol. 16, pages 577–587, 2006. (Cited on page 67.)
- [Thongchai 2001] S. Thongchai, M. Goldfarb, Sarkar N et K. Kawamura. *A Frequency Modeling Method of Rubbertuators for Control Application in an IMA Framework*. In In Proceedings of the 2001 Conference on American Control, Arlington, VA, USA, volume 4, pages 25–27, 2001. (Cited on page 67.)
- [Tian 2014] S. Tian, G. Ding, D. Yan, L. Lin et M. Shin. *Nonlinear Controlling of Artificial Muscle System with Neural Networks*. In In Proceedings of the 2004 IEEE International Conference on Robotics and Biomimetics, volume 4, pages 56–59, 2014. (Cited on page 67.)
- [Tiwari 2011] R Tiwari et E Garcia. *The state of understanding of ionic polymer metal composite architecture : a review*. Smart Materials and Structures, vol. 20, no. 8, page 083001, 2011. (Cited on page 26.)
- [Tondu 1995] B. Tondu et P. Lopez. *Theory of an Artificial Pneumatic Muscle and Application to the Modelling of McKibben Artificial Muscle*. C.R.A.S. French National Academy of Sciences, vol. 320, no. 4, 1995. (Cited on pages 28, 30, 59 and 65.)

- [Tondou 2000] B. Tondou et P. Lopez. *Modeling and Control of McKibben Artificial Muscle Robot Actuators*. IEEE Control Syst. Mag., vol. 20, page 15â38, 2000. (Cited on pages 31, 32, 67 and 68.)
- [Tondou 2006] B. Tondou et S.D. Zagal. *McKibben Artificial Muscle can be in Accordance with Hill Skeletal Muscle Model*. In IEEE/EMBS Int.Conf, BioMed. Rob. I& BioMechatronics, numéro 276, 2006. (Cited on pages 32 and 56.)
- [Tondou 2009] B. Tondou, K. Braikia, M. Chettou et S. Ippolito. *Second Order Sliding Mode Control for an Anthropomorphic Robot-Arm driven with Pneumatic Artificial Muscles*. In Int. Conf. on Humanoid Robotics (ICHR), pages 47–54, 2009. (Cited on page 3.)
- [Tondou 2012] B. Tondou. *Modelling of the McKibben artificial muscle : A review*. Journal of Intelligent Material Systems and Structures, vol. 23, no. 3, 2012. (Cited on pages 24, 56 and 58.)
- [Tondou 2013] B. Tondou. *Closed-Loop Position Control of Artificial Muscles with a Single Integral Action*. In In Proceedings of the IEEE International Conference on Mechatronics (ICM-2013), Vicence, Italy, volume 27, 2013. (Cited on page 69.)
- [Tondou 2015] B. Tondou. *Robust and accurate closed-loop control of mckibben artificial muscle contraction with a single integral action*. Actuators, vol. 3, pages 142–165, 2015. (Cited on page 41.)
- [Tondou 2016] B. Tondou. *What is an artificial muscle ? A systematic approach*. Actuators, vol. 4, pages 336–352, 2016. (Cited on page 40.)
- [Tonietti 2005] G. Tonietti, R. Schiavi et A. Bicchi. *Design and control of a variable stiffness actuator for safe and fast physical human/robot interaction*. In In IEEE Int. Conf. Robot. Autom, 2005. (Cited on page 10.)
- [Torop 2014] Janno Torop, Alvo Aabloo et Edwin WH Jager. *Novel actuators based on polypyrrole/carbide-derived carbon hybrid materials*. Carbon, vol. 80, pages 387–395, 2014. (Cited on page 27.)
- [Tozzi 2011] Piergiorgio Tozzi. *Artificial muscle : the human chimera is the future*. Swiss Med Wkly, vol. 141, page 13311, 2011. (Cited on page 24.)
- [Tsagarakis 2011] N. Tsagarakis, I. Sardellitti et D. Caldwell. *A new variable stiffness actuator (compact-usa) : Design and modelling*. In In Proc. IEEE/RSJ Int. Conf. on Intelligent Robots and Systems, 2011. (Cited on pages 11 and 19.)
- [Tuijthof 2000] G.J.M. Tuijthof et J.L. Herder. *Design, actuation and control of an anthropomorphic robot arm*. IEEE control systems magazine, vol. 35, pages 945–962, 2000. (Cited on page 68.)
- [Tunckol 2012] Meltem Tunckol, Jérôme Durand et Philippe Serp. *Carbon nanomaterial-ionic liquid hybrids*. Carbon, vol. 50, no. 12, pages 4303–4334, Octobre 2012. (Cited on page 27.)

- [van der Smagt 1996] P. van der Smagt, F. Groen et K. Schulten. *Analysis and control of a rubbertuator arm*. Biological Cybernetics, vol. 75, pages 433–440, 1996. (Cited on page 68.)
- [van Ham 1996a] R. van Ham, F. Daerden, B. Verrelst et D. Lefeber. *Control of a joint actuated by two pneumatic artificial muscles with fast switching on-off valves*. 6th National congress on theoretical and applied mechanics, vol. 75, 1996. (Cited on page 31.)
- [van Ham 1996b] R. van Ham, F. Daerden, B. Verrelst et D. Lefeber. *Control of a joint actuated by two pneumatic artificial muscles with fast switching on-off valves*. 6th National congress on theoretical and applied mechanics, vol. 75, 1996. (Cited on page 68.)
- [van Ham 2007] R. van Ham, , B. Vanderborght, M. V. Damme , B. Verrelst et D. Lefeber. *The mechanically adjustable compliance and controllable equilibrium position actuator : Design and implementation in a biped robot*. In Robotics and Autonomous Systems, 2007. (Cited on pages 10 and 17.)
- [van Ham 2009] R. van Ham, T. Sugar, B. Vanderborght, K. Hollander et D. Lefeber. *Compliant actuator designs*. IEEE Robot. Autom. Mag, vol. 16, pages 81–94, 2009. (Cited on pages 10, 12, 17, 18, 20 and 21.)
- [Vanderborght 2006] B. Vanderborght, B. Verrelst, B. Ham, R. Van Damme, M. Van Beyl et P. Lefeber. *Torque and compliance control of the pneumatic artificial muscles in the biped "Lucy"*. In ICRA, pages 842–847, 2006. (Not cited.)
:icra :2006 :icra :2006 :icra :2006 :icra :2006
- [Verrelst 2005] B. Verrelst, R. van Ham, , B. Vanderborght, F. Daerden et D. Lefeber. *The pneumatic biped lucy actuated with pleated pneumatic artificial muscles*. In Autonom. Robots, 2005. (Cited on page 10.)
- [Wang 2013] X. Wang, G. G. Alici et C. Nguyen. *Adaptive sliding mode control of tri-layer conjugated polymer actuators*. Smart Material Structures, vol. 22, pages 1–8, 2013. (Cited on page 40.)
- [Wolf 2008] S. Wolf et G. Hirzinger. *A new variable stiffness design Matching requirements of the next robot generation*. In Int. Conf. Robot. Autom, 2008. (Cited on page 10.)
- [Woods 2013] B.K.S. Woods, Y.T. Choi, C.S. Kothera et N.M. Wereley. *Control System Development for Pneumatic Artificial Muscle-Driven Active Rotor Systems*. AIAA J. Guidance Control Dyn, vol. 36, pages 1177–1185, 2013. (Cited on page 69.)
- [Xiangrong 2010] S. Xiangrong. *Nonlinear Model-based Control of Pneumatic Artificial Servo Systems*. Control Eng. Practice, vol. 18, page 311â317, 2010. (Cited on page 68.)
- [Yao 2008] Q. Yao, G. Alici et G. Spinks. *Feedback control of tri-layer polymer actuators to improve their positioning ability and speed of response*. Sensors and Actuators A, vol. 144, 2008. (Cited on pages 40 and 49.)

- [Zainudeen 2008] U.L. Zainudeen, M.A. Careem et S. Skaarup. *Pedot and ppy conducting polymer bilayer and trilayer actuators*. Sensors and Actuators B : Chemical, vol. 134, pages 467–470, 2008. (Cited on page 36.)
- [Zhang 2004] Mei Zhang, Ken R Atkinson et Ray H Baughman. *Multifunctional carbon nanotube yarns by downsizing an ancient technology*. Science, vol. 306, no. 5700, pages 1358–1361, 2004. (Cited on page 25.)
- [Zhang 2011] Zhiye Zhang et Michael Philen. *Review : Pressurized Artificial Muscles*. Journal of Intelligent Material Systems and Structures, 2011. (Cited on page 24.)
- [Zhu 2008] X. Zhu, G. Tao, B. Yao et J. Cao. *Adaptive Robust Posture Control of a Parallel Manipulator Driven by Pneumatic Muscles*. Automatica, vol. 44, pages 2248–2257, 2008. (Cited on page 68.)

Key words : Pneumatic systems, McKibben muscles, iLQR control, nonlinear control, agonist-antagonist actuation, bio-inspired robots, anthropomorphic systems, robots, grippers
